Calhoun
Institutional Archive of the Naval Postgraduate School

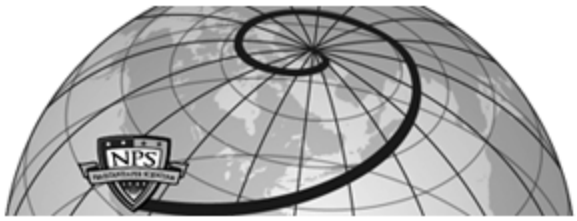

Author(s)	Anderson, Brian C.
Title	Assessing accuracy in varying Lidar data point densities in Digital Elevation Maps
Publisher	Monterey, California. Naval Postgraduate School
Issue Date	2008-09
URL	http://hdl.handle.net/10945/3928

This document was downloaded on May 04, 2015 at 22:04:55

DUDLEY KNOX LIBRARY

http://www.nps.edu/library

Calhoun is a project of the Dudley Knox Library at NPS, furthering the precepts and goals of open government and government transparency. All information contained herein has been approved for release by the NPS Public Affairs Officer.

Dudley Knox Library / Naval Postgraduate School
411 Dyer Road / 1 University Circle
Monterey, California USA 93943

NPS PRAESTANTIA PER SCIENTIAM 1909

http://www.nps.edu/

NAVAL POSTGRADUATE SCHOOL

MONTEREY, CALIFORNIA

THESIS

ASSESSING ACCURACY IN VARYING LIDAR DATA POINT DENSITIES IN DIGITAL ELEVATION MAPS

by

Brian C. Anderson

September 2008

Thesis Advisor:	R. C. Olsen
Second Reader:	James H. Newman

Approved for public release; distribution is unlimited

THIS PAGE INTENTIONALLY LEFT BLANK

REPORT DOCUMENTATION PAGE			Form Approved OMB No. 0704-0188
Public reporting burden for this collection of information is estimated to average 1 hour per response, including the time for reviewing instruction, searching existing data sources, gathering and maintaining the data needed, and completing and reviewing the collection of information. Send comments regarding this burden estimate or any other aspect of this collection of information, including suggestions for reducing this burden, to Washington headquarters Services, Directorate for Information Operations and Reports, 1215 Jefferson Davis Highway, Suite 1204, Arlington, VA 22202-4302, and to the Office of Management and Budget, Paperwork Reduction Project (0704-0188) Washington DC 20503.			
1. AGENCY USE ONLY ***(Leave blank)***	**2. REPORT DATE** September 2008	**3. REPORT TYPE AND DATES COVERED** Master's Thesis	
4. TITLE AND SUBTITLE Assessing Accuracy in Varying LIDAR Data Point Densities in Digital Elevation Maps		**5. FUNDING NUMBERS**	
6. AUTHOR B. C. Anderson			
7. PERFORMING ORGANIZATION NAME(S) AND ADDRESS(ES) Naval Postgraduate School Monterey, CA 93943-5000		**8. PERFORMING ORGANIZATION REPORT NUMBER**	
9. SPONSORING /MONITORING AGENCY NAME(S) AND ADDRESS(ES) N/A		**10. SPONSORING/MONITORING AGENCY REPORT NUMBER**	
11. SUPPLEMENTARY NOTES The views expressed in this thesis are those of the author and do not reflect the official policy or position of the Department of Defense or the U.S. Government.			
12a. DISTRIBUTION / AVAILABILITY STATEMENT Approved for public release; distribution is unlimited.		**12b. DISTRIBUTION CODE**	

13. ABSTRACT (maximum 200 words)

This thesis discusses the production of Digital Elevation Maps (DEM) using varying density of data points from a Lidar (Laser or Light Detection And Ranging) collection. Additionally, this thesis contains information on the multiple space missions that use laser altimetry or Lidar to gather data about planet earth, the moon, asteroids, Mars and Mercury. The thesis covers the accuracy of different amounts of data used when generating a DEM in Quick Terrain Modeler software package and the ILAP Bare Earth Extraction Plug-In and discusses the error analysis when comparing the different DEMs built by randomly selecting 90%, 66%, 50%, 30%, 10%, 5%, 3%, 1%, 0.5%, 0.3%, 0.05%, 0.03% and 0.01% of the data from an airborne Lidar collection from Honduras in 2008. Analyzing surface DEMs created in QTM, the results of the point reduction experiment indicate that a collection cloud point density of 60,000 points per square kilometer are required for an accurate surface DEM in this environment.

14. SUBJECT TERMS Lidar, Ladar, Laser Radar, Laser Altimetry, Foliage Penetration, FOPEN, poke-through, Digital Elevation Map, DEM, Lidar Space Missions			**15. NUMBER OF PAGES** 99
			16. PRICE CODE
17. SECURITY CLASSIFICATION OF REPORT Unclassified	**18. SECURITY CLASSIFICATION OF THIS PAGE** Unclassified	**19. SECURITY CLASSIFICATION OF ABSTRACT** Unclassified	**20. LIMITATION OF ABSTRACT** UU

NSN 7540-01-280-5500

Standard Form 298 (Rev. 2-89)
Prescribed by ANSI Std. 239-18

THIS PAGE INTENTIONALLY LEFT BLANK

Approved for public release; distribution is unlimited

ASSESSING ACCURACY IN VARYING LIDAR DATA POINT DENSITIES IN DIGITAL ELEVATION MAPS

Brian C. Anderson
Major, United States Marine Corps
B.S., Boston University, 1995

Submitted in partial fulfillment of the
requirements for the degree of

MASTER OF SCIENCE IN SPACE SYSTEMS OPERATIONS
and
MASTER OF SCIENCE IN APPLIED PHYSICS

from the

NAVAL POSTGRADUATE SCHOOL
September 2008

Author: Brian C. Anderson

Approved by: R. C. Olsen
Thesis Advisor

James H. Newman
Second Reader

Rudy Panholzer
Chairman, Space Systems Academic Group

James Luscombe
Chairman, Physics Department

THIS PAGE INTENTIONALLY LEFT BLANK

ABSTRACT

This thesis discusses the production of Digital Elevation Maps (DEM) using varying density of data points from a Lidar (Laser or Light Detection And Ranging) collection. Additionally, this thesis contains information on the multiple space missions that use laser altimetry or Lidar to gather data about planet earth, the moon, asteroids, Mars and Mercury. The thesis covers the accuracy of different amounts of data used when generating a DEM in Quick Terrain Modeler software package and the ILAP Bare Earth Extraction Plug-In and discusses the error analysis when comparing the different DEMs built by randomly selecting 90%, 66%, 50%, 30%, 10%, 5%, 3%, 1%, 0.5%, 0.3%, 0.05%, 0.03% and 0.01% of the data from an airborne Lidar collection from Honduras in 2008. Analyzing surface DEMs created in QTM, the results of the point reduction experiment indicate that a collection cloud point density of 60,000 points per square kilometer are required for an accurate surface DEM in this environment.

THIS PAGE INTENTIONALLY LEFT BLANK

TABLE OF CONTENTS

I. INTRODUCTION 1
A. PURPOSE OF RESEARCH 1
B. OBJECTIVE 1

II. BACKGROUND 3
A. LIDAR (LIGHT DETECTION AND RANGING) 3
B. FULL WAVEFORM ANALYSIS 8
C. STEP-STARE COLLECTIONS 9
D. ADVANTAGES OF LIDAR 10
E. DISADVANTAGES OF LIDAR 11
F. DIGITAL ELEVATION MAPS 11
1. Manual Surveys 11
2. Photogrammetry 12
3. Radar Imagery 12
G. MILITARY APPLICATIONS OF LIDAR 13

III. SPACE MISSIONS INCORPORATING LIDAR OR LASER ALTIMETRY 17
A. LASER ALTIMETRY AND THE APOLLO MISSIONS 19
B. WIDE-SWATH IMAGING LIDAR FOR SPACEBORNE APPLICATIONS 20
1. NASA Airborne Oceanographic Lidar 20
2. Vegetation Canopy Lidar 22
C. MARS 23
1. MOLA 23
2. Mars Polar Lander 25
D. EARTH 26
1. Shuttle Laser Altimeter Missions 26
2. Geoscience Laser Altimeter System 28
E. AEROSOLS AND CLOUDS 30
1. CALIPSO 30
2. NASA Mars Phoenix Mission 30
F. MERCURY AND ASTEROIDS 32
1. MESSENGER 32
2. Lidar to Observe Asteroids 34
G. THE MOON 35
1. Clementine 35
2. SELENE (Kaguya) 36
3. Chang'e 38
4. Future Lunar Missions 39
a. Lunar Reconnaissance Orbiter 39
b. Altair Lunar Lander 41

IV. EXPERIMENT 43

A. ASSESSING ACCURACY IN VARYING LIDAR DATA POINT DENSITIES IN DIGITAL ELEVATION MAPS 43
B. DATA DELIVERED 43
C. POST PROCESSING SOFTWARE 44
D. SITE DESCRIPTION 45
V. OBSERVATIONS 47
A. METHOD OVERVIEW 47
B. EVALUATION TECHNIQUES 51
VI. ANALYSIS 55
A. DIGITAL ELEVATION MAPS 55
B. LIDAR MODEL ARTIFACTS 63
1. Crystal Forest 63
2. Bomb Craters 64
C. VISUAL ANALYSIS 64
D. STATISTICS 65
VII. SUMMARY 69
VIII. CONCLUSION 71
LIST OF REFERENCES 73
APPENDIX – RANDOM_PTS_FROMXYZ.PRO IDL CODE 79
INITIAL DISTRIBUTION LIST 81

LIST OF FIGURES

Figure 1. Lidar range calculation (Optech Inc.) 3
Figure 2. Rangefinder Scanning and Aircraft Orientation (Optech Inc.) 4
Figure 3. Low density Lidar point cloud that clearly shows the scan lines of the scanning mirror as the airplane moved along the collection line (After NGA data Strip 10) 5
Figure 4. Example point cloud collected from first and last Lidar returns in a forest (Hohl 3) 7
Figure 5. A single pulse can return a single signal with different shapes or multiple returns per pulse from numerous objects in the beams path (Quick Terrain Modeler Training 3) 7
Figure 6. Principle of echo digitization (Ullrich 3) 9
Figure 7. Innovative Lidar Applications Program Step-Stare mode (a) first step, (b) second step, (c) third step (Roth 2) 10
Figure 8. Flow chart of high scale map production from space images (Dini 1652) 12
Figure 9. Flood simulation tool can be used to model impact of rising water on transportation infrastructure (Applied Imagery) 15
Figure 10. Roof faces from an aerial scan, building from a terrestrial scan and combination of both data sets (IKG Research) 16
Figure 11. Cross-sectional profile of Pass 912 obtained at night under summer foliage conditions during September 1980. Top curve is “AOL Surface”, lower symbols are “AOL Waveform Bottom” (Krabill 692) 21
Figure 12. VCL’s MBLA design had five lasers arranged in a pentagon for a circular field-of-view that is centered on nadir (Dubayah 5) 23
Figure 13. Using MOLA data through June of 2000, the MOLA Science Team has produced very high resolution topographic shade maps of Mars. This figure is from 0 to 360 degrees E (MOLA) 25
Figure 14. Ground Tracks plotted for Shuttle Laser Altimeter (SLA) mission SLA-01 and SLA-02 (LAPF) 27
Figure 15. Histogram of all sea surface height measurements from SLA-01 (LAPF) 28
Figure 16. (Bottom) Photo of the ICESat ground track where the Lidar data (top) was collected off the coast of Saharan Africa (WFF GLAS) 29
Figure 17. A color-modulated, altitude-time image of CALIOP 532 nm Total (Parallel + Perpendicular) attenuated backscatter (/km/sr) (CALIPSO Products) 30
Figure 18. This graph shows Lidar data for a 15-minute period around noon on Sol 4. Higher concentrations of dust (as shown in red and orange) move over the lander near the end of the measurement (Phoenix News) 31
Figure 19. “A close-up of the Mercury Laser Altimeter (MLA) profile of Mercury acquired during MESSENGER’s first Mercury flyby on 14 January 2008. Comparison with an Arecibo radar image mosaic (bottom) provided by Harmon and co-workers shows that the two largest depressions are adjacent impact craters. The craters have rim-to-rim diameters of 107 km

(left) and 122 km (right). The root mean square roughness of the floor the larger crater is ~35 m. The vertical exaggeration in the figure is 35:1" (Messenger).....33
Figure 20. The LIDAR spots on the surface of asteroid Itokawa covered over 87% of the total surface. Since the spin axis of the asteroid is along the z-axis in the images, the density of spots in both polar regions is relatively low (Mukai 190) 34
Figure 21. A topographic map of the Moon's surface based on Clementine's laser altimeter (science@NASA) 36
Figure 22. Topographic profile of Pythagoras crater (63.5N, 63.0W). Outer ring and central peak are clearly displayed. Data obtained 25 November 2007. Horizontal axis is lunar latitude (One degree corresponds to 30.3km) (Araki 1510).....37
Figure 23. Topography of the Mare Orientale from observation data from LALT and the stereoscopic Terrain Camera for high resolution lunar maps (Kaguya) 38
Figure 24. China released this Digital Elevation Map from Chang'e data on 9 December 2007 (Chang'e).....39
Figure 25. LOLA Pulse Detection Time-of-Flight Altimeter 5-spot Pattern. Red represents the laser spots on the ground while the grey circles represent the receiver FOV (Keller 6).....40
Figure 26. NASA artist's rendering of Altair lunar lander on the lunar surface (NASA "Altair" Lunar Lander) 41
Figure 27. The top of the figure shows the steps necessary to detect landing hazards and select a safe landing site in topographic data provided by a LIDAR. The bottom left shows how two LIDAR scans are aligned to estimate surface relative velocity. Bottom right shows the result of aligning a small 3D scan taken by a Lidar with a larger topographic map to estimate the position of the lander relative to the desired landing site (ALHAT) 42
Figure 28. Map of Central America including Mocoron, Honduras (Google).....46
Figure 29. Subset30-36_10000pct_surface DEM 1625 meters by 875 meters.....49
Figure 30. Quick Terrain Modeler Height Coloration Palette.....50
Figure 31. Subset30-36_10000pct_surface DEM with Height Coloration 50
Figure 32. Surface DEM using 100% of the subset point cloud 55
Figure 33. Surface DEM using 90% of the subset point cloud 56
Figure 34. Surface DEM using 66% of the subset point cloud 56
Figure 35. Surface DEM using 50% of the subset point cloud 57
Figure 36. Surface DEM using 30% of the subset point cloud 57
Figure 37. Surface DEM using 10% of the subset point cloud 58
Figure 38. Surface DEM using 5% of the subset point cloud 58
Figure 39. Surface DEM using 3% of the subset point cloud 59
Figure 40. Surface DEM using 1% of the subset point cloud 59
Figure 41. Surface DEM using 0.50% of the subset point cloud 60
Figure 42. Surface DEM using 0.30% of the subset point cloud 60
Figure 43. Surface DEM using 0.10% of the subset point cloud 61
Figure 44. Surface DEM using 0.05% of the subset point cloud 61

Figure 45. Surface DEM using 0.03% of the subset point cloud 62
Figure 46. Surface DEM using 0.01% of the subset point cloud 62
Figure 47. Crystal Forest Lidar artifact from TINning of 3% subset point cloud surface with returns misidentified as ground. Arrow indicates one bad point. 63
Figure 48. Correlation Factor for each DEM 65
Figure 49. RMS difference between the base DEM image and the 10% data reduction DEM. Bright areas indicate where the two maps differ most. 66
Figure 50. Percentage of surface points identified through the Bare Earth Extractor compared to the total cloud points in the reduced data set 67

THIS PAGE INTENTIONALLY LEFT BLANK

LIST OF TABLES

Table 1. Lidar Transportation Applications and tools available to support them (Applied Imagery).....14
Table 2. Chronological Order of space missions using Lidar or laser altimetry instruments (After NSSDC).....18
Table 3. Comparison of Lunar Elevations Determined by Eight Independent Experiments (Sjogren 7).....20
Table 4. Subset30-36 Strip Data tabulated mission information (After strip_summary.xls).....48
Table 5. Subset30-36 Original and Reduced Point Cloud Data Points.....51
Table 6. Experimental Point Density.....69

THIS PAGE INTENTIONALLY LEFT BLANK

ACKNOWLEDGMENTS

Special Thanks to:

Dr. R. C. Olsen, Naval Postgraduate School

Dr. Jim Newman, Naval Postgraduate School

Angela Puetz, Naval Postgraduate School

Mike Umanski, Applied Imagery

The Staff at the Trident Room

The Staff at the Britannia Arms “Staff the Brit”

My fellow Rocket Scientists

Yellow Cab

GNO

And most important:

My family without whose support this whole thing would have been untenable.

Thank you! Angi, Charles, Samuel Anderson

THIS PAGE INTENTIONALLY LEFT BLANK

I. INTRODUCTION

A. PURPOSE OF RESEARCH

Forces operating on the ground anywhere in the world depend on accurate knowledge of the terrain in order to plan and conduct their missions. Their ability to either fight on the ground or provide logistic support across the terrain will necessarily be affected by ground cover, slope and either natural or man-made obstacles. Lidar has shown great potential for providing data that can be converted into terrain maps with impressive accuracy. The point cloud returned from airborne Lidar collection contains data that indicates with high precision where objects are in three dimensional space. The term airborne laser scanning (ALS) describes a widely used measurement method for acquiring three-dimensional data on a surface. ALS applications range from the generation of digital terrain models to three-dimensional city models and to vegetation (e.g. forest parameters) or corridor (e.g. power lines) mapping (Ullrich 1).

In regions with extensive multiple canopied jungle, forests or heavy ground cover, Lidar can record multiple returns from energy pulses, gathering data on multi-story ground cover which includes ground returns from foliage penetration (FOPEN) or poke-through. A bare earth digital elevation map (DEM) can be extracted to provide a georeferenced surface map of an area of interest that is covered in dense foliage. The purpose of this thesis is to determine an acceptable density of returns in a Lidar point cloud to generate an accurate DEM of the area obscured under canopy.

B. OBJECTIVE

The primary objective of this thesis is to determine an acceptable spatial density of returns in a Lidar point cloud to create an accurate digital elevation map of some area of interest. DEMs were prepared using data collected by the National Geospatial Intelligence Agency in February 2008 in areas of differing ground cover amounts.

The following chapters will provide a brief background on Lidar, a detailed description of the data and the results of the research.

Chapter II will provide a background introduction to Lidar and the post-processing software available for viewing and analyzing the data. Advantages and disadvantages Lidar offers over other systems for terrain analysis under canopy are discussed along with the collection methods.

Chapter III identifies space mission applications and provides a detailed history of the many missions flown with laser altimetry or Lidar at their heart.

Chapter IV will provide details of the research performed along with detailed descriptions of the applications used for computer analysis.

Chapter V breaks down the details of the problem and describes the project undertaken for delimiting the data collected on the regions and outlines the statistical methodology used to assess research accuracy. Finally, the evaluation techniques used to evaluate the DEMs created with the Lidar data are discussed.

Chapter VI includes the results of the experiment and provides interpretations for each DEM evaluated along with a description of artifacts commonly found in Lidar models. The visual and statistical analyses of the DEMs is included here.

Chapters VII and VIII provide a summary of the research and the conclusions drawn from the research.

II. BACKGROUND

A. LIDAR (LIGHT DETECTION AND RANGING)

Lidar is the commonly used acronym for LIght Detection And Ranging. (Less common is ladar or LAser Detection And Ranging, which I mention since it appears in the literature, but I will not use this term for the physical process described herein.) Similar to radar (RAdio Detection And Ranging) in operation, Lidar actively uses energy in the electromagnetic spectrum to detect objects in three dimensions and obtain a range and bearing from the sensor. However, the frequencies of energy used by Lidar systems usually exist in the infrared with wavelength ranges of 500-1000 nm as radar frequencies are lower and have wavelengths of 1-10 cm. A laser emits discrete pulses of radiation at a particular frequency. By using "narrow pulses of light rather than broad radio waves" a Lidar system can very accurately send out, "time, count and process the returning light." (Optech Inc.) Unlike photogrammetry, Lidar is an active sensor which enables data collection against a target day or night. The electromagnetic energy commonly emitted is invisible to the human eye, but powerful enough to cause eye damage. "You only get to look at the laser twice" as David Kalin said at the FOPEN Workshop.

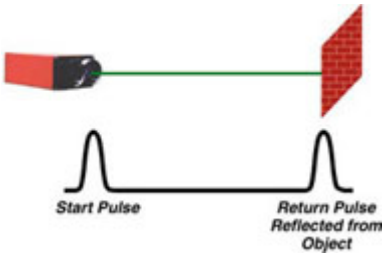

Figure 1. Lidar range calculation (Optech Inc.)

Range to target is determined using the constant speed of light and measured time between the pulse and the return. This path is from the laser to the target and back to the sensor, so the total time of flight is divided in half to obtain the one way travel time (t/2). The distance is found by multiplying this time by the speed of light (c).

$$Range = \frac{ct}{2}$$

With precise knowledge of the laser's position in three dimensional space, range to target and the direction to look for the target gives that specific target's own precise location in three dimensional space. When the Lidar sensor is geodetically referenced, then all the returns are also mapped to a location in space. This is represented in an X, Y, Z format with east, north and height. Height is referenced above ground level (AGL) from reference data.

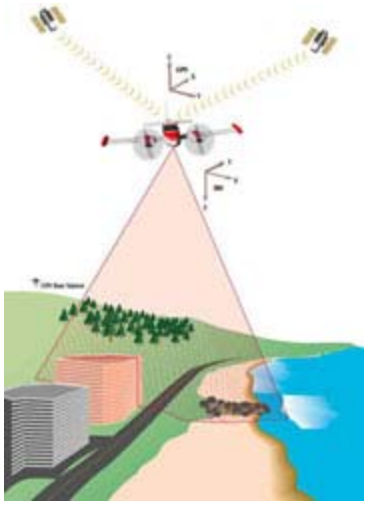

Figure 2. Rangefinder Scanning and Aircraft Orientation (Optech Inc.)

When collected in the field, the sensor is tracked for its exact location to provide a "target horizontal (X-Y) spacing capability to 30 centimeters and a vertical (Z) resolution from 10 – 20 centimeters" (Quick Terrain Modeler Training 2). A Global Positioning System (GPS) receiver in the aircraft records the position at fixed intervals and a second ground-based receiver provides differential correction for a more accurate position estimate. For the airborne sensors, the airplane's motion is also tracked using an inertial reference system (IRS) for post-processing. The laser may also be installed on a stabilized, gimbaled platform to minimize the effect of the airplane motion on the data measurement.

The laser emitter is fixed in position and the beam is scanned across the distant target using a scanning mirror. Each pulse returns range data.

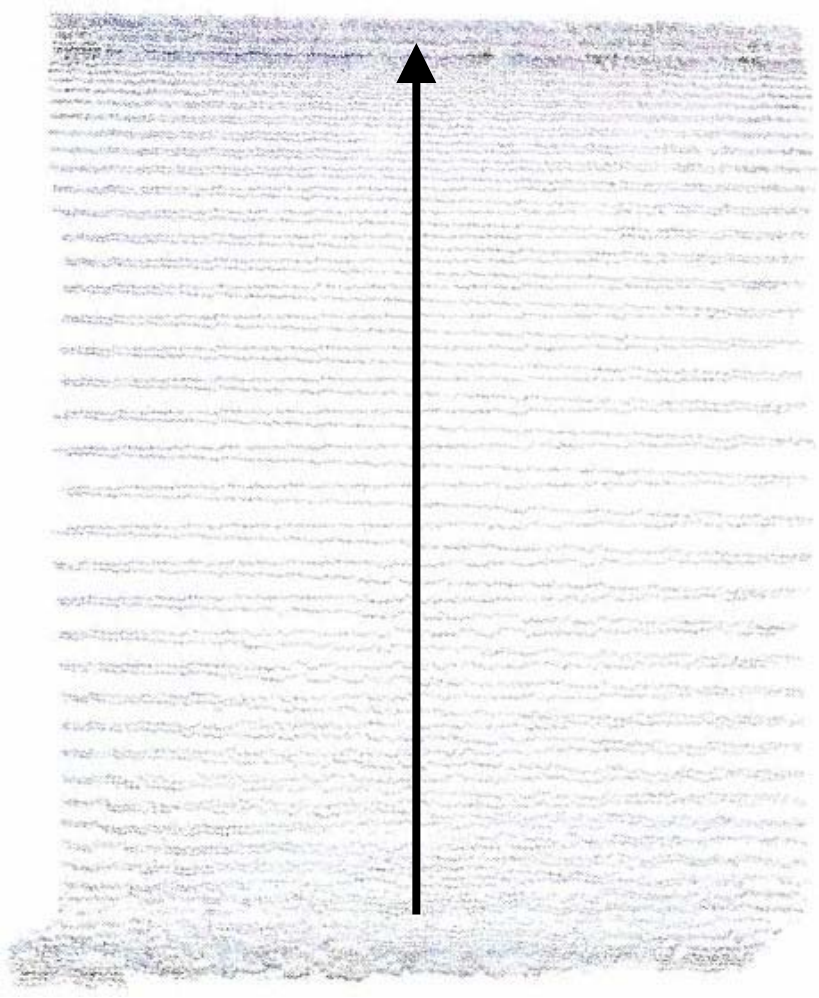

Figure 3. Low density Lidar point cloud that clearly shows the scan lines of the scanning mirror as the airplane moved along the collection line (After NGA data Strip 10)

The pulse repetition frequency (PRF) indicates how many times per second the Lidar emits a pulse. A modern PRF is measured in thousands of pulses per second. Firing the laser at thousands of pulses per second and scanning the beam across the terrain using a scan mirror generates a dense distribution of ranges to the surface. The denser the points, the better the resolution of the point cloud will be when processed in visualization software. Additionally, more pulses per second increase the likelihood of

collecting returns from a “poke through” pulse that has reached the ground under foliage and returned to the sensor which enables a better ground reference for the point cloud.

Further adding benefits to a higher PRF is that the airborne Lidar can be flown at higher altitudes and still obtain the same point cloud density as a lower-flying sensor with a lower PRF. For a fixed mirror scan angle on both systems considered, the ground swath will be wider for the sensor flying at the higher altitude which gives a greater area collected (and mapped) for each pass. This becomes important when collecting against hostile targets in a military or intelligence arena or for efficiency in flying regular mapping and research flights.

Where h is altitude AGL, θ is scan angle and w is scan width, the equation to show swath width from scan angle:

$$w = h \sin \theta$$

For any fixed scan angle, we can see from this formula that there is a direct relationship between the altitude flown to collect the data points and the width of the scan path. Since current Lidar systems are capable of a laser repetition rate of over 100 kHz, including Optech’s newest Lidar the Airborne Laser Terrain Mapping (ALTM) Gemini 167 kHz model (Optech Gemini Product Information 2), it is possible to fly the mission to collect data at the maximum altitude for the range of the system. For the Gemini, this operational ceiling is 4000 meters (13,123 ft) AGL with a programmable scan angle from 0-50 degrees in 1 degree increments.

These new systems also collect up to four range captures per pulse for 1st, 2nd, 3rd and last returns. Each has a horizontal accuracy based again on the altitude flown during the collection and is affected by scan angle, the beam divergence and atmospheric conditions for both its horizontal and elevation accuracy (Optech Inc). As the beam reflects off objects in its path, the Lidar records the range from each of the returns to build its point cloud. As long as the reflecting objects are able to be individually resolved as a pulse in time, the system can record range to separate branches and leaves in the understory, ground cover and the actual ground return.

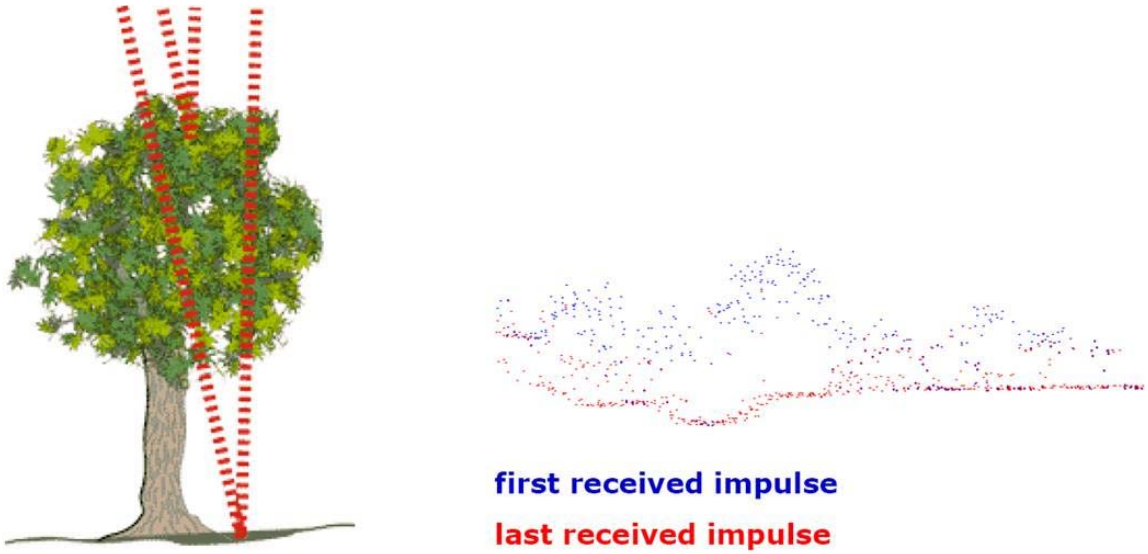

Figure 4. Example point cloud collected from first and last Lidar returns in a forest (Hohl 3)

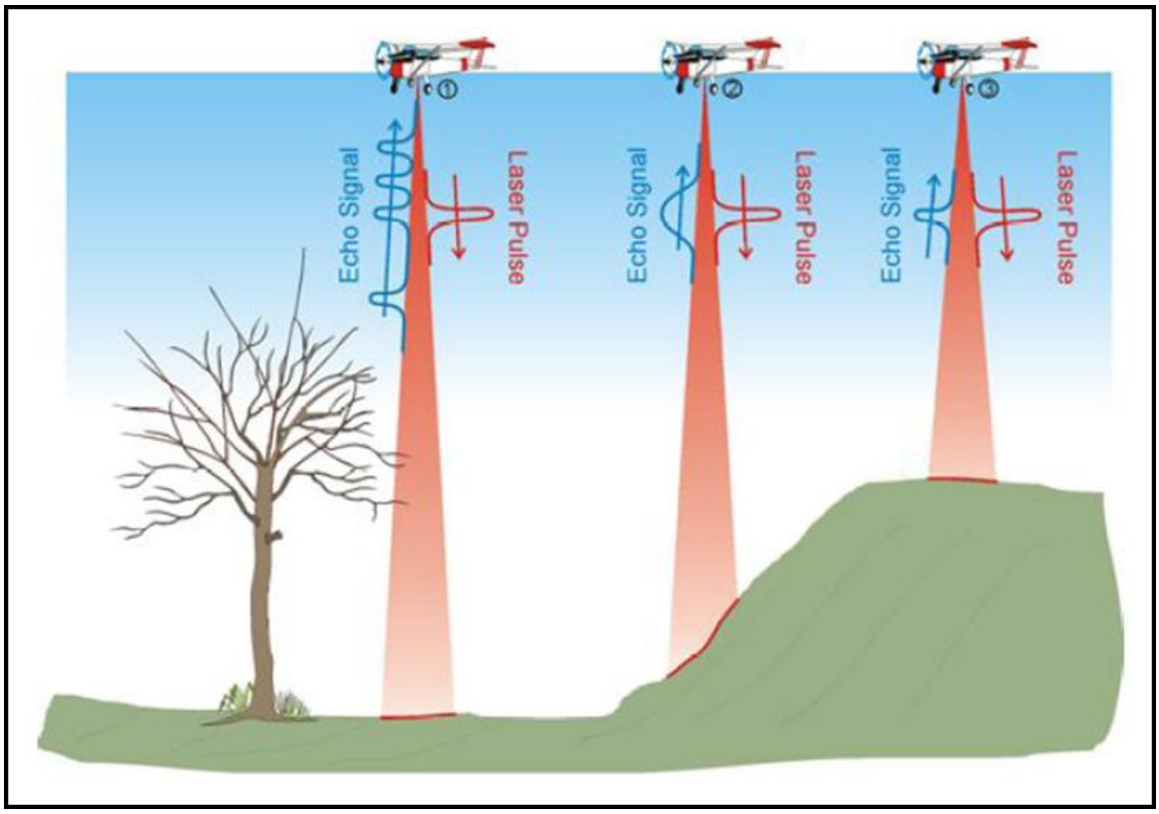

Figure 5. A single pulse can return a single signal with different shapes or multiple returns per pulse from numerous objects in the beams path (Quick Terrain Modeler Training 3)

In post-flight processing, the laser range, scan angle, GPS data and IRS data are combined to accurately determine the position of a point on the earth's surface (Optech Inc.). All this allows collection of a dense set of individual range returns (called a point cloud) from relatively safe operational altitudes. The military and intelligence implications of these technical improvements are significant and give Lidar a potential advantage for these collect missions.

B. FULL WAVEFORM ANALYSIS

Compared to laser radar systems based on the conventional discrete echo approach, direct detection laser radar systems with echo signal digitization and subsequent full-waveform analysis provide valuable additional information on the target's properties. Classification into ground returns and non-ground returns is a required post-collection processing task to generate high-quality digital terrain models. "Due to unknown characteristics of the target (size, reflectance, laser radar cross-section), the intensity values" are of less use to infer physical characteristics of the backscattering target (Ullrich 1-2). Usually, filtering techniques based on geometry and topology relationships within the three dimensional data are employed to separate ground and off-terrain points. For discrete echo detection, the system requires a successful separation of close targets by the minimum range resolution which is based on pulse width, system bandwidths and other system related parameters of signal detection and signal processing.

$$\text{Resolution} = \frac{c\tau}{2}$$

The pulse duration τ measured in seconds, multiplied by the speed of light c gives the pulse length. "Objects separated by a slant range distance equal to or less than $c\tau/2$ will produce reflections that arrive at the antenna as one continuous pulse, dictating that they will be imaged as one large object" (Olsen 182). If the slant-range separation is greater than $c\tau/2$, the pulses will not overlap and their signals will be recorded separately. In radar systems (SAR), range resolution is enhanced through frequency modulation (called chirp). In Lidar, it is done by capturing the leading edge of the nanosecond pulse return. However, full-waveform systems sample for range returns at constant time intervals and the return signal is converted to a digital data stream.

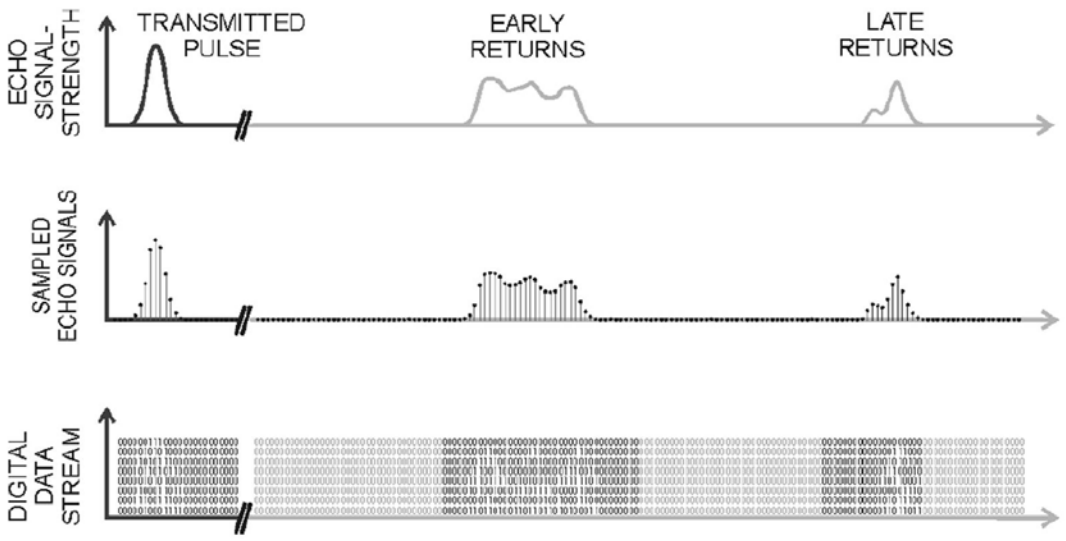

Figure 6. Principle of echo digitization (Ullrich 3)

The time of receipt of the return gives range to target and the characterization of the return waveform width provides information on surface roughness and slope of the target, or depth of a volumetric target. The amplitude of the echo signal provides information on the target's laser radar cross-section or directly on the target's reflectance. Through processing of the full-waveform data within a forested area, small artifacts caused by bushes, brushwood, or piles of twigs can be successfully removed, which would not be possible during processing of only three-dimensional coordinates with standard geometric and topographic filters. Full-waveform laser scanning shows advantages which add possibilities for foliage penetration and increasing terrain model accuracy (Ullrich 3-8).

C. STEP-STARE COLLECTIONS

Foliage penetration with gimbaled Lidar enables higher ground resolution by "integrating multiple looks from several angles" (Roth 1). An Optech system operated by JHU modified with a stabilized, two-axis gimbal allows the Lidar to give the same area multiple "looks" during the line of flight. An area of interest (AOI) is selected which may be off-axis (or roll offset) and off-nadir. The area is scanned as the aircraft moves along. Then the sensor pivots to look again, rotates and looks again. This process is

possible as long as the AOI is within the field of regard of the Lidar. For example, from 6000 ft AGL, a 100m x 100m area can be scanned 22 times (Roth 2).

Figure 7. Innovative Lidar Applications Program Step-Stare mode (a) first step, (b) second step, (c) third step (Roth 2)

Multiple scans can greatly increase point cloud density and number of ground returns on a single pass. These higher point densities generate better elevation maps which provide a tactical improvement for a visual appreciation of the specific area in which the customer wants or needs to see.

D. ADVANTAGES OF LIDAR

Graeme Aggett, of Riverside Technologies, Inc. and Rural Geospatial Innovations lists the following advantages in the presentation to the 2005 GIS Conference:

- Active sensor so survey can be accomplished day or night and includes shadowed areas
- Surveying can be accomplished on steep slopes or in hard to reach locations like mud flats or ocean jetties
- Useful for mapping areas with towers and power lines since power lines are visible in the data
- Accuracy and quick turnaround (days versus weeks or longer)
- Can be integrated with traditional aerial photography
- Able to map bare earth elevations in vegetated areas – only single pulse needs to reach ground (photogrammetry requires 2 look angles)
- Post spacing much denser than traditional methods

- Dense elevation data obtained at far less cost than traditional methods, especially when automated post-processing is used to generate bare earth information (50-51)

E. DISADVANTAGES OF LIDAR

Following up the advantages, Aggett lists these disadvantages to the Lidar technologies:

- Surveying is not advisable in hazy or low cloud cover conditions
- Surveying is not possible in rainy or misty conditions
- Not able to accurately delineate stream channels, shorelines, ridge lines often visible on photographic images (ill-suited for breaklines which need to be generated independently or from intensity image)
- Generated contours not hydrologically corrected (to enforce flow-direction)
- Generated contours not aesthetically appealing
- Lidar returns on water are unreliable
- Lidar is still a quite new technology – standard procedures comparable with those in photogrammetric applications have yet to become commonplace, though industry is active in defining these with user input (52-53)

F. DIGITAL ELEVATION MAPS

Digital Elevation Maps have been developed using different means to obtain the data that goes into these maps.

1. Manual Surveys

Land surveyors take numerous survey points and build elevation contour maps in a time consuming, expensive and difficult, though time-tested, process. Although this method of leveling produces high quality results in elevation maps, it is not nearly as practical as airborne Lidar for large scale mapping applications.

2. Photogrammetry

Overhead stereoscopic imagery has been used to build elevation maps using optical and electro-optical parallax methods to analyze the elevation contours. Photogrammetrists and cartographers measure, map and chart the Earth's surface. They collect, analyze and interpret both spatial data such as latitude, longitude, elevation and distance to produce maps. The process of using images taken on orbit to make high scale topographic maps is complex. "For creation, Digital elevation Model (DEM) and correction of space images need Ground Control Points (GCP) that should be measured," orthorectified and georeferenced (Dini 1651).

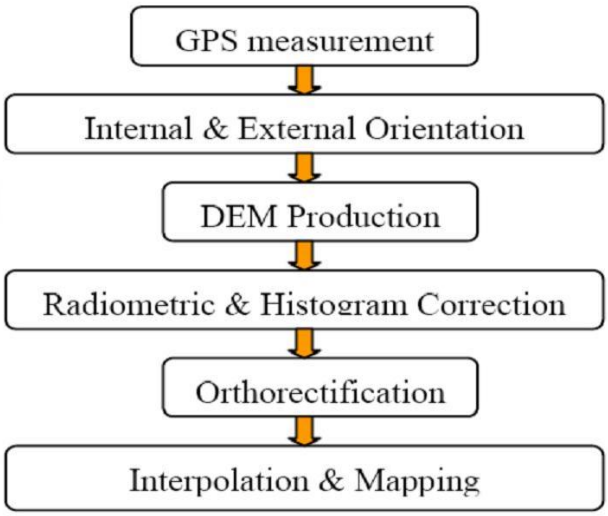

Figure 8. Flow chart of high scale map production from space images (Dini 1652)

3. Radar Imagery

Imaging radar is another method to produce elevation maps. The GeoSAR mapping system developed by the NASA Jet Propulsion Laboratory employs Interferometric Synthetic Aperture Radar in the X and P bands with wavelengths of 3 cm and 85 cm respectively. IFSAR has an advantage over Lidar because it can obtain images through cloud cover to produce orthorectified radar reflectance maps with 1.5 meter resolution and DEMs to 5 meter resolution with similarly rapid, large scale mapping flights. The radar energy will propagate until it reflects from any object with a

radar cross-section near its wavelength. The 3 cm X-band energy will scatter off leaves, but the longer 85 cm P-band gives better foliage penetration as well as very bright returns from power lines or other long wire objects. Because of the ability of radar energy to penetrate the surface layers of the earth before reflecting, comparisons between Lidar and IFSAR raise issues about what, precisely, constitutes the surface of the earth. Currently, this IFSAR project processes a 3 meter resolution DEM using the X-band data (Shaffer 4-18). Although this airborne IFSAR approach is promising, Lidar data has better FOPEN characteristics and because of that, produces a better bare earth extraction surface digital elevation model for areas under canopy.

G. MILITARY APPLICATIONS OF LIDAR

The United States military has already found numerous uses for Lidar among its many missions. The National Geospatial-Intelligence Agency (NGA) is a Department of Defense combat support agency and a member of the national Intelligence Community (IC). NGA develops imagery and map-based intelligence solutions for U.S. national defense, homeland security and safety of navigation. Many of the leading researchers in the field work for or with the NGA to develop the necessary tools and products needed by the operational forces of the Department of Defense.

Lidar transportation support tools are employed to determine the slope and contour of avenues of approach and mobility corridors. Quick Terrain Modeler has specific tools contained within the software to enable transportation planning. See the following table for details.

Transportation LiDAR Application	Relevant Quick Terrain Modeler Tools
Basic roadway inventory, maintenance and planning.	Quickly build huge models (up to 77 mi^2) without decimation or tiling, navigate through models in real time. Overlay GIS transportation layers (shape files) on 3D models.
Transportation corridor mapping.	Build contour maps, evaluate impact of high water conditions, measure distances. Use change detection tool to compare sequential surveys of the same area
Landslide and hazard assessment. Cross slope analysis for surface runoff and drainage.	Slope analysis tool and cross section tools quickly find and analyze steep terrain.
Grade and side slope analysis for traffic flow, safety and pollution applications.	Slope analysis and cross section tools can highlight steep grades as well as side slopes.
Evaluation of driver sight distances for safety analysis.	Use line of sight analysis in combination with mensuration tools to determine driver sight distances and stopping sight distances.
Visualization for planning and public debate.	Overlay aerial imagery on 3-D DEM, create AVI fly-through's for wide distribution and playback on standard Windows media players.
Cut and fill volume estimation.	Use the volume calculation tool to estimate volumes volume changes in sequential surveys.

Table 1. Lidar Transportation Applications and tools available to support them (Applied Imagery)

The Line of Sight (LOS) tools available also are used to determine when and where objects are visible along a route of travel from any points on or above a digital surface model. This aids the development of targeting and fires vulnerability. Lidar data can be used to detect buildings and camps in heavy foliage and under canopy. Flood modeling tools within Lidar visualization software packages can clip out points that will be under water as streams, lakes rise. For planning prior to military actions, this can aid personnel in route planning in the event of major storms or intentional destruction of levees and dams during combat operations.

Figure 9. Flood simulation tool can be used to model impact of rising water on transportation infrastructure (Applied Imagery)

With visualization tools and access to an unmanned aerial system constantly sending Lidar data of its flight path, troops in the future will be better able to appreciate the terrain ahead with near real-time updates as opposed to relying on maps and imagery which may be up to decades out of date due to new streaming tools developed to allow fast visualization of Lidar data by quickly generating previews for rapid inspection, verification and presentation within a geospatial context (Isenburg).

In addition to airborne Lidar scanning, terrestrial-based scanning can aid military forces in urban terrain. Ground-based Lidar sensors can be free-standing or mounted on vehicles to take data and generate the point cloud of returns in urban valleys to create accurate images of buildings and generate three dimensional maps for Line of Sight analysis. These tools give ground forces abilities to predict and counter enemy snipers during military operations in urban terrain. By merging complementary airborne and terrestrial Lidar data collections, the benefits from the individual advantages of both produce “higher reliability and accuracy” (IKG Research) in the fused image.

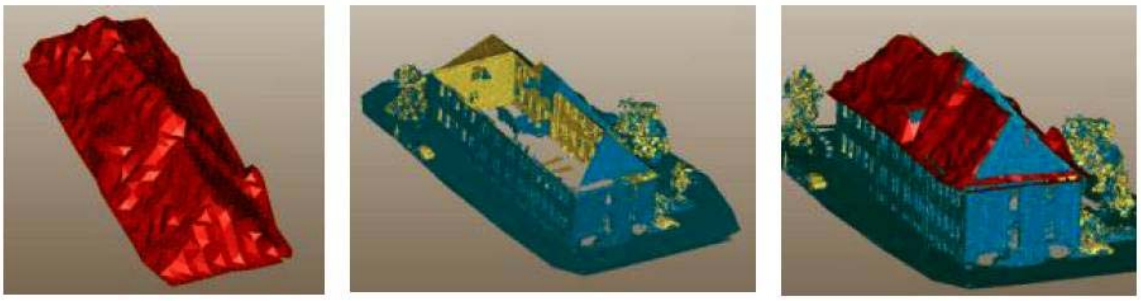

Figure 10. Roof faces from an aerial scan, building from a terrestrial scan and combination of both data sets (IKG Research)

III. SPACE MISSIONS INCORPORATING LIDAR OR LASER ALTIMETRY

The invention of the laser, which is actually an acronym from light amplification by stimulated emission of radiation, can be dated to 1958 with the publication of the scientific paper, “Infrared and Optical Masers”, by Arthur L. Schawlow, then a Bell Labs researcher, and Charles H. Townes, a consultant to Bell Labs, using microwave wavelengths. The maser was used to amplify radio signals and as an ultrasensitive detector for space research. This technology took off quickly and earned these two physicists a Nobel Prize for their research. In 1960, while working at Hughes Aircraft Laboratories, Thomas Maiman invented the first ruby laser which worked using optical wavelengths. John Degnan writes in his history of Satellite Laser Ranging (SLR), “Laser ranging to an artificial satellite equipped with retroreflectors was first successfully demonstrated by a team of engineers and scientists from the NASA Goddard Space Flight Center in 1964” (1). Flying with an inclination of 79.7 degrees, Explorer 22/Beacon Explorer-B presented nearly 5 million square meters of optical radar cross-section to the northern hemisphere to return laser echoes to scientists at NASA’s GSFC. These ranging returns were accurate to 2-3 meters and represented a major leap in orbit determination over the 50 meter accuracy of the microwave radars from that period (Degnan 1). Six SLR retroreflector equipped satellites were flying in 1967 in support of an international effort for the National Geodetic Satellite Program which resulted in laser site position errors which were a factor of four better than other optical measurements (Degnan 3).

Apollo 11, the first manned mission to land on the moon, carried the first laser retroreflector array there in July 1969. The Lunar Ranging Experiment (LURE) at the McDonald Observatory at the University of Texas soon recorded laser returns from this site and other reflectors were added in the following years by Apollo 14, Apollo 15, as well as two unmanned Russian missions (Lunakhod I and II). Shortly thereafter, the SLR community specified one centimeter accuracy for laser ranging. “The precision of the SLR technique has improved by an order of magnitude in each of its [first] three decades of existence” (Degnan 9).

Experiment Name	Mission	Spacecraft Name	Launched
Satellite Laser Ranging	Earth	Explorer-22/Beacon Explorer-B	19641010
Lunar Ranging Experiment (LURE)	Moon	Apollo 11, 14, 15, Lunakhod I, II	19690716
Laser Altimeter	Moon	Apollo 15 Command and Service Module	19710726
Laser Altimeter	Moon	Apollo 16 Command and Service Module	19720416
Laser Altimeter	Moon	Apollo 17 Command and Service Module	19721207
Mars Observer Laser Altimeter (MOLA)	Mars	Mars Observer	19920925
Clementine LIDAR	Moon	Clementine	19940125
Lidar In-Space Technology Experiment	Earth	STS/LITE	19940201
Shuttle Laser Altimeter-01	Earth	Space Shuttle Endeavour	19960111
Mars Orbiter Laser Altimeter (MOLA)	Mars	Mars Global Surveyor	19961107
Shuttle Laser Altimeter-02	Earth	Space Shuttle Discovery	19970807
Light Detection and Ranging (LIDAR)	Mars	Mars Polar Lander	19990103
Geoscience Laser Altimeter System (GLAS)	Earth	ICESat/EOS-ALT1	20030113
Light Detection and Ranging Instrument (LIDAR)	Asteroid Itokawa	Hayabusa (Muses-C)	20030509
Mercury Laser Altimeter (MLA)	Mercury	MESSENGER	20040803
Cloud Aerosol Lidar with Orthogonal Polarization	Earth	CALIPSO	20060428
MET Lidar	Mars	Phoenix	20070804
Laser Altimeter (LALT)	Moon	Kaguya	20070914
Laser Altimeter	Moon	Chang'e 1	20071024
Lunar Orbiter Laser Altimeter (LOLA)	Moon	Lunar Reconnaissance Orbiter (LRO)	Future

Table 2. Chronological Order of space missions using Lidar or laser altimetry instruments (After NSSDC)

A. LASER ALTIMETRY AND THE APOLLO MISSIONS

Three of the Apollo Missions (15, 16, 17) used a laser altimeter experiment to obtain data on the altitude of the Command Service Module (CSM) above the lunar surface. These data, acquired with a 1-m resolution, "were used to support mapping and panoramic camera photography, to provide altitude data for other orbital experiments, and to relate lunar topographical features for a better definition of lunar shape" (Laser Altimeter). The laser altimeter was hard-mounted and aligned with the mapping camera subsystem mounted on the top shelf in the CSM scientific experiment module (SIM) and automatically emitted a laser pulse to correspond to a mid-frame ranging for each frame of film exposed by the metric camera. On the Apollo 15 CSM, the altimeter operated normally until revolution 24, at which time it started to fail, became progressively worse and failed completely by revolution 38. Data was sampled every 20 seconds which provided an observation every 30 km or 1 degree along the orbit track (Sjogren 2). The Apollo 16 laser altimeter recorded 2395 measurements which gradually deteriorated down to 50% reliability by rev 60, and then on the last photographic pass, "decreased abruptly to 5% on rev 63. The measurements were sufficient to provide the necessary cartographic control" (Laser Altimeter). In his final report on the Apollo laser altimeter experiment, William Sjogren found that the agreement of the laser data with previous independent spacecraft topography was excellent and with the Apollo 16 orbital inclination difference of 38 degrees the lunar global shape parameters yielded a "best fitting ellipsoid [that] was nearly a sphere with radius 1737.7 km. The old astronomers did a fairly good job, for their value was 1738.0 ± 1 km" (4).

GROUP	EXPERIMENT	ELEVATION (KM)	LOCATION		UNCERTAINTY 1-σ (KM)	REMARKS	REFERENCE
			LAT, DEG	LONG, DEG			
1 MARE COGNITUM	RANGER VII	1735.5	-10.6	-20.6	0.3	IMPACT TIME	1
	LASER ALTIMETER	1735.4	- 9.0	-20.6	0.4	APOLLO 16	2
2 MARE TRANQUILLITATIS	RANGER VI	1735.3	9.3	21.5	0.3	IMPACT TIME	1
	RANGER VIII	1735.2	2.7	24.7	0.3	IMPACT TIME	1
	LUNAR ORBITER V/H	1735.4	1.0	23.2	0.7	SET III	3
	PHOTOGRAMMETRY	1735.4	1.7	24.0	0.2	LUNAR ORBITER SITE II P636	4
	RETROREFLECTOR	1735.6	0.7	23.5	0.05	APOLLO 11	5
	LANDMARK TRACKING	1735.3	1.3	23.7	0.4	APOLLO 11	6
3 OCEANUS PROCELLARUM	SURVEYOR I	1735.5	-2.5	-43.3	1.3	LANDER TRACKING	7
	LUNAR ORBITER V/H	1735.6	-2.1	-43.8	0.7	SET IXa	3
	PHOTOGRAMMETRY	1735.7	-2.1	-43.8	0.2	LUNAR ORBITER SITE P-9.2AB	4
	LASER ALTIMETRY	1735.3	-5.2	-43.3	0.4	APOLLO 16	2
4 MARE SERENITATIS	PHOTOGRAMMETRY	1734.6	21.3	27.6	0.2	LUNAR ORBITER SITE V-24	4
	SOUNDER	1734.2	20.0	27.6	0.4	APOLLO 17	8
	LASER ALTIMETRY	1734.2	23.9	27.0	0.4	APOLLO 15	2
5 PALUS PUTREDINIS	LANDMARK TRACKING	1735.6	3.7	26.1	0.4	APOLLO 15	6
	RETROREFLECTOR	1735.6	3.6	26.1	0.05	APOLLO 15	5
	LASER ALTIMETRY	1735.7	3.4	26.0	0.4	APOLLO 15	2

Table 3. Comparison of Lunar Elevations Determined by Eight Independent Experiments (Sjogren 7)

B. WIDE-SWATH IMAGING LIDAR FOR SPACEBORNE APPLICATIONS

1. NASA Airborne Oceanographic Lidar

Laser altimetry is being accepted by the global Earth science community as a source for accurate topographic data and the advantages of this technology can be applied to large area mapping. The NASA Airborne Oceanographic Lidar (AOL) was used since the 1970s and had been conceived for marine applications of laser hydrography. Dr. Krabill and his team from Goddard Space Flight Center ran a "spin-off" experiment in 1979-1980 to test the AOL system "aimed at evaluating the potential of an airborne laser ranging system to provide cross-sectional topographic data on flood plains that are difficult and expensive to survey using conventional techniques" as a more cost effective means of providing needed data products (Krabill 685). To measure water depth for hydrography, the AOL system recorded two returns from the surface of the water and from the bottom, similar to a forest canopy "surface" and ground "bottom" returns. In his

1984 paper, Krabill concluded that the results of the test over the Wolf River Basin "were sufficient to show the feasibility of performing airborne laser surveys" but would "require further investigation and analysis" (694).

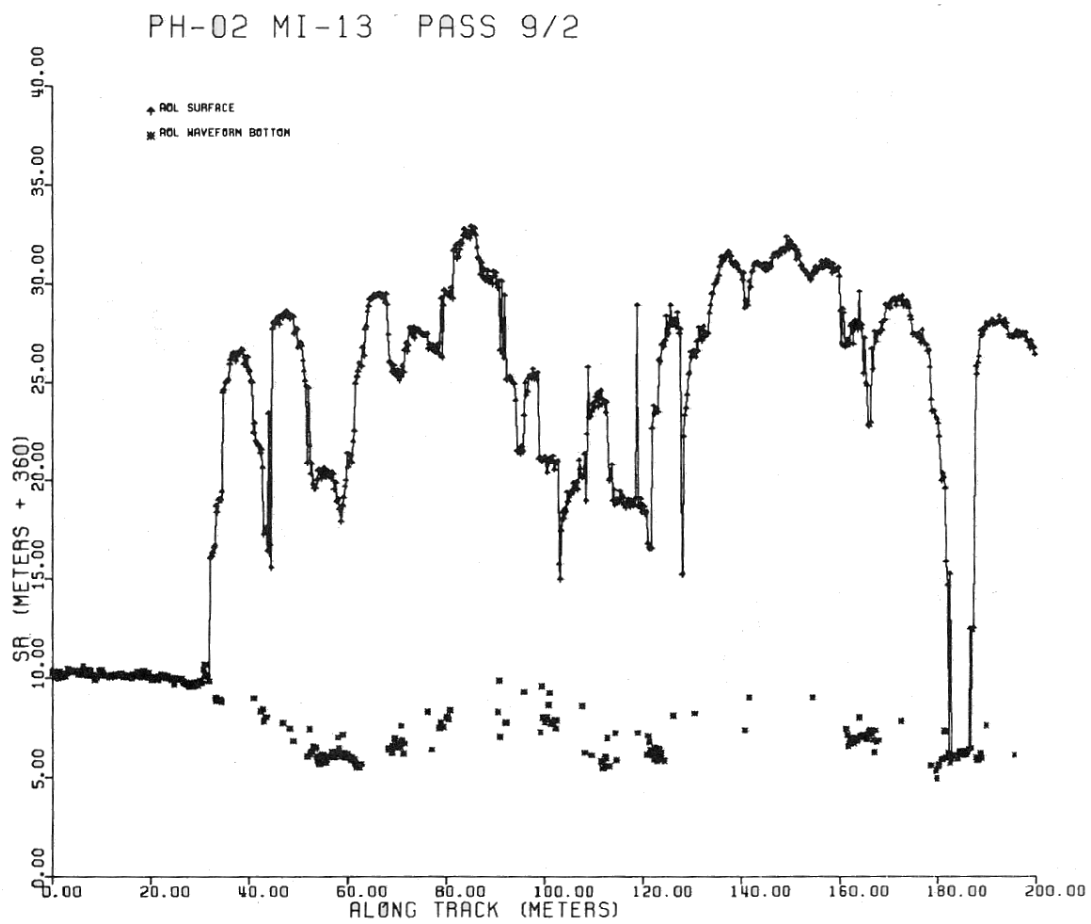

Figure 11. Cross-sectional profile of Pass 912 obtained at night under summer foliage conditions during September 1980. Top curve is "AOL Surface", lower symbols are "AOL Waveform Bottom" (Krabill 692)

Much work has been done in the intervening years to improve accuracy and develop Lidar technology. Since current airborne laser systems provide data at several meter resolution and across swaths up to 1-2 km in width, there are commercial economic factors to widen swaths further. However, as off-nadir incident angles increase, there is degradation in accuracy that significantly diminishes the ability to penetrate dense vegetation canopies. This effectively limits swath width. Higher operational altitudes directly increase swath width for a selected angular range according the equation

discussed above. However, higher altitude operations require significantly more laser output power, smaller divergence angles and higher beam quality to achieve smaller footprints. The scientists at NASA Goddard Space Flight Center have developed prototype spaceborne instrumentation and science applications of wide-swath Lidar in aircraft. Bryan Blair writes that a spaceborne implementation of wide-swath imaging Lidar technology will enable:

- Landscape scale (10 km swath) imaging
- Full Earth imaging at <10m pixels within 1 year
- Near-100% coverage/illumination
- Topography measurements at decimeter-level absolute vertical accuracy
- Vegetation canopy height and structure measurements
- Change detection measurements at sub-centimeter relative vertical accuracy
- Subtle topographic change beneath vegetation
- Vegetation and land cover changes (2)

"The wide-swath spaceborne imaging Lidar can provide data at the DTED3 level (10m posting) with accuracies exceeding DTED5 levels (5m absolute) by an order of magnitude" (Blair 2). This led to the development of several satellite laser altimeters such as the Shuttle Laser Altimeter (SLA) and Vegetation Canopy Lidar (VCL) (Blair 1).

2. Vegetation Canopy Lidar

The NASA/University of Maryland Vegetation Canopy Lidar (VCL) mission was designed to create the first maps of the three-dimensional structure of vegetation in the world's forests. Originally scheduled for launch in September 2000, the mission was selected as part of NASA's Earth System Science Pathfinder project but is no longer being actively developed (Earth Observatory; VCL).

The VCL was designed with a Multi-Beam Laser Altimeter (MBLA) which is comprised of five laser transmitters in a single altimeter instrument. By reconstructing the reflected light from its five laser emitters, the satellite would have produced an accurate map of both the heights of the trees as well as the topography of the underlying

terrain to an accuracy of one meter for biomass calculations (VCL). Each laser would send 242 pulses per second at the Earth's surface. Each beam covers an area 75 feet across. "Each laser beam operates at the 1064 nm fundamental wavelength of the neodymium-doped yttrium aluminum garnet (Nd:YAG) solid-state laser, are arranged in a pentagon inside a 20 mrad telescope circular field-of-view that is centered on nadir" (Dubayah 5). By spacing the five beams a little over a mile apart, each VCL orbit was planned to sample an area 5 miles across. VCL was to be "the first multi-beam, waveform-recording Lidar to fly in space" (Earth Observatory).

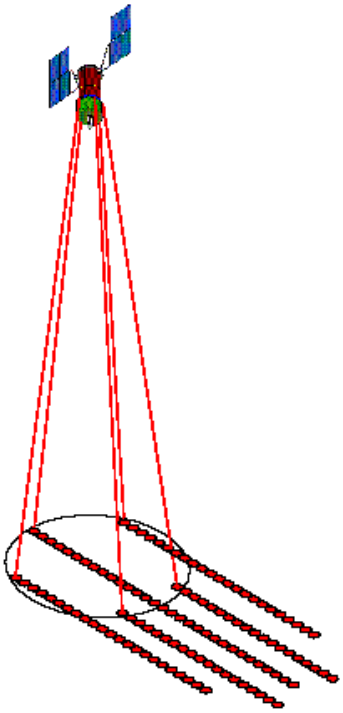

Figure 12. VCL's MBLA design had five lasers arranged in a pentagon for a circular field-of-view that is centered on nadir (Dubayah 5)

C. MARS

1. MOLA

NASA has designed and launched two spacecraft destined for Mars incorporating a laser altimeter. The Mars Observer and the Mars Orbiter (Global Surveyor) both contained an instrument for laser altimetry named MOLA. The Mars Observer was

launched from Cape Canaveral in September of 1992 and contact with the spacecraft was lost and never reestablished just three days prior to its Mars orbit insertion on 21 August 1993 after the cruise mode between planets (Mars Observer). No data were collected by this instrument.

The Mars Orbiter Laser Altimeter on the Mars Global Surveyor was designed to map the Martian global topography and can also be used to measure the height of water and carbon dioxide clouds. The Mars Global Surveyor (MGS) was developed by NASA and the Jet Propulsion Laboratory to collect data on the surface morphology, topography, composition, gravity, atmospheric dynamics and magnetic field to investigate the surface processes, geology, distribution of material, internal properties, evolution of the magnetic field and the weather and climate of Mars. The spacecraft was launched in November 1996 and marked the United States return to Mars after a 20-year absence. After arriving to orbit Mars and planned aerobraking ended in February 1999, MGS was in a 118 minute circular polar science mapping orbit with an index altitude of 378 km. The orbit is sun-synchronous (2 a.m./2 p.m.) and maps over the 2 p.m. crossing from south to north (Mars Global Surveyor). Mars was mapped in 26 day cycles and the primary mission lasted one Martian year (687 Earth days) through January 2001. Mission extensions were added until contact with the spacecraft was lost on 2 November 2006. According to the official MGS mission, the data collected is used for the following scientific objectives:

1. To study the surface processes on Mars, including the formation and evolution of volcanoes, basins, channels and the polar ice caps combined with gravity and other data.
2. To study the structure and evolution of the interior of Mars, including the lithospheric thickness and strength, internal convection, composition, thermal history and release of water and carbon dioxide to the surface.
3. To calculate the volume and seasonal changes in the polar ice deposits.
4. To measure the altitude and distribution of water and carbon dioxide clouds, for the purpose of constraining the volatile budget in the Martian atmosphere.

The MOLA instrument's laser transmitter is a diode pumped, Q-switched Nd:YAG laser with a pulse energy of 40-45 mJ and a PRF of 10 pulses/sec, each pulse having a beam diameter of 1 cm and a divergence of 0.45 mrad. The vertical resolution

is 2 m local (relative) and 30 m global (absolute). The horizontal resolution is 160 m. Using MOLA data through June of 2000, the MOLA Science Team produced very high resolution topographic shade maps of Mars. Polar views are in a polar stereographic projection and have a resolution of 300 or 600 m. The MOLA instrument resolves slopes on Mars to no worse than 1 part in 1000 on any length scale greater than about 330 meters and so digital images made from the elevations are able to resolve subtle slopes that are not visible in camera images. The rich detail in the northern hemisphere lowlands, which appear mostly featureless in previous global-scale image mosaics of Mars is clearly observable with the processed altimetry data (MOLA).

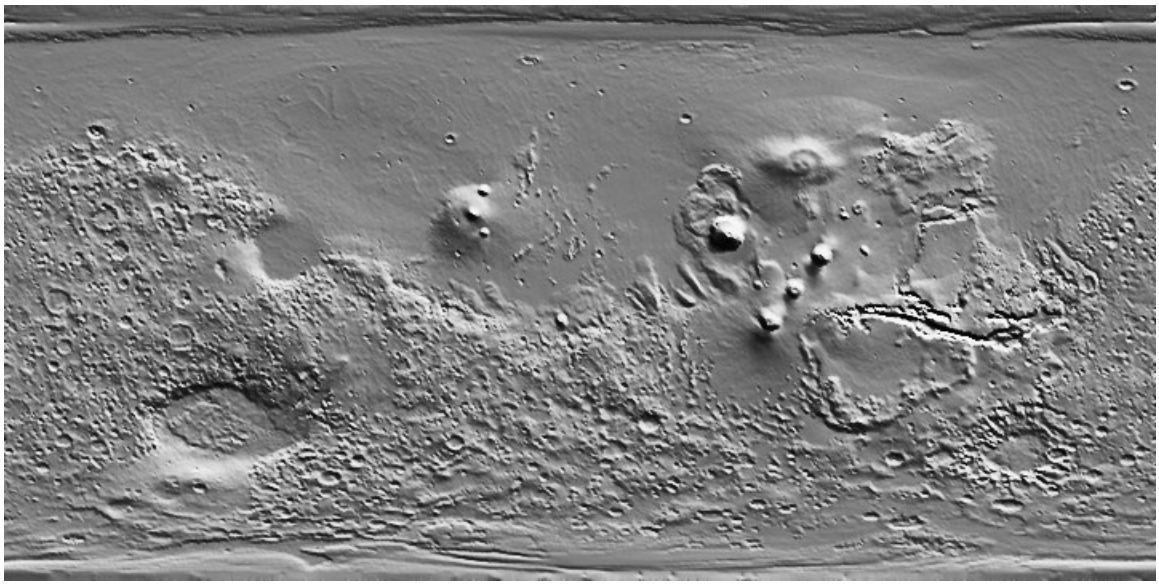

Figure 13. Using MOLA data through June of 2000, the MOLA Science Team has produced very high resolution topographic shade maps of Mars. This figure is from 0 to 360 degrees E (MOLA)

2. Mars Polar Lander

NASA launched the Mars Polar Lander on 3 January 1999 with a mission to "study the Martian weather, climate and water and carbon dioxide budget, in order to understand the reservoirs, behavior and atmospheric role of volatiles" (Mars Polar Lander). The instrument package included a Lidar built by the Russian Space Agency to characterize ice, aerosol and dust hazes in the atmosphere to a level of 2 to 3 kilometers.

The 400 nJ Gallium-Aluminum-Arsenic diode was designed to emit 100 nanosecond pulses at wavelengths of 0.88 micrometer with a pulse repetition frequency of 2.5 kHz up into the atmosphere. The last telemetry from Mars Polar Lander was sent just prior to atmospheric entry on 3 December 1999. No further signals have been received from the lander; the cause of this loss of communication is not known.

D. EARTH

1. Shuttle Laser Altimeter Missions

Following the successful Lidar In-Space Technology Experiment (LITE), developed by NASA/Langley Research Center, which was flown on the Space Shuttle in 1994 (STS/LITE), the Shuttle Laser Altimeter (SLA) experiments were flown in 1996 and 1997. These missions collected accurate laser ranging data from an orbital platform. "Profiling laser altimeter observations from orbital platforms provide the opportunity to obtain elevation data of very high vertical accuracy in a consistent, Earth-centered reference frame" (Harding, et al. 1). The SLA, developed at NASA's Goddard Space Flight Center, was designed as a pathfinder experiment to evaluate engineering and algorithm techniques for obtaining high-resolution, orbital laser altimeter observations of terrestrial surfaces. SLA-01 data was used to evaluate the vertical accuracy of GTOPO30, a global digital elevation model with a grid spacing of approximately 1 km. GTOPO30 is a compilation of eight sources of elevation information, including raster and vector data sets. SLA-01 employed a 1064 nm wavelength and collected approximately 475,000 geolocated returns from 3 million transmitted pulses. SLA-02 also used a 1064 nm laser and collected approximately 342,000 and 562,000 geolocated returns from land and ocean surfaces, respectively (LAPF). These two flights characterized returns in 100 meter diameter laser footprints spaced every 700 meters along a nadir profile and the resulting digital elevation maps along the ground track were compared to the existing surveys. Pointing angles were computed from the Earth Center Fixed coordinates of the unit laser pointing vector at the Shuttle's position after pointing corrections were applied

and the location of the bounce point on the surface of the Earth. A coordinate transformation to Topocentric coordinates is made to calculate the vector's orientation at the bounce-point location.

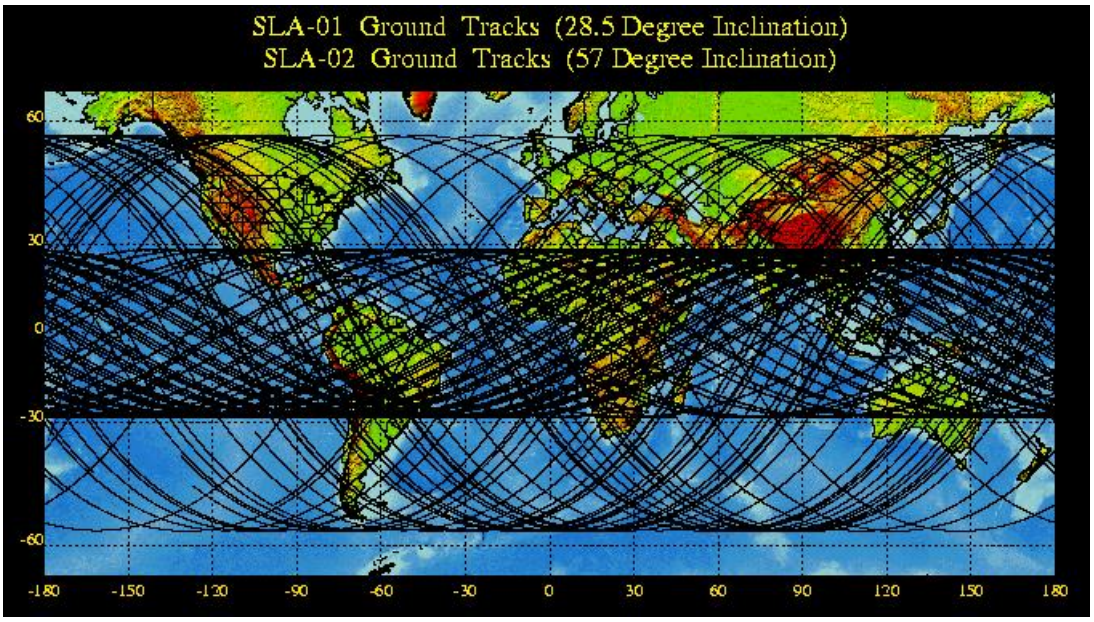

Figure 14. Ground Tracks plotted for Shuttle Laser Altimeter (SLA) mission SLA-01 and SLA-02 (LAPF)

Random SLA error arose due to the spatially heterogeneous nature of vegetation and urban cover where the first-return SLA measured building tops or overhead canopy rather than bare earth. However, "[t]he consistent reference frame, high absolute accuracy and ability to range to all types of land surfaces, regardless of cover or relief conditions, make orbital laser altimeter observations well suited for characterization of systematic biases in global DEM's" (Harding, et al. 4).

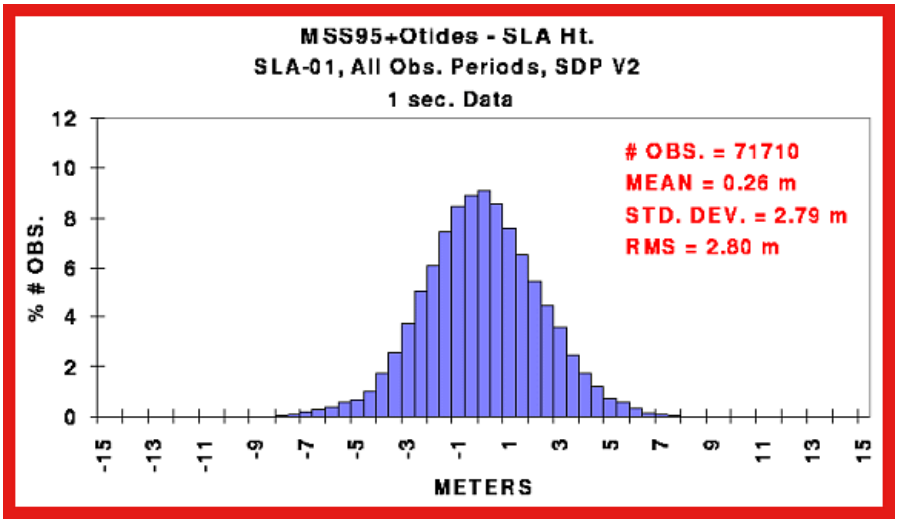

Figure 15. Histogram of all sea surface height measurements from SLA-01 (LAPF)

2. Geoscience Laser Altimeter System

NASA's Earth Observing System (EOS) involves a series of satellites first launched in 1998 and thereafter, providing coverage of the Earth to study polar ice over a period of fifteen to twenty years. The EOS-ALT was designed to fly the Geoscience Laser Altimeter System (GLAS) instrument.

Launched in early 2003 as part of NASA's Earth Observing System, EOS-ALT 1, also known as the Ice, Cloud and land Elevation Satellite (ICESat), uses its single scientific instrument to determine the mass balance of the polar ice sheets to predict future changes in ice volume and sea-level changes. The GLAS maps topography and vegetation heights of land surfaces, measures snow-cover and sea-ice surface characteristics and measures cloud heights and the vertical structure of atmospheric aerosols (ICESat). The Lidar flying on ICESat uses a nadir pointing Nd:YAG laser in two wavelengths of 1064 and 532 nm transmitted in 4 ns pulses at a PRF of 40 pulses per second. "The green laser (532 nm) reflects from the atmosphere and the IR laser reflects from the ice" (GLAS).

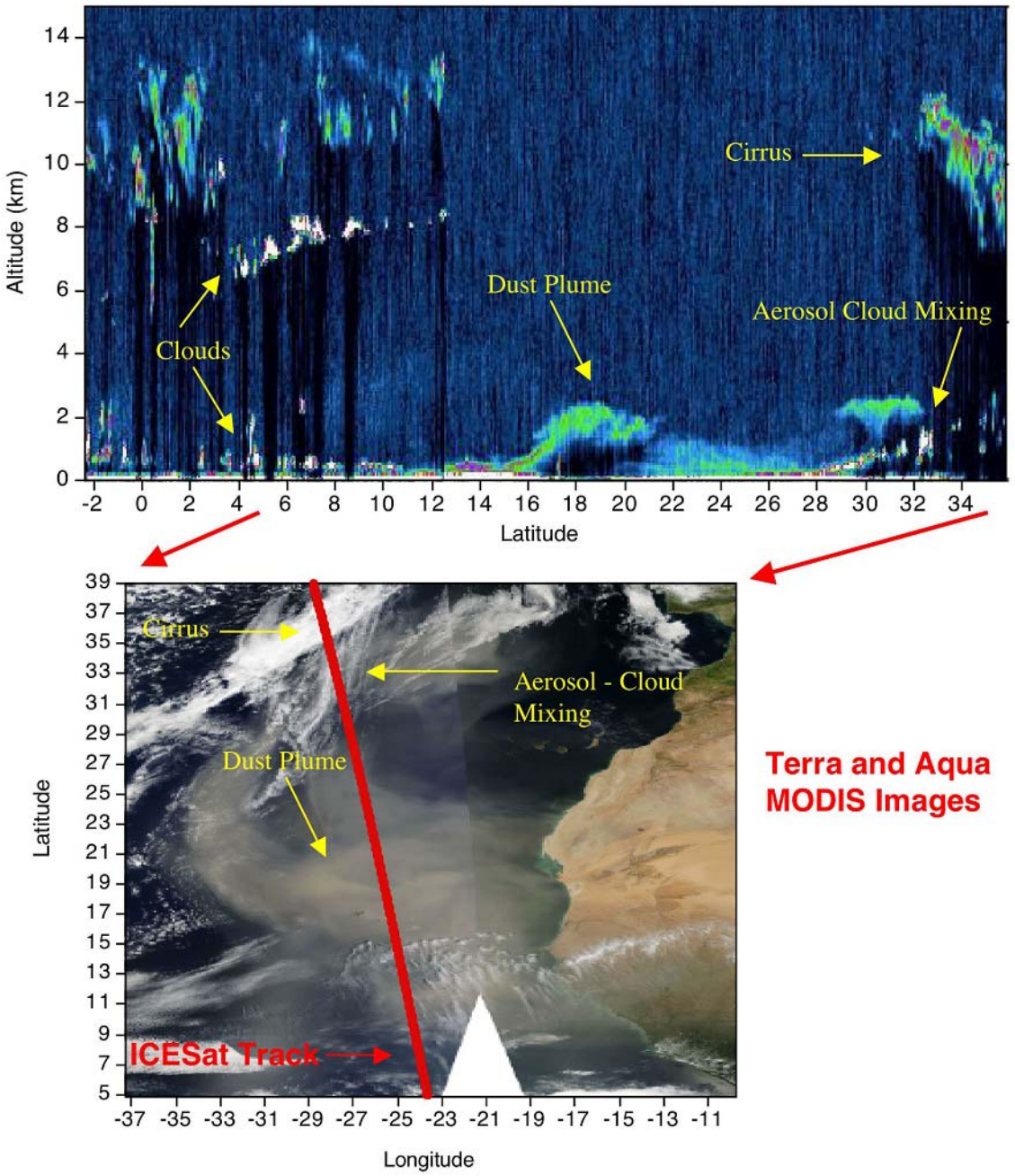

Figure 16. (Bottom) Photo of the ICESat ground track where the Lidar data (top) was collected off the coast of Saharan Africa (WFF GLAS)

E. AEROSOLS AND CLOUDS

1. CALIPSO

The Cloud-Aerosol Lidar and Infrared Pathfinder Satellite Observation was launched from Vandenberg AFB on 28 April 2006 as an American-French (NASA-CNES) meteorological satellite. CALIPSO carries three instruments including the Cloud Aerosol Lidar with Orthogonal Polarization. This Lidar carries an Nd:YAG, diode-pumped, Q-switched, frequency doubled (two-wavelength 1064 nm and 532 nm) pulsed transmitter and receivers fed by a one-meter diameter telescope. The 1064 nm channel monitors the reflected intensity and two other channels monitor the two orthogonal polarizations. It enables derivation of the vertical distribution of aerosols and water vapor at a resolution of 40 meters (CALIOP).

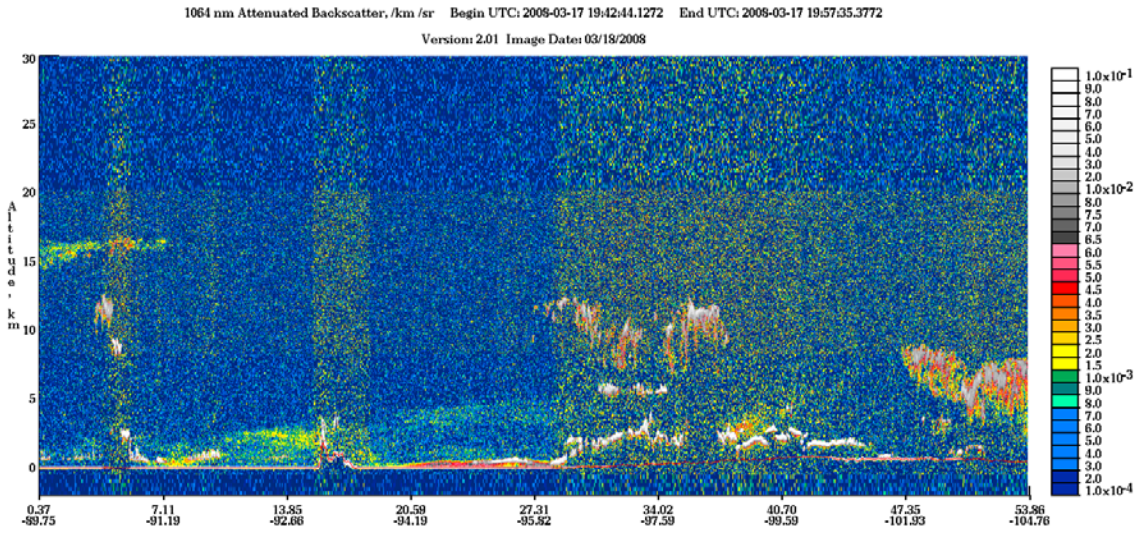

Figure 17. A color-modulated, altitude-time image of CALIOP 532 nm Total (Parallel + Perpendicular) attenuated backscatter (/km/sr) (CALIPSO Products)

2. NASA Mars Phoenix Mission

Launched in August 2007 and successfully landing on Mars in May 2008, Phoenix is a robotic spacecraft that is part of the Mars Scout Program. The instruments aboard the Phoenix lander search for environments suitable for microbial life on Mars

and to research the history of water there. The operational funding for the mission will extend through 30 September 2008. The Meteorological Station (MET) on Phoenix that "will bounce laser pulses off passing clouds and atmospheric dust overhead to determine their composition, movement and size" (Optech Inc). It was designed in Canada and supported by the Canadian Space Agency. The vertical pointing Lidar detects multiple types of backscattering by atmospheric particles to determine the altitude at which scattering occurs. Phoenix system is a "Q-switched Nd:YAG laser" (Carswell 1) which transmits at both 532 nm and 1064 nm "so that it can give accurate measurements of cloud height to within 10 metres" (Canadian Space Agency). Wavelength dependence of scattering makes it possible to discriminate between ice and dust and serve as an indicator of the effective particle size.

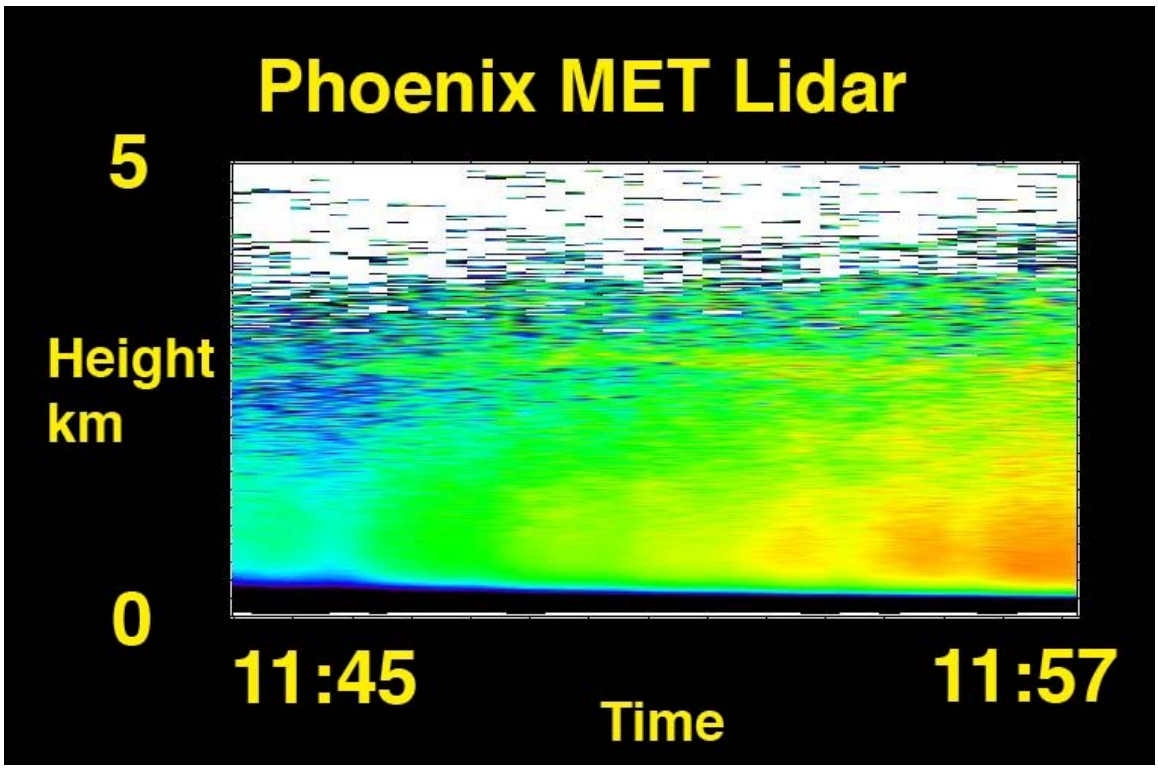

Figure 18. This graph shows Lidar data for a 15-minute period around noon on Sol 4. Higher concentrations of dust (as shown in red and orange) move over the lander near the end of the measurement (Phoenix News)

The MET Lidar began operation on 29 May 2008 recording the first surface extraterrestrial atmospheric profile. This first profile indicated well mixed dust in the first few kilometers of the atmosphere of Mars, where the planetary boundary layer was observed by a marked decrease in scattering signal. The plot shows the amount of dust as a function of time and altitude, with warmer colors indicating more dust and cooler colors indicating less dust. A Layer at 3.5 km can be observed in the plot, which could be extra dust, or less likely given the time of sol this was acquired, a low altitude ice cloud (Phoenix News).

F. MERCURY AND ASTEROIDS

1. MESSENGER

Currently approaching an orbit around the planet Mercury, the NASA probe MErcury Surface, Space ENvironment, GEochemistry and Ranging (MESSENGER) was launched 3 August 2004 to study the characteristics and environment of Mercury from orbit. Specifically, the mission is to characterize the chemical composition of Mercury's surface, the geologic history, the nature of the magnetic field, the size and state of the core, the volatile inventory at the poles and the nature of Mercury's exosphere and magnetosphere over a nominal orbital mission of one Earth year (Messenger). The first altitude measurements from any spacecraft at Mercury also found that craters on the planet are about a factor of two shallower than those on Earth's moon. The measurements also show a complex geologic history for Mercury (Harrington 1).

The mission is the first to visit Mercury in over 30 years; the only previous probe to visit Mercury was Mariner 10, which completed its mission in March 1975. The MESSENGER has vastly improved scanning capability, with cameras capable of resolving surface features to 18 meters (59 ft) across compared to the 1.6 kilometers (0.99 mi) resolution of the Mariner 10. Using the Mercury Laser Altimeter (MLA), MESSENGER will also be able to image the entire planet with the day or night capability of its photon-counting, 1064 nm infrared Lidar with a PRF of 8 Hz. "MLA can view the planet from up to 1500 kilometers (930 miles) away with an accuracy of 30 cm" (MLA).

On 14 January 2008, as part of the initial fly-by measurements, MESSENGER's MLA became the first instrument to measure the distance between a spacecraft and the surface of Mercury. "The instrument acquired the surface at a slant range of about 600 kilometers and tracked the surface through closest approach near 200 km and out to a distance of about 1500 km" (Messenger). Laser altimetry data will used to map the planet's gravitational field and also to track the planet's slight, forced libration – a wobble about its spin axis – which will tell researchers about the state of Mercury's core.

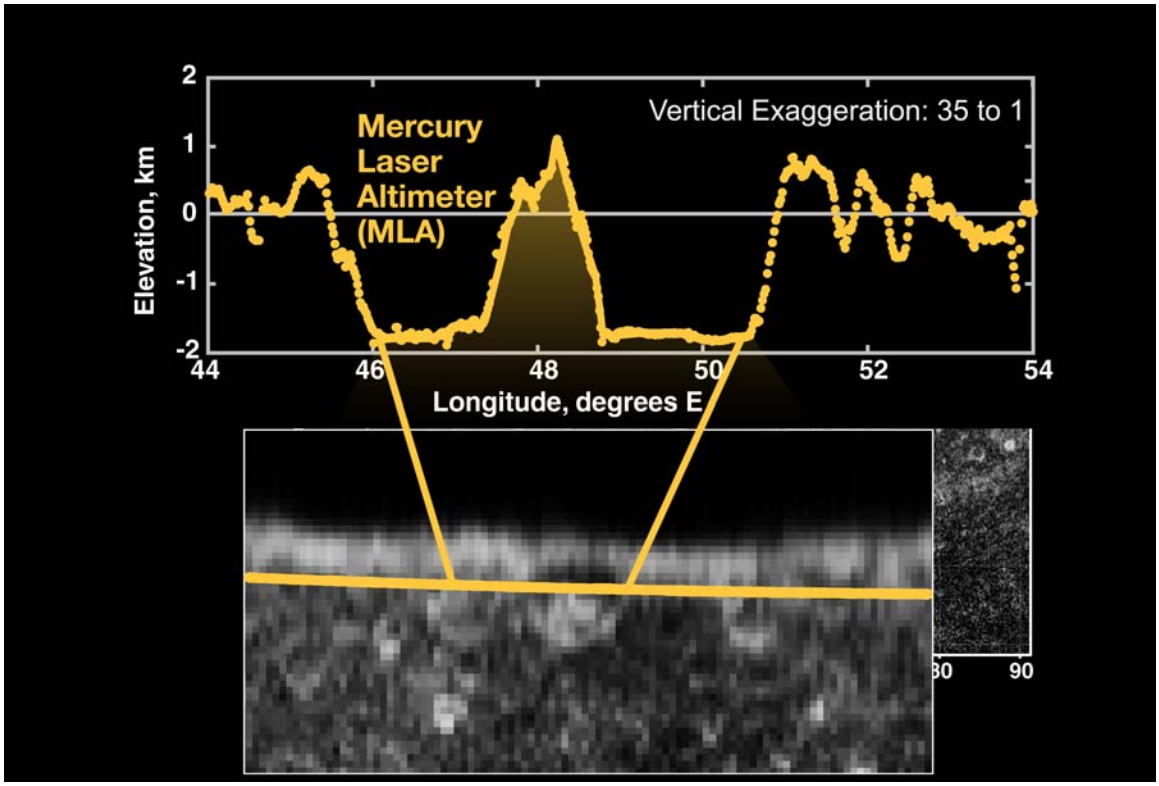

Figure 19. "A close-up of the Mercury Laser Altimeter (MLA) profile of Mercury acquired during MESSENGER's first Mercury flyby on 14 January 2008. Comparison with an Arecibo radar image mosaic (bottom) provided by Harmon and co-workers shows that the two largest depressions are adjacent impact craters. The craters have rim-to-rim diameters of 107 km (left) and 122 km (right). The root mean square roughness of the floor the larger crater is ~35 m. The vertical exaggeration in the figure is 35:1" (Messenger)

2. Lidar to Observe Asteroids

Hayabusa is an unmanned space mission led by the Japan Aerospace Exploration Agency to observe and return a sample of material from small near-Earth S-Type asteroid 25143 Itokawa (dimensions 540 meters by 270 meters by 210 meters) to Earth for further analysis. The Hayabusa spacecraft was launched on 9 May 2003 and rendezvoused with Itokawa in mid-September 2005; the spacecraft is slated to return to Earth by June 2010. One objective was a "determination of the bulk density of the asteroid using a laser altimeter and visible camera" (Mukai 187). The laser was an Nd:YAG laser with 1064 nm wavelength and the intensity of the detected returns was used to provide information on surface albedo. Despite the failure of two of three reaction wheels, which reduced total laser hits, a two-dimensional map of the surface was generated with a resolution of 3-4 meters (Mukai 188) which revealed surface boulders a few meters in size. From the returned data, mass was calculated at 3.51 x 10^{10} kg a density of 1.95 g/cc and "Itokawa is the first recognized small S-type asteroid with a rubble pile structure" (Mukai 191).

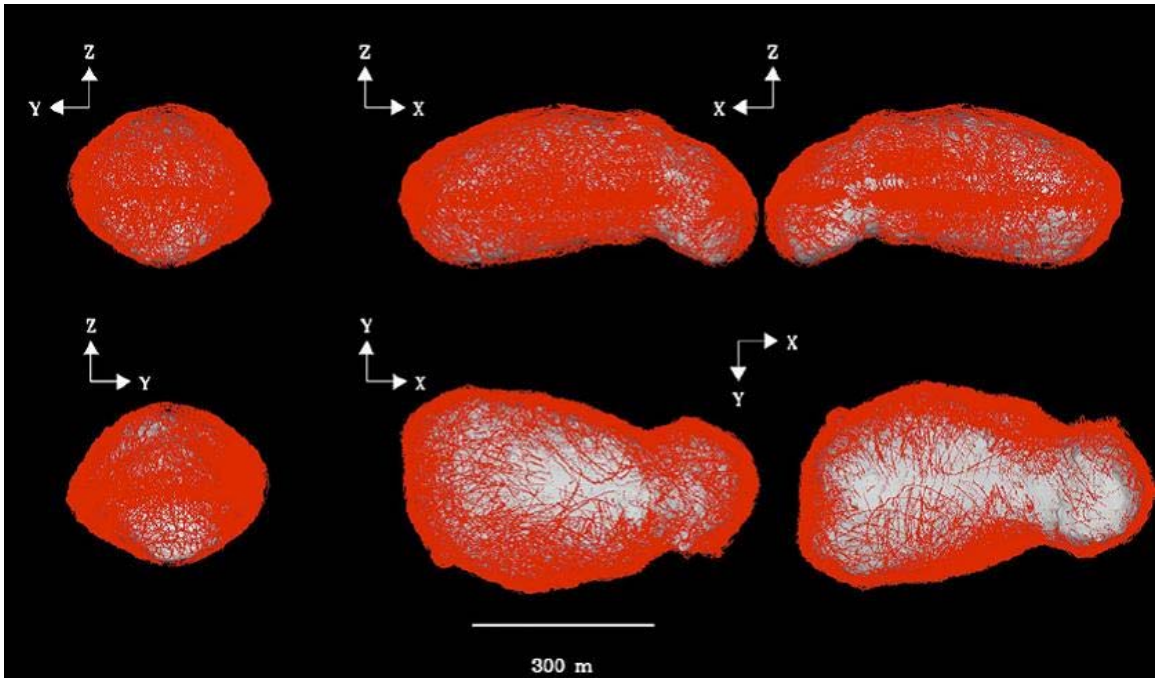

Figure 20. The LIDAR spots on the surface of asteroid Itokawa covered over 87% of the total surface. Since the spin axis of the asteroid is along the z-axis in the images, the density of spots in both polar regions is relatively low (Mukai 190)

G. THE MOON

1. Clementine

Launched on 25 January 1994, Clementine was a joint project between the Ballistic Missile Defense Organization and NASA. The mission objectives were to make scientific observations of the Moon and the near-Earth asteroid 1620 Geographos and to test sensors and spacecraft components under extended exposure to the space environment. The spacecraft carried a laser altimeter as one of its seven scientific instruments "to obtain a multispectral imaging of the entire lunar surface" (Clementine). The orbital parameters of the mission put the laser altimeter into an elliptical orbit with a periapsis at 400 km to obtain altimetry and imagery at an inclination of 60 degrees. The instrument had a 1064 nm wavelength Nd:YAG laser transmitter with a pulse width <10 ns, a PRF of 1 pulse per second and a beam divergence less than 500 microrad. The Lidar could store up to six detections and would then discriminate between missed and false detections. The instrument produced range resolutions of 40 m vertical and 100 m horizontal with across track spacing at the equator of 40 km and along track spacing of 1-2 km. To produce the topographic model of the Moon and since the detailed topography is largely unknown, a filter, "based on a priori knowledge of the surface properties, returned at most a single valid range value for each bounce point. After filtering, a few dozen ranges, corresponding to known impact features, were manually included, and several suspect ranges excluded" (Clementine).

While the altimetry along-track is fairly dense, the east-west coverage is limited by the 2.8 degree spacing of the groundtracks, repeating every 132 orbits.

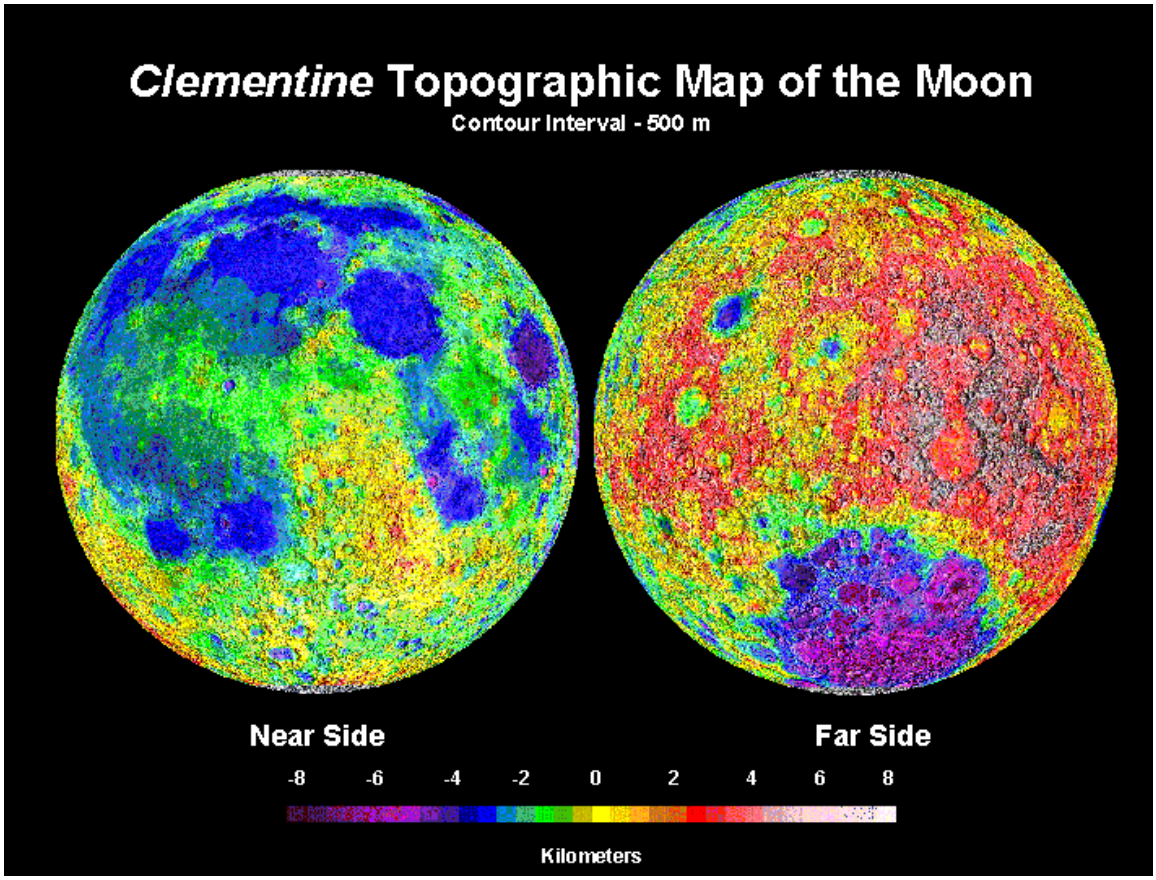

Figure 21. A topographic map of the Moon's surface based on Clementine's laser altimeter (science@NASA)

2. SELENE (Kaguya)

The Japan Aerospace Exploration Agency (JAXA) developed the SELenological and ENgineering Explorer or SELENE, better known in Japan by its nickname Kaguya, as the second Japanese lunar orbiter spacecraft. "The major objectives of the KAGUYA (SELENE) mission are to obtain scientific data on lunar origins and evolution, and to develop the technology for future lunar exploration" (Kaguya). The spacecraft was launched 14 September 2007 and carries a laser altimeter as one of its fifteen scientific instruments. SELENE has a mission to map the lunar surface using its Laser Altimeter (LALT) which incorporates very compact Q-switched Cr doped Nd:YAG laser system which transmits 20 ns laser pulses. The beam divergence is 0.4 mrad and the beam spot size on the lunar surface is typically 40m when the main orbiter altitude is 100 km. Range

accuracy between SELENE orbiter and the lunar surface is ±5m (Araki 1510). Ranging began on 25 November 2007 and nominal observation started on 30 December 2007. The LALT demonstrated that it can detect precise topographic features and was expected to obtain a "global and precise topographic data set of the moon, including the polar regions higher than 75 degrees that have never been explored" (Kaguya).

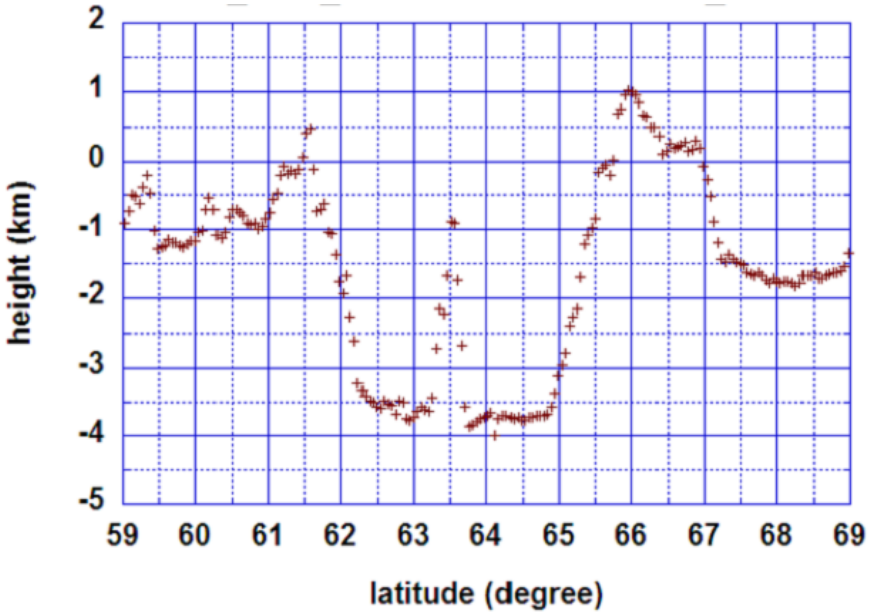

Figure 22. Topographic profile of Pythagoras crater (63.5N, 63.0W). Outer ring and central peak are clearly displayed. Data obtained 25 November 2007. Horizontal axis is lunar latitude (One degree corresponds to 30.3km) (Araki 1510)

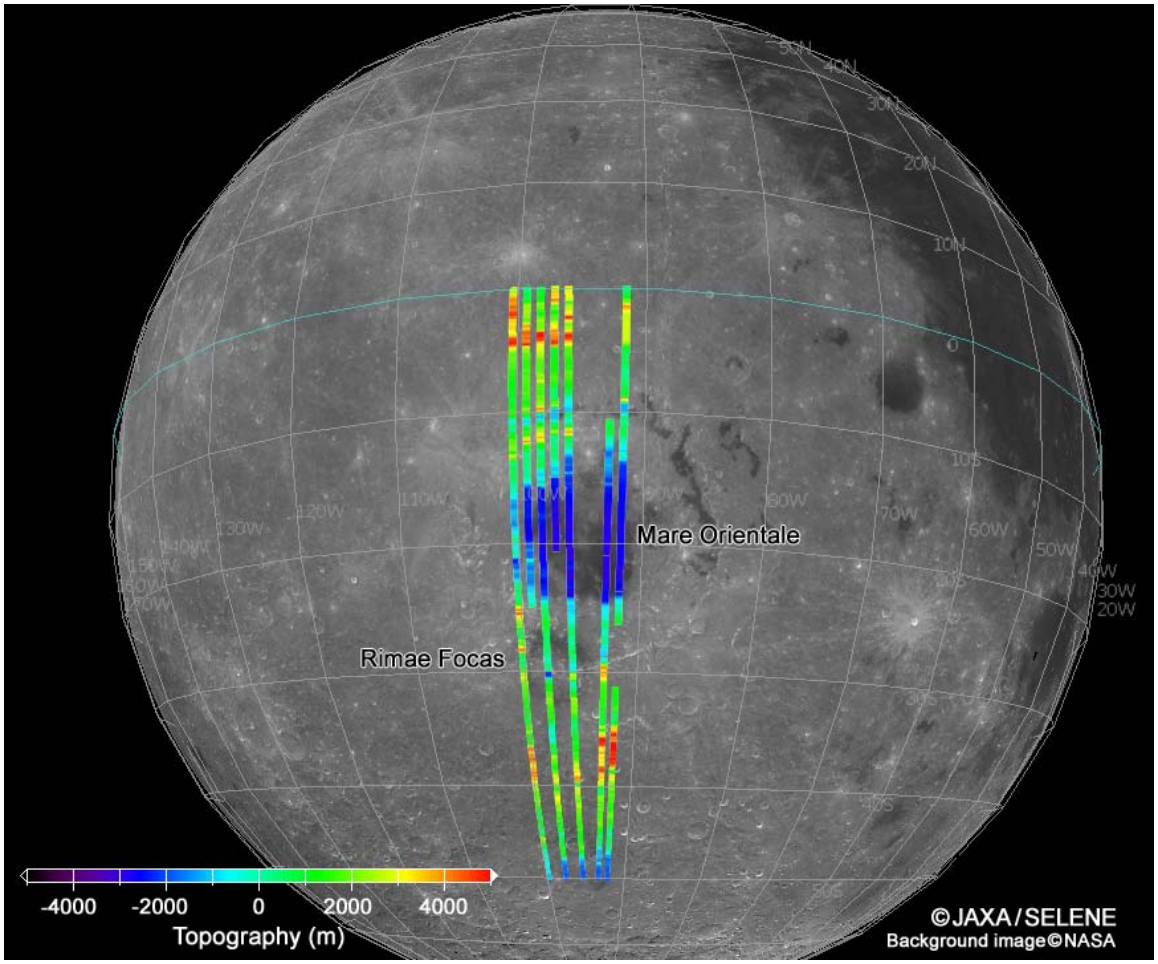

Figure 23. Topography of the Mare Orientale from observation data from LALT and the stereoscopic Terrain Camera for high resolution lunar maps (Kaguya)

3. Chang'e

Named after the Chinese goddess of the moon, the Chang'e 1 lunar orbiter, launched from Xichang Satellite Launch Center on 24 October 2007, is the first Chinese mission to the Moon. This mission's objectives were to "develop and launch China's first lunar orbiter, validate the technology necessary to fly lunar missions, build a basic engineering system for lunar exploration, start scientific exploration of the Moon" (Chang'e). The eight instrument payload includes a nadir-pointing laser altimeter to measure topography with 1064 nm wavelength, 150 mJ laser pulses from the spacecraft traveling at 1.59 km/s in a 127 minute, high-inclination circular lunar science orbit at 200 km above the surface.

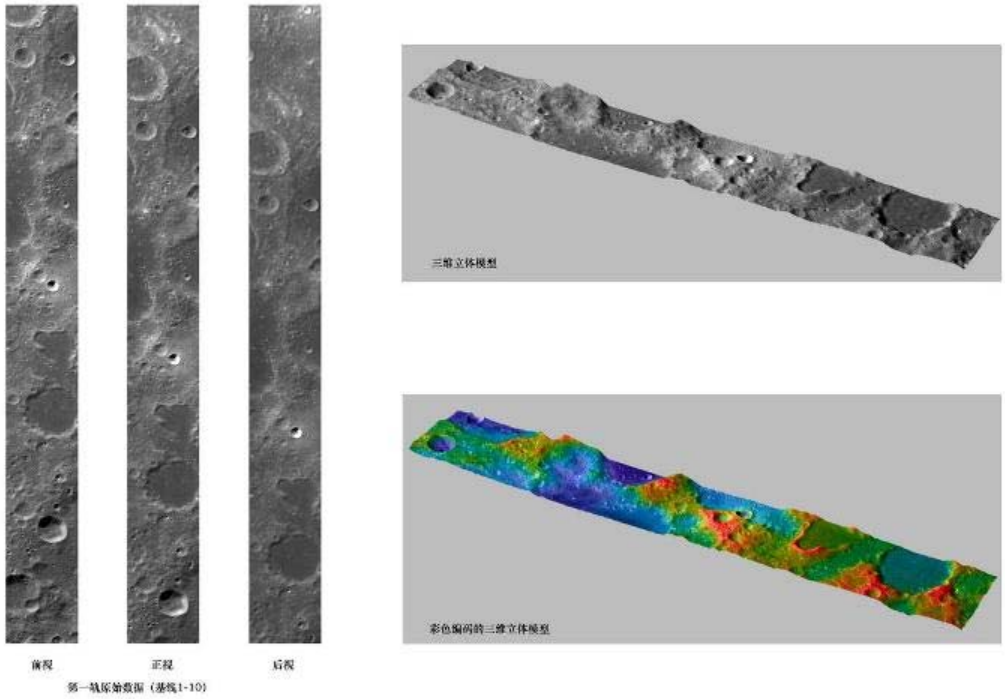

Figure 24. China released this Digital Elevation Map from Chang'e data on 9 December 2007 (Chang'e)

4. Future Lunar Missions

a. Lunar Reconnaissance Orbiter

The Lunar Reconnaissance Orbiter (LRO), planned for an early 2009 launch, has mission objectives that are to find "safe landing sites, locate potential resources, characterize the radiation environment and demonstrate new technology" (Mission Overview). The Lunar Orbiter Laser Altimeter (LOLA) investigation will provide a precise global lunar topographic model and geodetic grid at scales from local to global that are necessary for landing safely. This mission will preserve the record of the evolution of the surface which contributes to decisions as to where to explore. "The topographic model provided by LOLA will be at a level that will allow safe landings and enhance exploration - driven mobility once on the lunar surface" (LOLA). An active

laser instrument will be able to image permanently shadowed polar regions of the Moon to identify possible locations of surface ice crystals in shadowed polar craters. The LOLA instrument pulses a single laser through a Diffractive Optical Element (DOE) to produce five beams that illuminate the lunar surface. LRO's high-resolution mapping will show some of the larger pieces of equipment previously left on the Moon and will return approximately 70–100 TB of image data. "With its two-dimensional spot pattern, LOLA unambiguously determines slopes along and across the orbit track" (LOLA). The instrument "measures the precise distance to the lunar surface at 5 spots simultaneously, thus providing 5 profiles across the lunar surface. Each spot within the five-spot pattern has a diameter of five meters; the spots are 25 meters apart and form a cross pattern" (Keller 6).

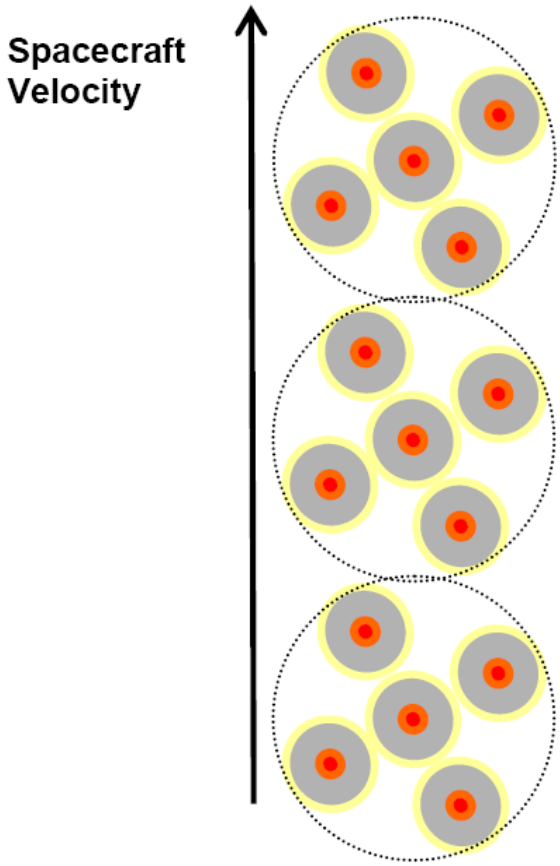

Figure 25. LOLA Pulse Detection Time-of-Flight Altimeter 5-spot Pattern. Red represents the laser spots on the ground while the grey circles represent the receiver FOV (Keller 6)

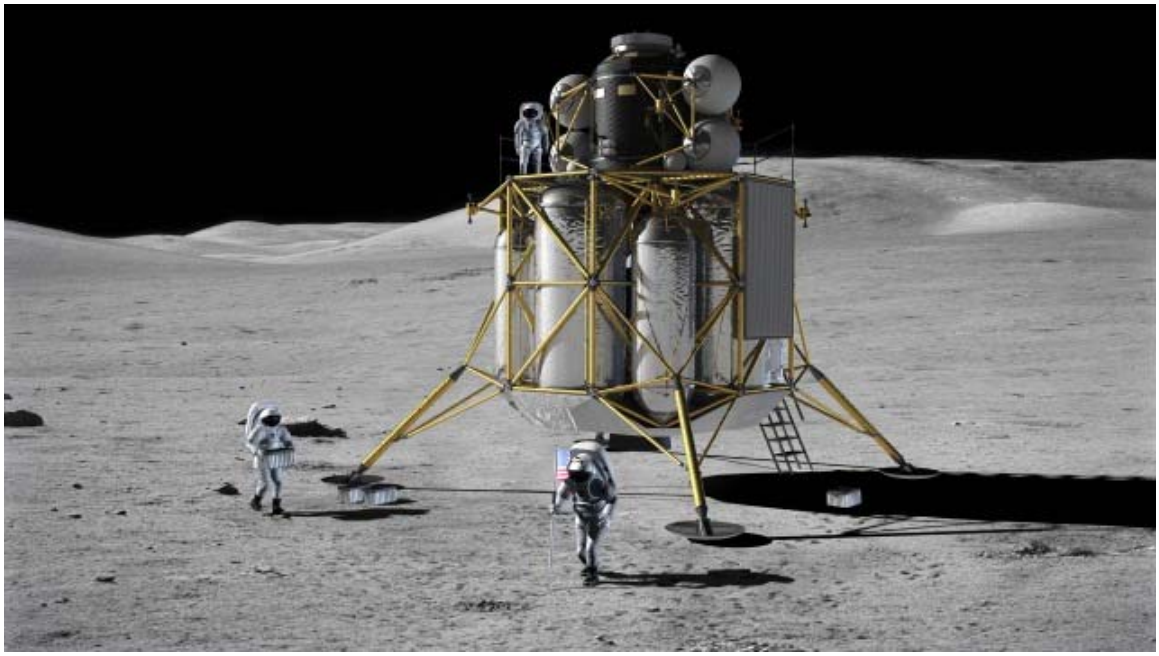

Figure 26. NASA artist's rendering of Altair lunar lander on the lunar surface (NASA "Altair" Lunar Lander)

b. Altair Lunar Lander

The Altair project is the landing vehicle part of NASA's Constellation program. "Altair will be capable of landing four astronauts on the moon, providing life support and a base for weeklong initial surface exploration missions, and returning the crew to the Orion spacecraft that will bring them home to Earth" (NASA "Altair" Lunar Lander). The Lunar Surface Access Module (LSAM) will need autonomous landing and hazard avoidance capabilities. At the Tempe conference in March 2008, the Altair group's Chirold Epp discussed the landing task for ALHAT (Autonomous Landing and Hazard Avoidance) using Lidar to create detailed real-time digital elevation maps for landing software to find a safe touchdown site. Using Lidar to identify obstacles like boulders and craters, the LSAM can actively adjust to avoid danger. The current challenge is to develop lightweight systems that have fast enough processors to cope with a real-time descent to the lunar surface (Jones 22).

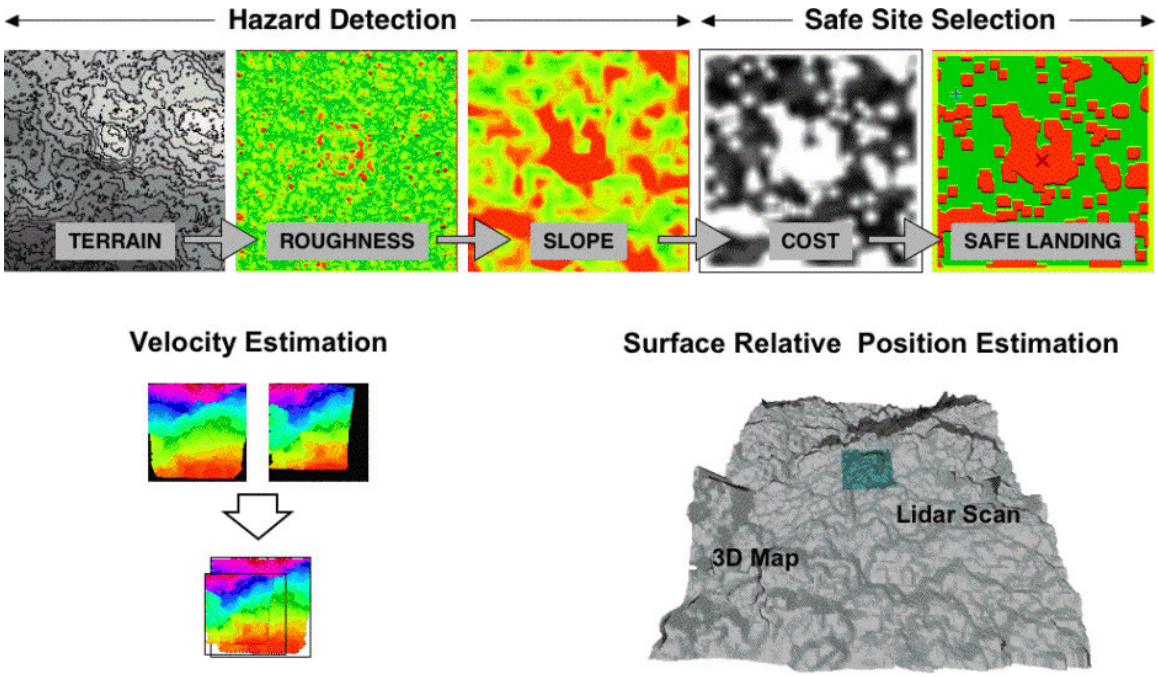

Figure 27. The top of the figure shows the steps necessary to detect landing hazards and select a safe landing site in topographic data provided by a LIDAR. The bottom left shows how two LIDAR scans are aligned to estimate surface relative velocity. Bottom right shows the result of aligning a small 3D scan taken by a Lidar with a larger topographic map to estimate the position of the lander relative to the desired landing site (ALHAT)

IV. EXPERIMENT

A. ASSESSING ACCURACY IN VARYING LIDAR DATA POINT DENSITIES IN DIGITAL ELEVATION MAPS

The purpose of this thesis is to assess the production of Digital Elevation Maps (DEM) using varying density of data points from a Lidar (Laser or Light Detection And Ranging) collection. The thesis covers the accuracy of different amounts of data used when generating a DEM in Quick Terrain Modeler software package and the bare earth extraction plug-in. A large portion of this thesis will also discuss the error analysis when comparing the different DEMs built by randomly selecting 90%, 66%, 50%, 30%, 10%, 5%, 3%, 1%, 0.5%, 0.3%, 0.1%, 0.05%, 0.03% and 0.01% of the data from an airborne Lidar collection to the 100% file.

The techniques and steps that will be taken in this thesis include analyzing data collected in different files, selecting a region of interest within the data set, extracting a bare earth surface from the point cloud and statistically comparing different percentages of data from that region when processed into a surface Digital Elevation Map.

Differences in the surfaces from the Triangulated Irregular Network (TIN) overlaid on a grid will be assessed using multiple methods and software packages. The DEMs will be qualitatively assessed within Quick Time Modeler and quantitatively analyzed using a root mean squares method in ENVI.

B. DATA DELIVERED

The data used in this research was collected over jungle sites in Honduras by the National Geospatial Intelligence Agency during February 2008. Each mission to collect data was flown between the 11th and the 20th of that month, during day and night missions. The data chosen for the analysis was collected on a mission using a real-time GPS solution. This mission is titled 20080211a and consisted of 36 numbered strips flown by the aircraft during collection.

The data examined consists of X and Y coordinates corresponding to north and east coordinates in WGS84. The World Geodetic System defines the size and shape of the earth as well as the origin and orientation of the coordinate systems used to map the world (NGA). Each point has elevation and intensity data with each point. All this is contained in a .LAS file. The data, which combines GPS, IMU and laser pulse range data to produce X, Y and Z point data, will generally be put into this format. This data format provides a suitable, open format which allows different LIDAR vendors to output data which a variety of LIDAR software vendors can share in a supportable environment (Spatial Resources).

The binary representative LAS format can reduce files sizes significantly over the same data using ASCII storage. Depending on the number of attributes stored in the ASCII text file, the LAS format can reduce the file size by as much as 35% to 80%. "Given that LIDAR projects are typically on the order of hundreds of gigabytes, LAS over ASCII results in huge savings in file sizes over the entire project" (Spatial Resources).

Quick Terrain Modeler visualization software was used to convert the binary .LAS files into something useful for imagery analysis.

C. POST PROCESSING SOFTWARE

There are several software programs commercially available for post-processing and viewing Lidar data. Quick Terrain Modeler was used with a Bare Earth Extraction plug-in that more easily enabled analysis of the Lidar data sets for this research. Quick Terrain Modeler is a 3-D modeling software package created to view and manipulate large amounts of complex data. The software was developed by JHU/APL and is now available for purchase commercially from Applied Imagery LLC. QTM is capable of using standard formats of Lidar data (LAS, ASCII XYZ, etc.) to build cloud and surface models within the software.

The Bare Earth Extraction Plug-in, developed by JHU/APL, "is a digital elevation model processing utility with functionality designed to facilitate the detection of manmade objects under canopy" (ILAP Bare Earth Plug-In 3). The plug-in sorts XYZ points representing foliaged areas into three distinct point files: surface, cloud and object.

The surface file is the estimated bare earth surface. This file can be constructed as either a QTC point cloud model or a QTT surface model. The second type, cloud file, represents foliage returns. The object file includes points classified as non-surface but whose height above the estimated ground level (AGL) falls below the user-specified limit. Both cloud and object files are imported as QTC point clouds (ILAP Bare Earth Plug-In 7). For this research, the surface file was consistently imported as a QTT file. The cloud and object files were generated from the XYZ data files, but not used in the analysis of the Digital Elevation Maps.

D. SITE DESCRIPTION

The missions flown to collect this Lidar data were flown near Mocoron, Honduras. "Honduras is a vibrant country, brimming with clear turquoise waters, pristine beaches, lush jungles, breathtaking mountains, challenging rivers, and fascinating ancient ruins" (Country of Honduras). The site chosen for analysis was selected from visual observations of multiple data sets within QTM because it included a river waterway, open area savannah plain, manmade objects including buildings and a road and jungle foliage. This diversity gave it an interesting overview of different topography and how the DEM looked with only the surface files imported through the Bare Earth Extractor.

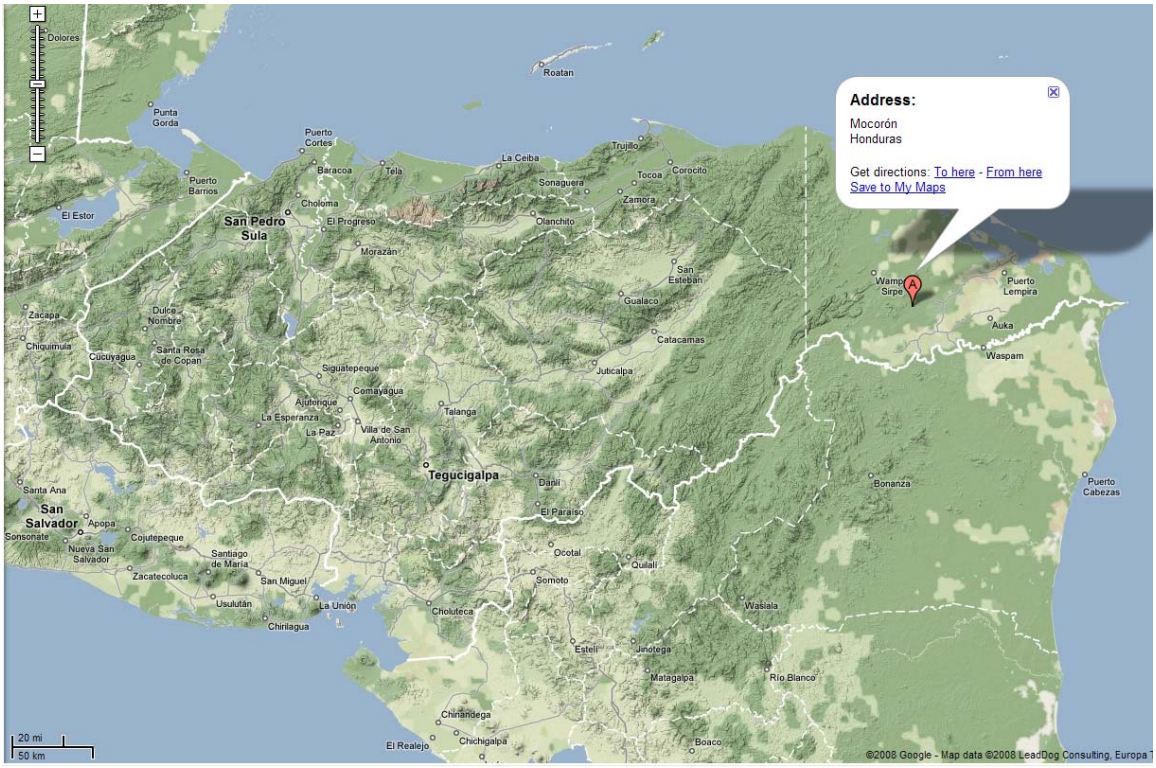

Figure 28. Map of Central America including Mocoron, Honduras (Google)

V. OBSERVATIONS

A. METHOD OVERVIEW

The research steps taken during the experiment to evaluate the digital elevation models generated from varying densities of a Lidar point cloud are detailed in the paragraphs below.

Initially, work was done for familiarization with the software. The operator's manual for Quick Terrain Modeler was read and tutorial examples were followed to gain comfort with the capabilities of this program to import and export data of different formats for useful analysis. Upon receipt of the specific Lidar dataset for this research, multiple different LAS files were reviewed for displayed content. These files were compared to the accompanying strip summary notes on each of the missions flown during the collection. Weather factors and specific target-sets collected excluded many of the days collections. Atmospheric conditions affected the data and when heavy clouds were in the collection area, the data was significantly reduced in valuable returns from ground targets. Many strips were eliminated from consideration for this reason. The objective of the search was a surface DEM which contained a substantial area with interesting features for comparison from the 100% DEM to each of the reduced point datasets. By importing multiple strips of LAS data and selecting a subset area which covered multiple flight lines, each reduced data set was compared to the base area with linear road and water features, slopes and foliage. This comparison was done using the QTC point cloud first, then applied this analyst's visual filter to the subsequent QTT surface models.

Of the data, a subset of strips was chosen from mission 20080211a which was flown on 11 February 2008. Thirty-six flight lines were collected on this data set. As the strip summary notes indicated on calibration runs and other factors, the best data to assess came from the last seven flight lines collected. The 20080211a mission strips 30 through 36 were imported into QTM as LAS files and evaluated first as a QTC point cloud, then again as a QTT surface. A subset area that covered a rectangular area 1625 meters by 875 meters was cropped out. This was not a true north-east rectangle, but it was arranged

along the flight path headings. The flight paths were flown alternating between a heading of 135 degrees for strips 30, 32, 34 and 36 and 315 degrees for strips 31, 33, 35 and 37. Each strip abutted and slightly overlapped its predecessor.

20080211a	DATE	DAY	FLIGHT #	TAKE OFF	LANDING	LOCATION	SYSTEM	OBJECTIVES
	11-Feb	Mon	1	0630 Roatan	1121 Roatan	Mocoron	Lidar & N-cam	1.A Mocoron Village Checkout
	(Note: All Take Off and Landing Times are given in local time - CST)							II. A. 3) Camp Victoria 1 (2kft)

Plan	strip#	plan#	heading (°)	course	speed	PRF (kHz)	scan_angle	on_sec
MocoronTrails2.pln	30	5	135	134.372	128.477	100	10	66.01
MocoronTrails2.pln	31	6	315	315.794	138.806	100	10	75.17
MocoronTrails2.pln	32	7	135	132.887	121.723	100	10	76.79
MocoronTrails2.pln	33	8	315	315.465	128.38	100	10	65.4
MocoronTrails2.pln	34	9	135	134.38	124.021	100	10	69.28
MocoronTrails2.pln	35	10	315	315.621	128.419	100	10	70.37
MocoronTrails2.pln	36	11	135	134.422	123.081	100	10	75.15

Table 4. Subset30-36 Strip Data tabulated mission information (After strip_summary.xls)

Once the subset was selected, all data outside this area were cropped away and a new data set was exported from Quick Terrain Modeler as an XYZ file for subsequent work on the subset.

The Bare Earth Plug-In designed by the Johns Hopkins University Applied Physics Laboratory works on XYZ files. Initially, the entire file was selected for the extractor to build the 100% DEM using every single point within the subset collected on the mission. This established the reference file which all reduced datasets were compared against. There are over 8.6 million points included in the 100% subset. The Bare Earth extractor generated the three files: surface, cloud and object. The surface file was very fine and contained 4,260,249 points for the surface model.

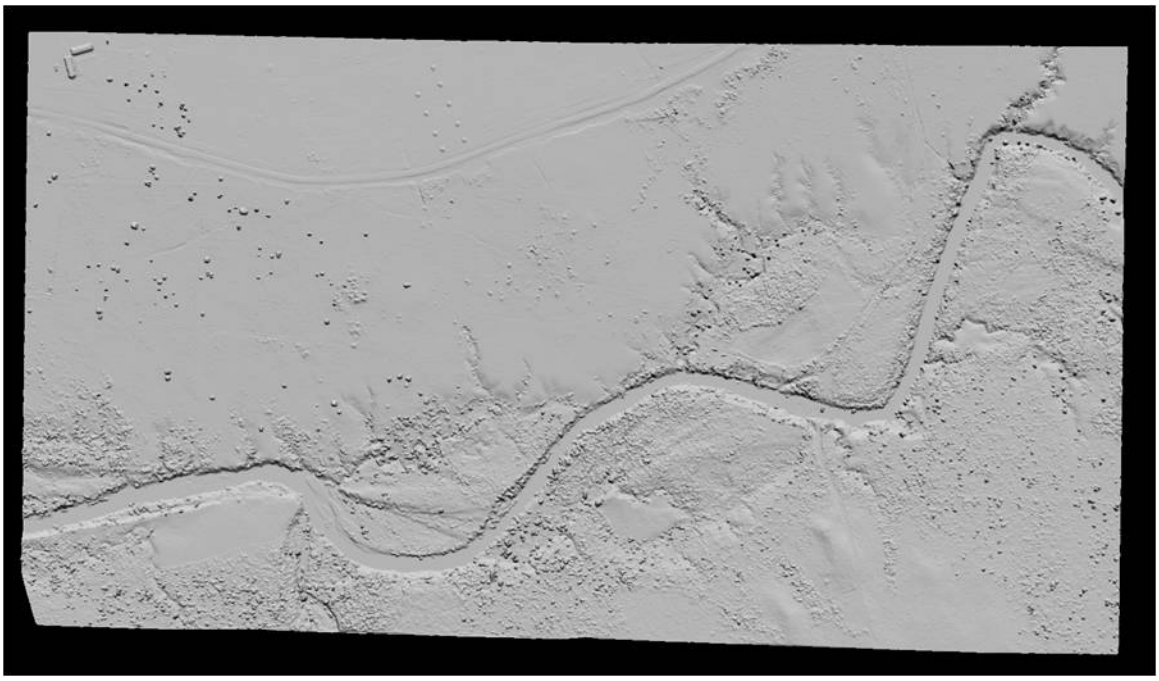

Figure 29. Subset30-36_10000pct_surface DEM 1625 meters by 875 meters

Quick Terrain Modeler can display the surface model with height coloration turned on or off for different visualization purposes. The earth colors palette was chosen to look more like standard printed cartographic or topographic products in use with similar color schema. The figure below shows how the elevation data was represented by color on the following DEM, which is the same 100% DEM displayed with the coloration added. The range of elevation data shown on this map is 32 meters elevation up to an elevation of 48 meters.

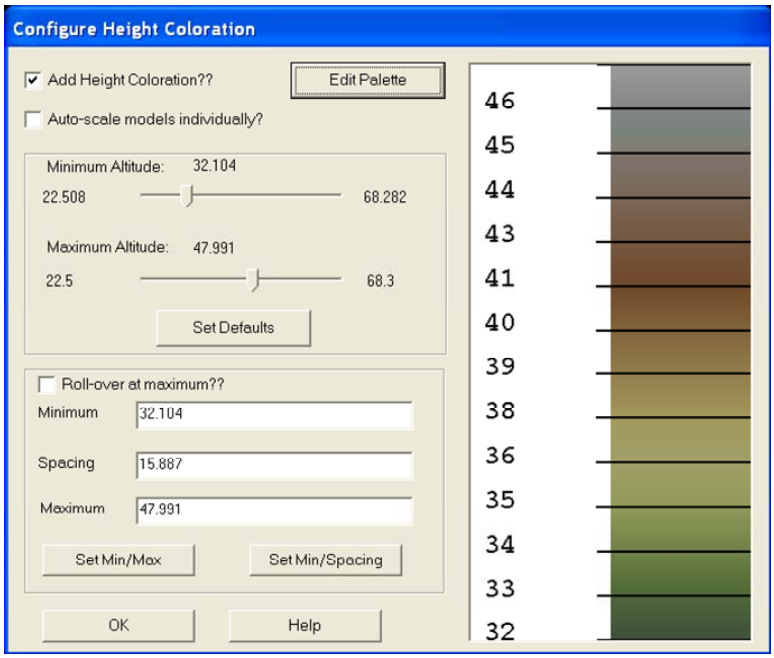

Figure 30. Quick Terrain Modeler Height Coloration Palette

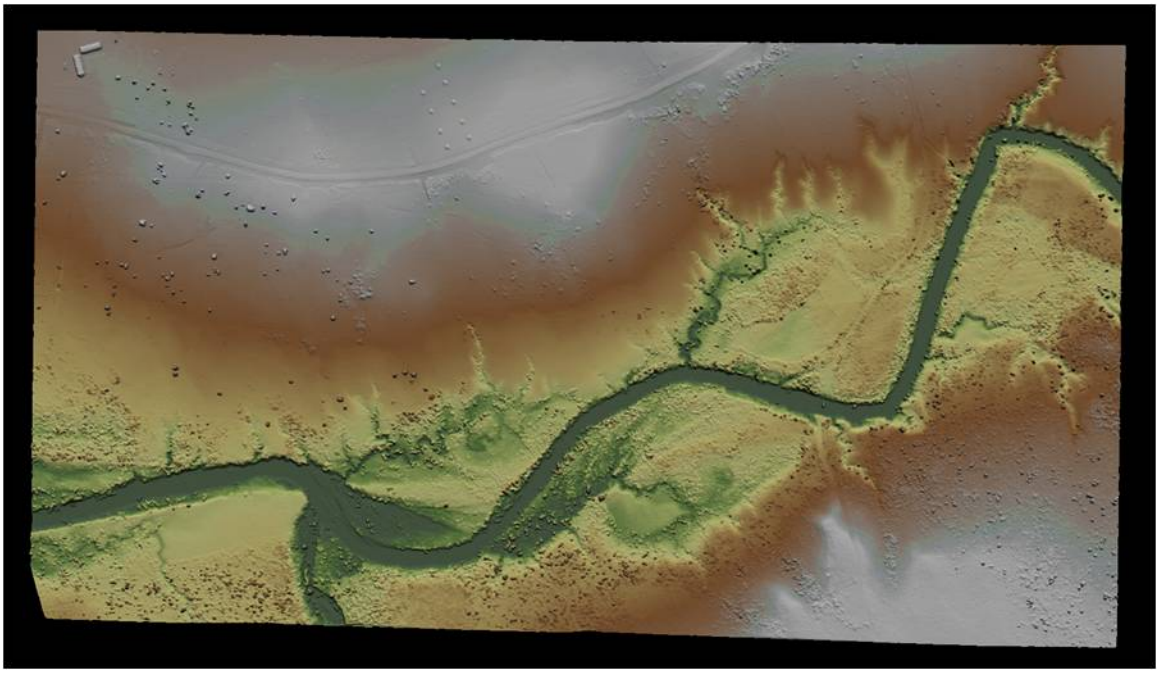

Figure 31. Subset30-36_10000pct_surface DEM with Height Coloration

B. EVALUATION TECHNIQUES

Interactive Data Language computer code (IDL) was written by Angela Puetz of the Naval Postgraduate School Remote Sensing Center that would take the 100% source file in XYZ format and randomly select the assigned percentage of points from there to be saved as a new XYZ file. This code is contained in the Appendix. The user would modify the source file as necessary, input the fractional percent of points to be selected from the file at random and indicate where the new file would be stored. For this research, the total percentage was stepped down from 100% to 90%, 66%, 50%, 30%, 10%, 5%, 3%, 1%, 0.5%, 0.3%, 0.05%, 0.03% and 0.01%. From the original XYZ file of subset30-36, which comprised 8,622,343 separate geolocated points, each of the new files was reduced from that. These percent reduced XYZ files were run through the JHU/APL Bare Earth Plug-In to generate surface, cloud and object files for further generation of the QTT surface model Digital Elevation Map. Results tabulated below.

Percent Reduction	*Point Cloud Total Points*	*Surface Points*
100	8622343	4260249
90	7760109	3942705
66	5690746	2921962
50	4311172	2235412
30	2586703	1403544
10	862234	417996
5	431117	158246
3	258670	72682
1	86223	14738
0.5	43112	6763
0.3	25867	3584
0.1	8622	1030
0.05	4311	314
0.03	2587	105
0.01	862	7

Table 5. Subset30-36 Original and Reduced Point Cloud Data Points

Each of the fifteen DEMs was loaded into Quick Terrain Modeler for viewing. The models can be all loaded at once and viewed separately or together for visual comparison and analysis. The files were verified that the region was correct and an initial analysis was made on each as a relative quality of "goodness," a non-technical term for how the DEM looked as a map that a typical user would want on any type of military ground operation. The subjective nature of this analysis was insufficient, so more work was done to compare each file to the 100% point cloud DEM.

Each surface file was exported from Quick Terrain Modeler into a file type that can be read in ENVI. A powerful visualization and analysis software package, ENVI (Environment for Visualizing Images) is the premier software solution for extracting information from geospatial imagery (ENVI Capabilities). The files were exported as GeoTIFF files from QTM. GeoTIFF is a public domain metadata standard which allows georeferencing information to be embedded within a TIFF file. The potential additional information includes projections, coordinate systems, ellipsoids, datums and everything else necessary to establish the exact spatial reference for the file (GeoTIFF).

Once all fifteen GeoTIFF files were loaded into ENVI, the image could be manipulated in order to be processed for visualization and statistical methods. As the reduced files source data diminished, the surface created by QTM changed its exterior dimensions as the perimeter points were lost through the random down selection. As the perimeter points were negatively affected, the DEM generation process of taking a Triangulated Irregular Network (TIN) and draping it over the grid caused increasing visualization differences from the 100% source DEM. These differences needed to be reduced in order to conduct the statistical analysis on the collected files. The smallest percentage of points DEMs required warping in ENVI to produce a regular outline and that all the files be masked to this shape to eliminate bad or erroneous data from corrupting the statistical analysis. In the process of warping, when the datasets are loaded into ENVI the images will be referenced to a "pseudo" geographic map projection using the latitude/longitude positions for the 4 corners read from the original data file's header. "Since the images are not truly georectified, the only pixels that have 100% accurate map location metadata information are these four corner pixels, and the geographic location of

every other pixel in the image is merely a 1st degree polynomial warp approximation" (ENVI Capabilities). The mask feature in ENVI, Mask Image "instructs the toolkit to create an ENVI mask image (1 = good data, 0 = bad data) for the data set that suppresses the data acquired" outside user set parameters (ENVI Capabilities).

From the appropriately warped and masked files, extensive statistics are run comparing each file to the 100% source and RMS error between each is calculated and correlated. For this analysis, Angela Puetz wrote additional code in IDL to execute the RMS calculations on the files. Histograms of the data contained can be extracted for additional visualization of the data.

THIS PAGE INTENTIONALLY LEFT BLANK

VI. ANALYSIS

A. DIGITAL ELEVATION MAPS

The following figures are the Digital Elevation Maps of the subset area created using Quick Terrain Modeler with the Bare Earth Extraction Plug-In. The first is the most dense with the initial point distribution at 100% and following that are the surfaces created from each of the reduced data sets. These DEMs have details that are easily seen in grayscale and are included like this rather than in the colorized palette for ease of reproduction.

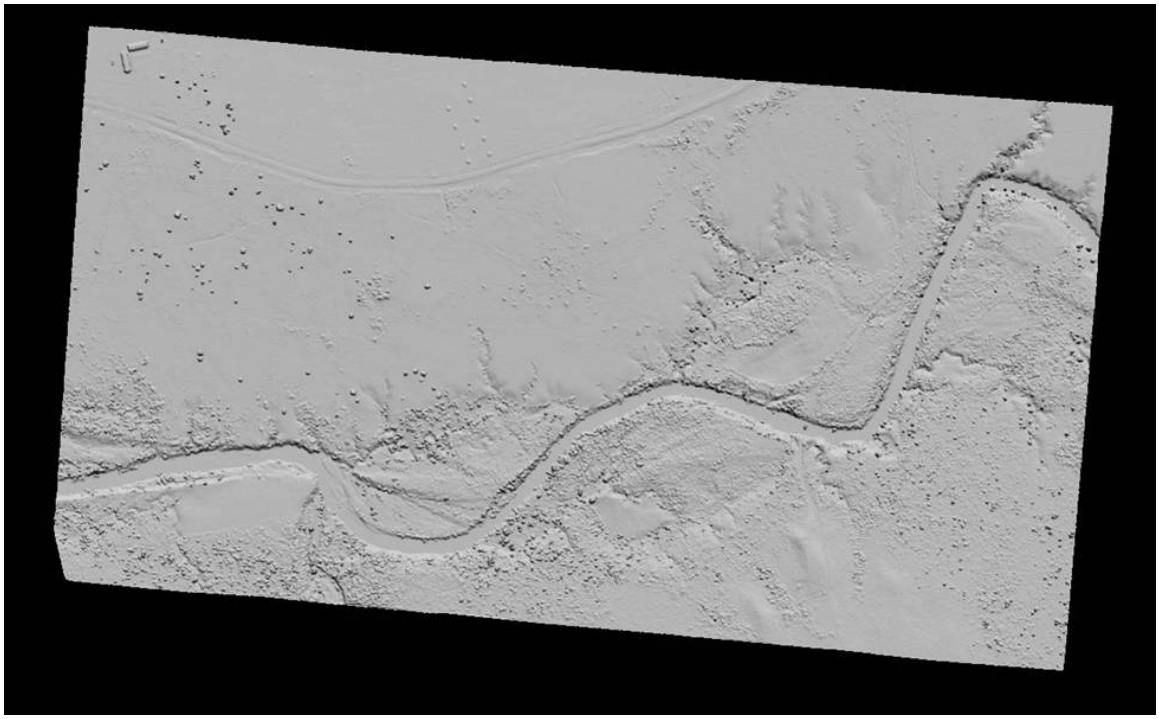

Figure 32. Surface DEM using 100% of the subset point cloud

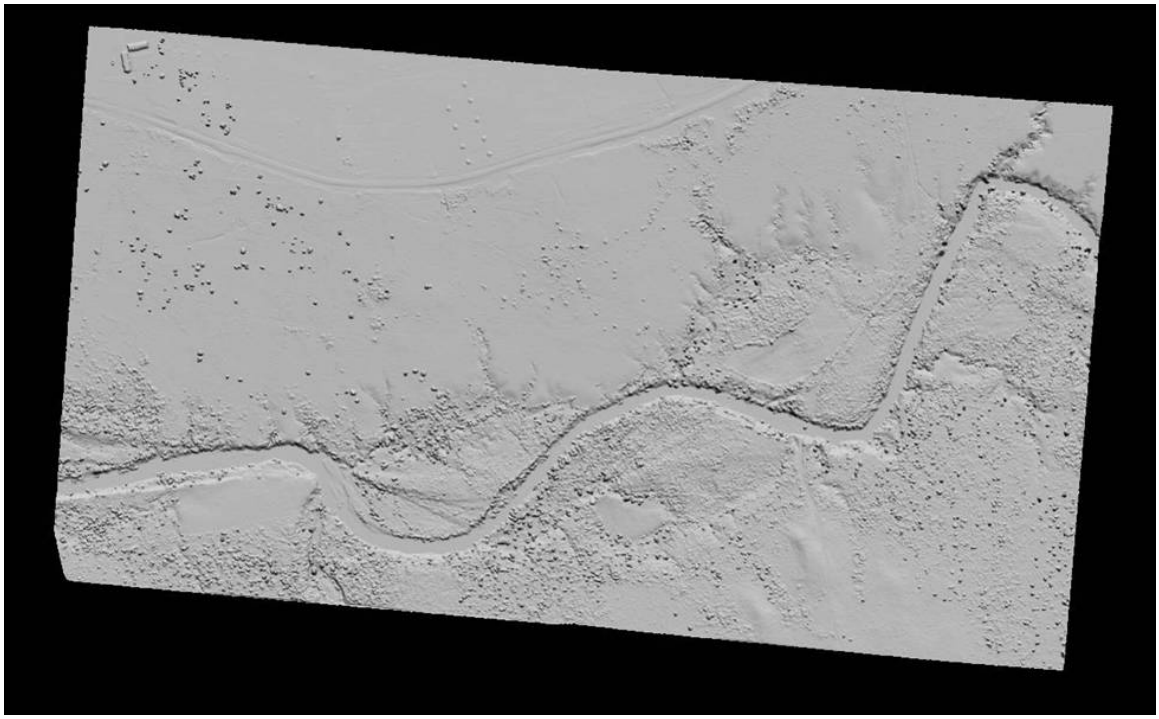

Figure 33. Surface DEM using 90% of the subset point cloud

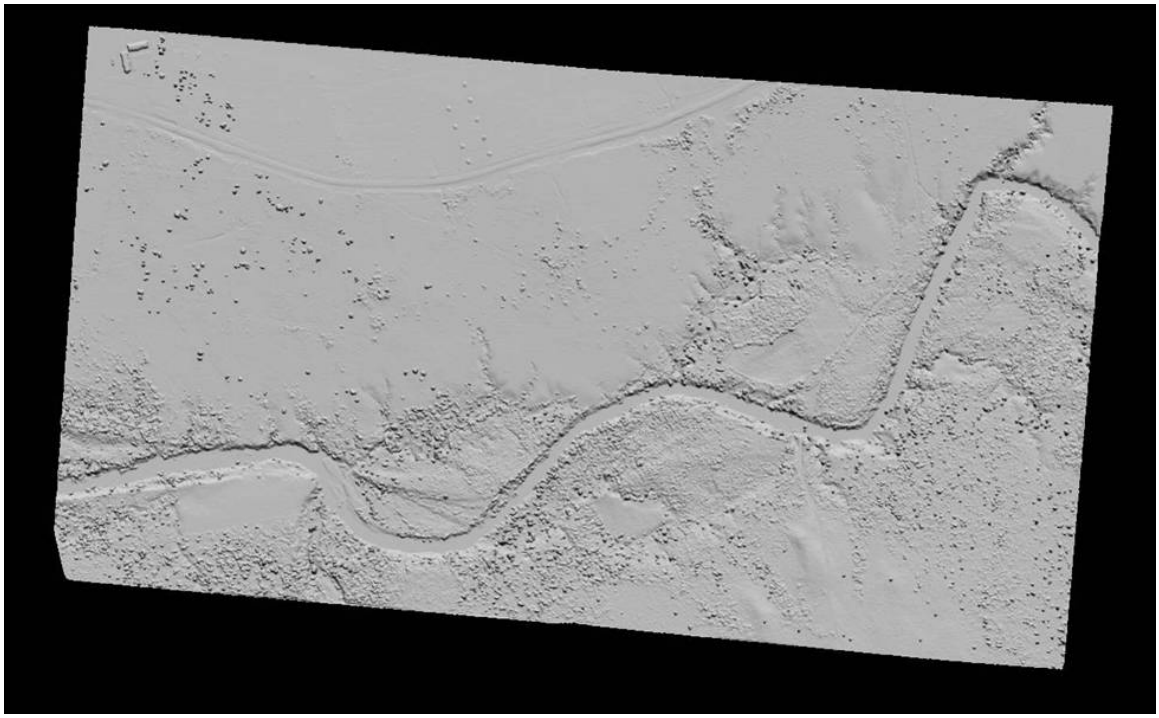

Figure 34. Surface DEM using 66% of the subset point cloud

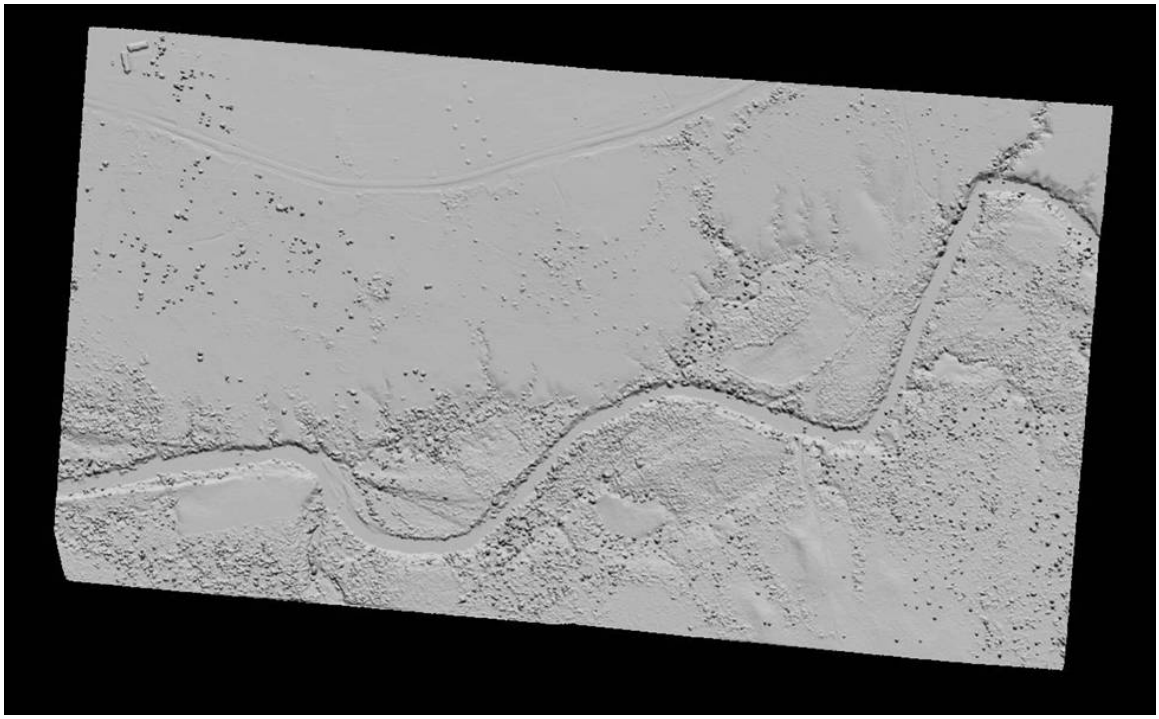

Figure 35. Surface DEM using 50% of the subset point cloud

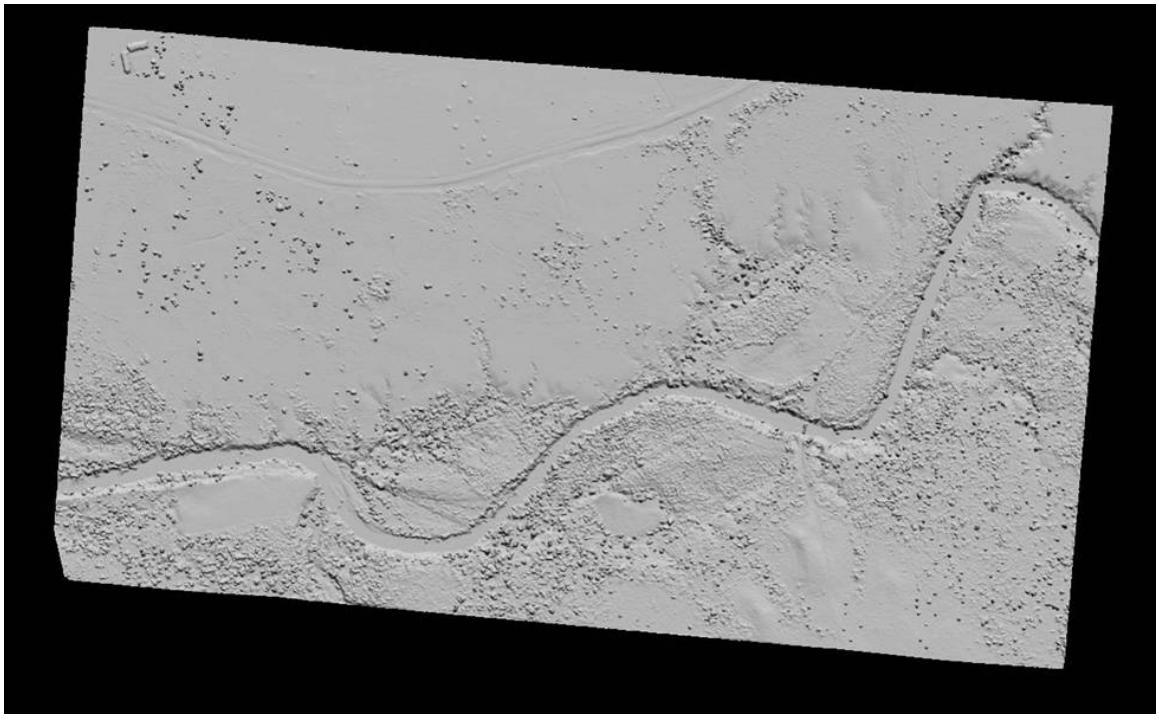

Figure 36. Surface DEM using 30% of the subset point cloud

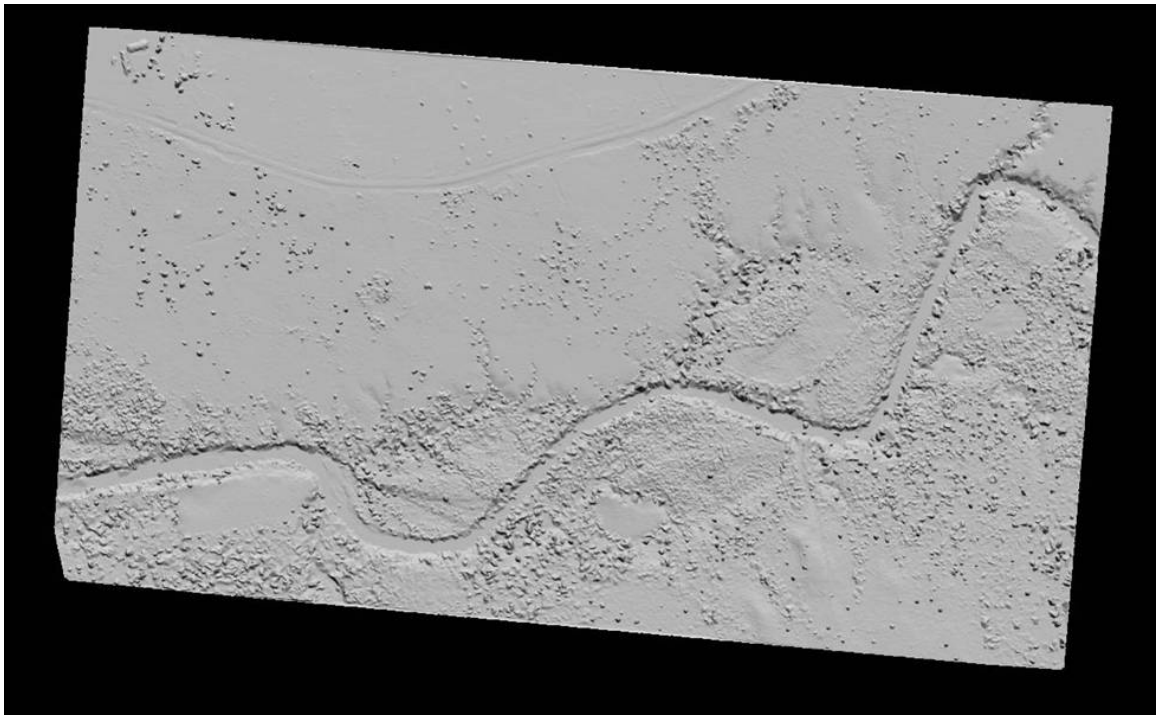

Figure 37. Surface DEM using 10% of the subset point cloud

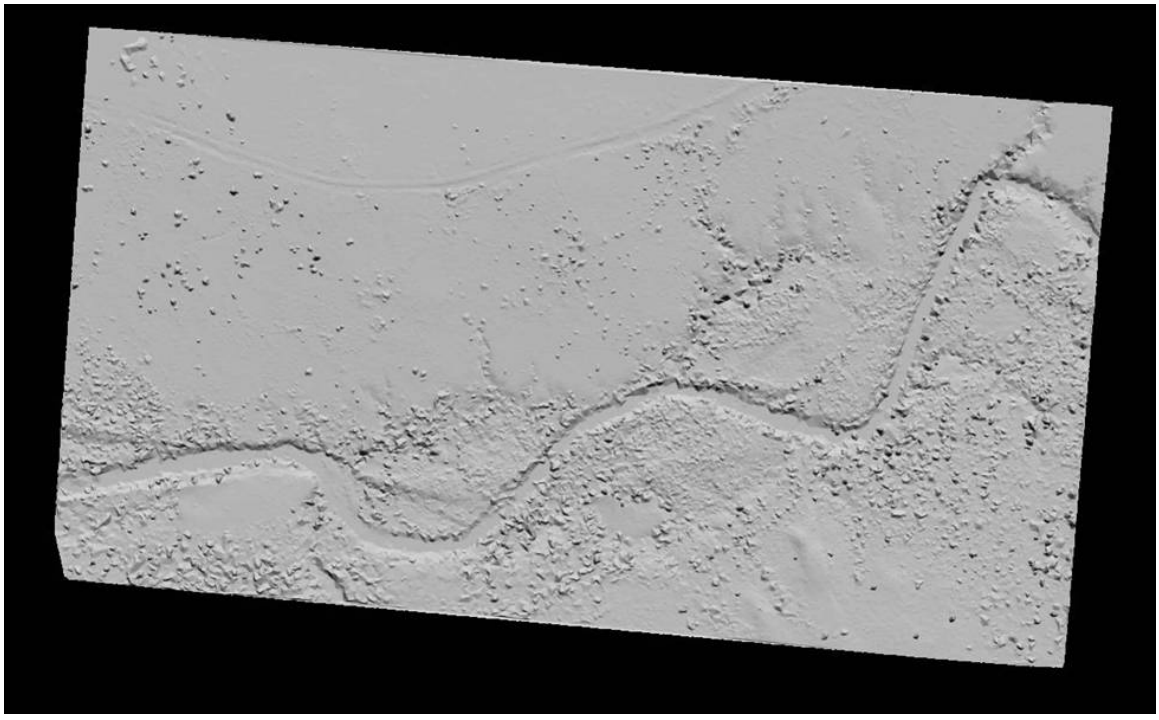

Figure 38. Surface DEM using 5% of the subset point cloud

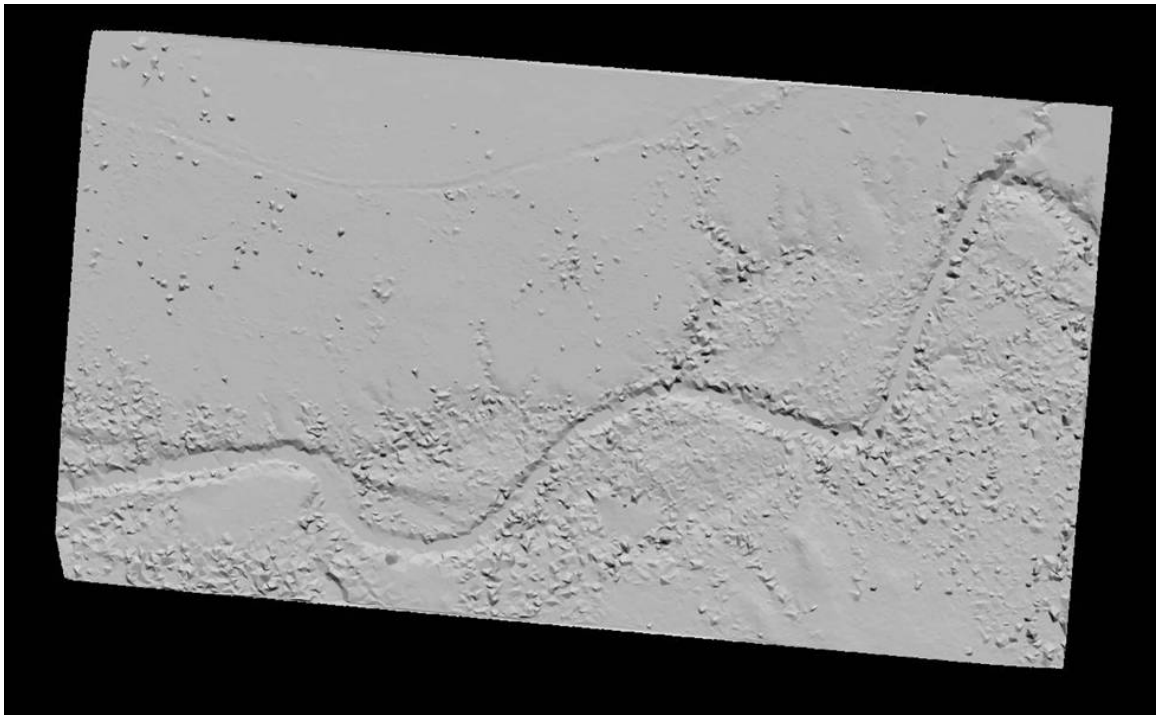

Figure 39. Surface DEM using 3% of the subset point cloud

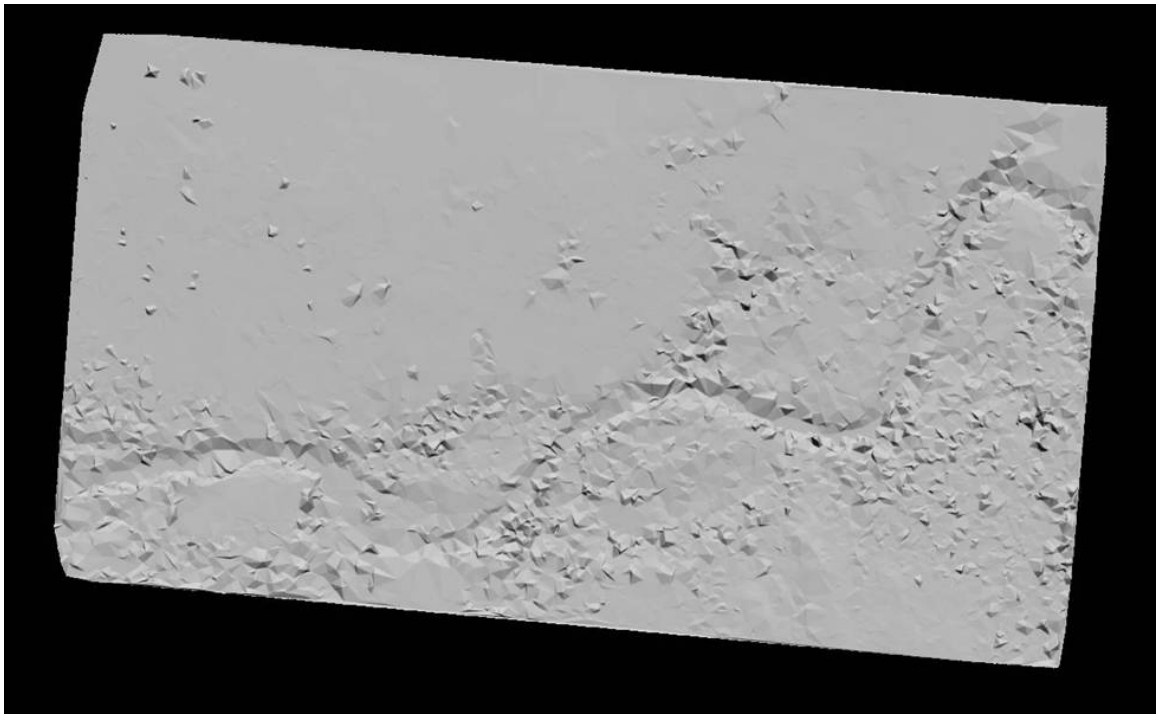

Figure 40. Surface DEM using 1% of the subset point cloud

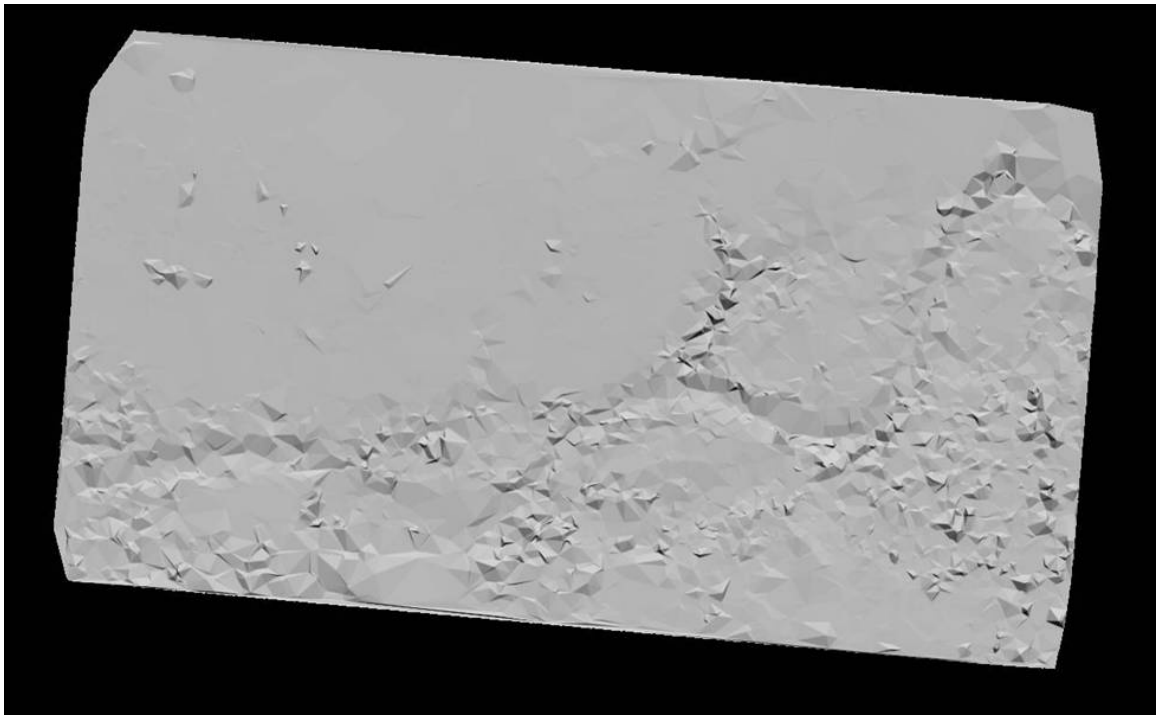

Figure 41. Surface DEM using 0.50% of the subset point cloud

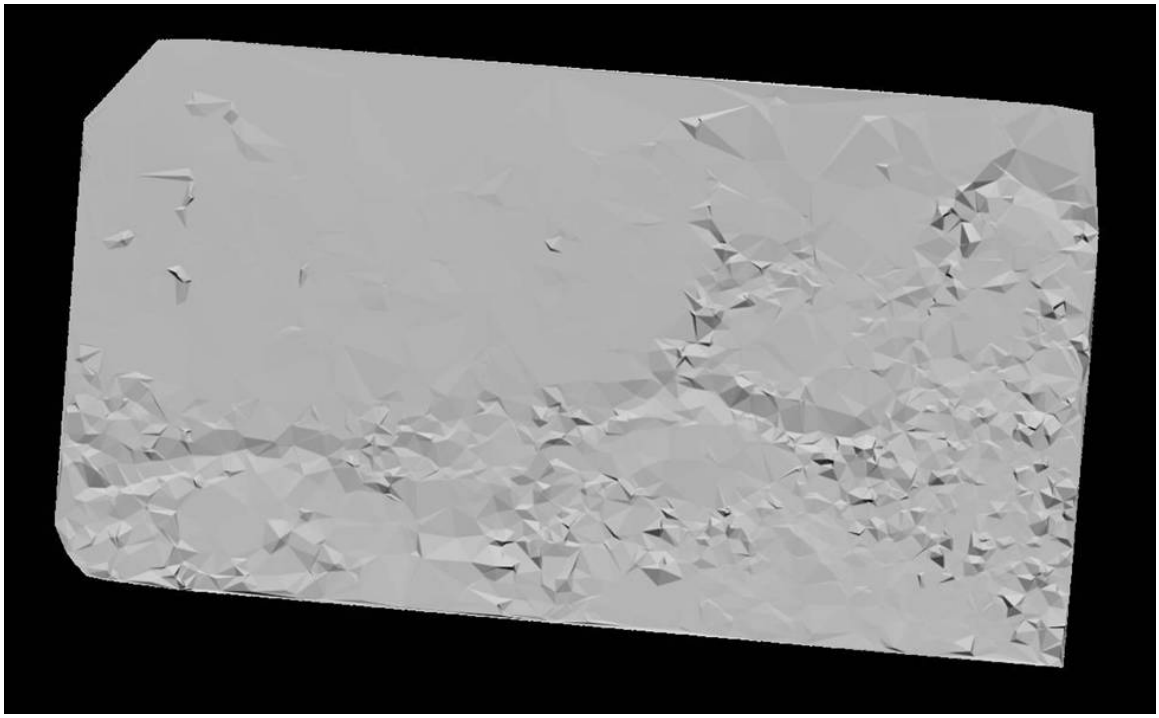

Figure 42. Surface DEM using 0.30% of the subset point cloud

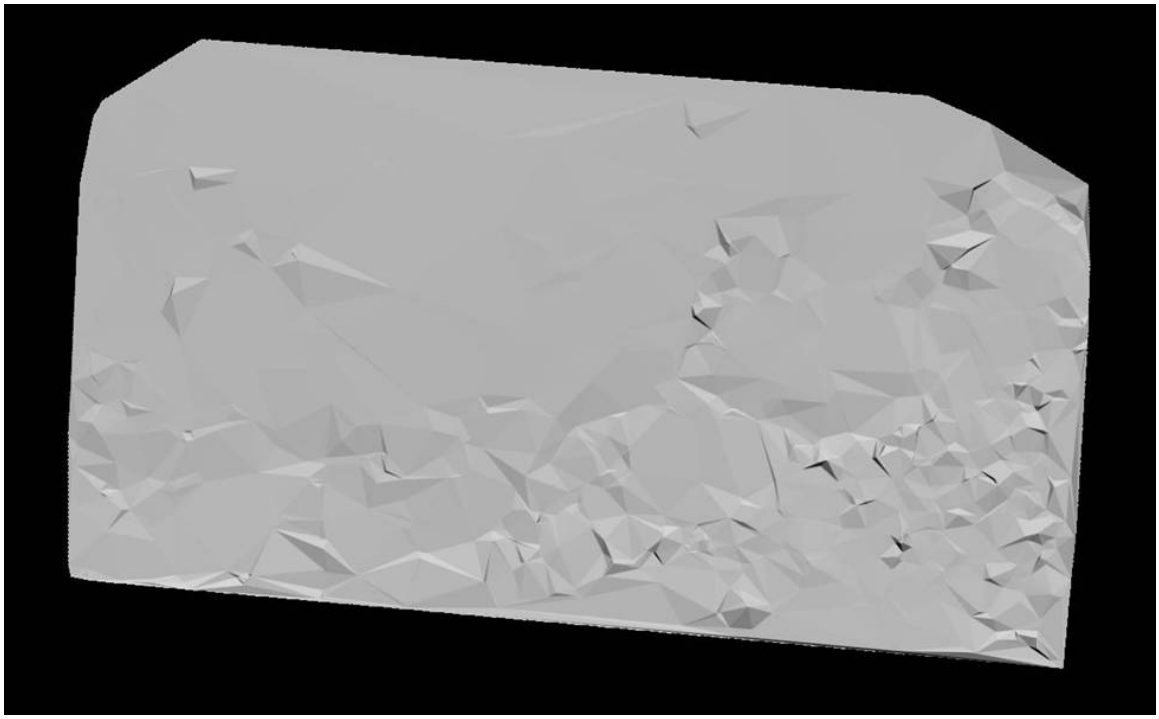

Figure 43. Surface DEM using 0.10% of the subset point cloud

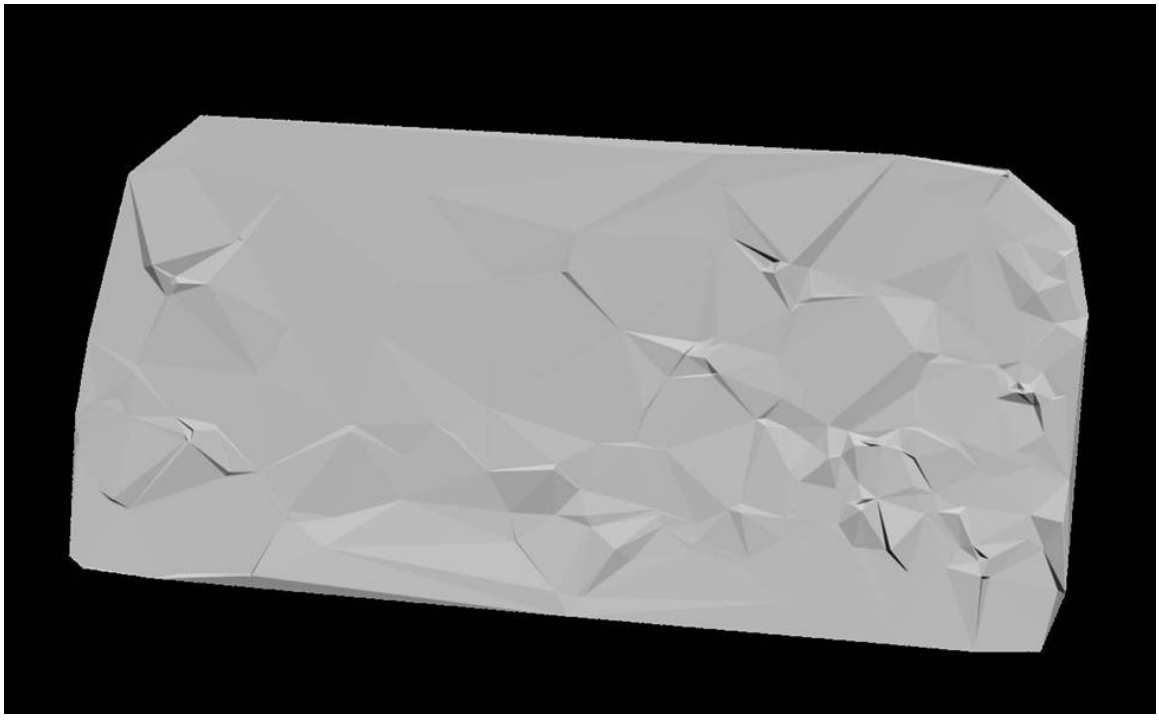

Figure 44. Surface DEM using 0.05% of the subset point cloud

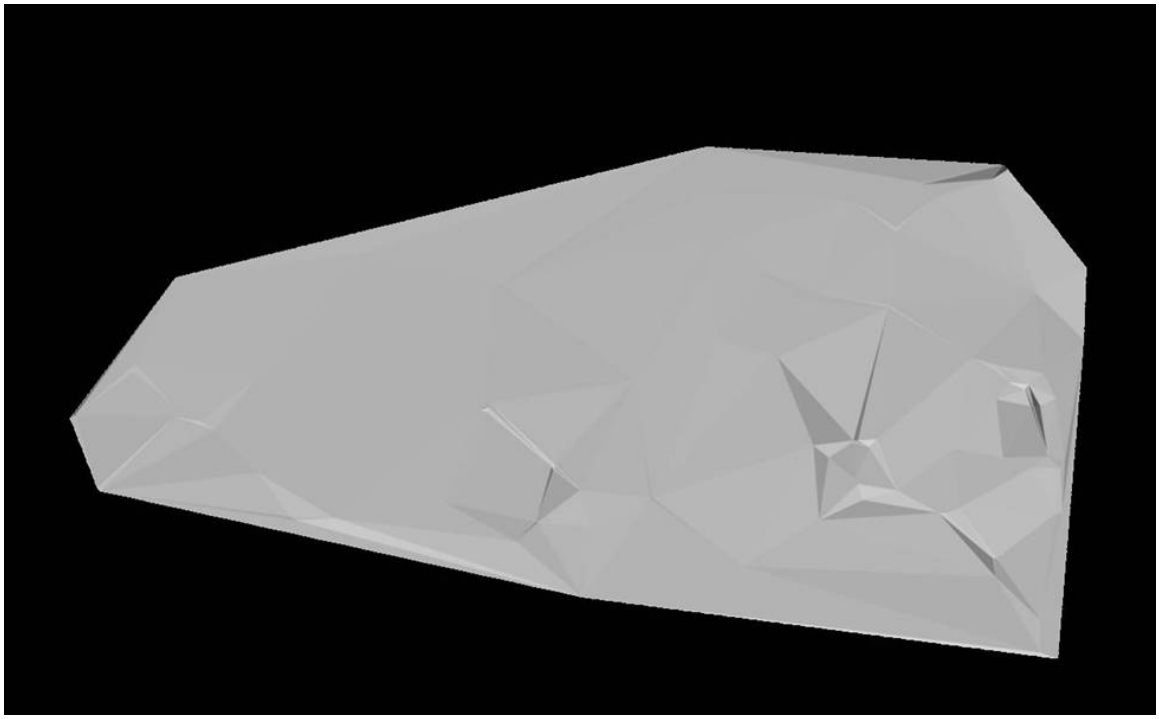

Figure 45. Surface DEM using 0.03% of the subset point cloud

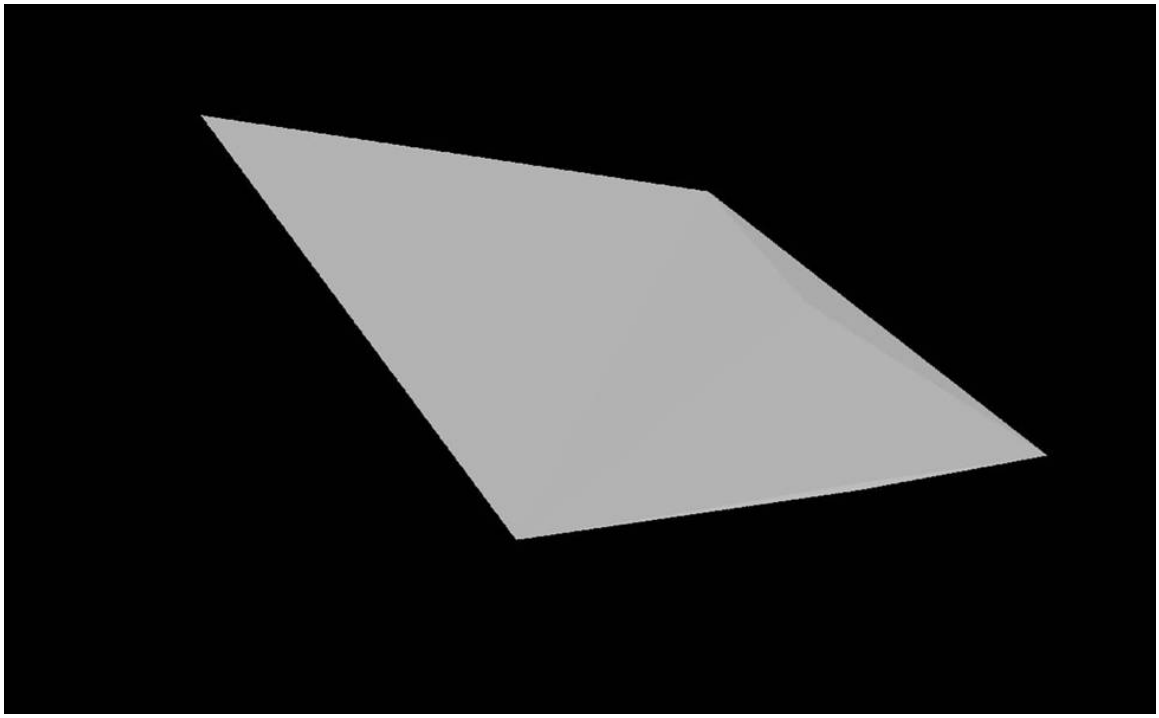

Figure 46. Surface DEM using 0.01% of the subset point cloud

B. LIDAR MODEL ARTIFACTS

When surface models are generated with a visualization software package, the data points are processed using algorithms which classify each point as either a ground, object or cloud point based on the physical location in three-dimension space of the surrounding points. Surface points are then draped over a uniform grid with spacing set by the user that should match closely with the point density of the data collected. These points are connected to one another in multiple triangles in a process to develop the Triangular Irregular Network (TIN). There are many different filtering processes from which to choose, depending on point density, relief, terrain and vegetation. When filtering basic Lidar, "a minimum of 89 percent of all artifacts are removed automatically. A minimum 90 percent of all outliers will be removed without any manual editing" (Young). Processes may vary within the project to account for variances in vegetation, features and terrain. As an analyst views the surface models, certain Lidar artifacts will appear. Some of the artifacts encountered while conducting this research and potential causes are explained below. Clearly visible in the following examples, areas of a DEM with these artifacts are of little use operationally and should be readdressed in the processing of the data.

1. Crystal Forest

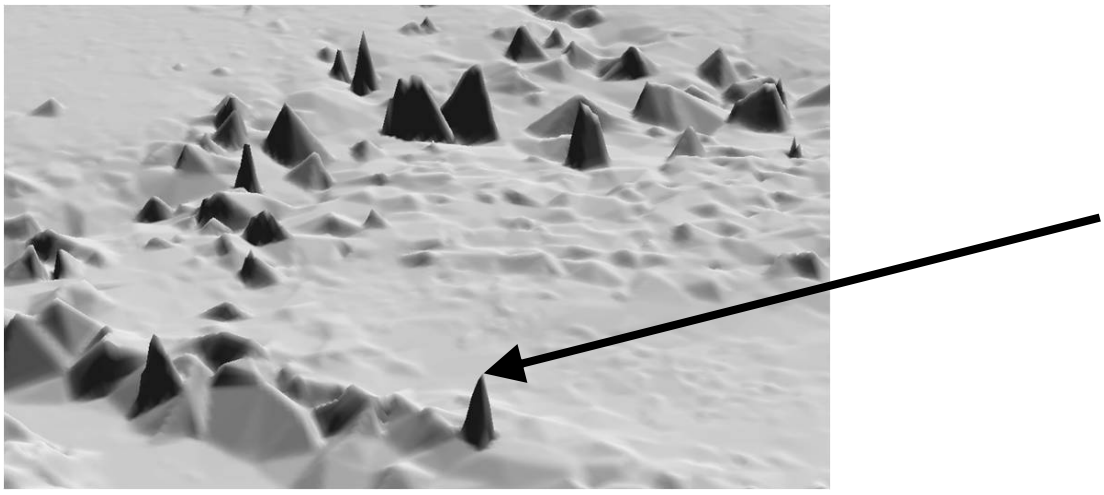

Figure 47. Crystal Forest Lidar artifact from TINning of 3% subset point cloud surface with returns misidentified as ground. Arrow indicates one bad point.

"Where there are few survey points (i.e., bare-earth surfaces in heavy timber, where there are few ground reflections), TINning the points produces large triangular facets where the surface has significant curvature" (PSLC). Additionally, it is possible to see similar textures where the vegetation reflections are incorrectly classified as ground rather than being filtered as object or cloud points. "Elevations are likely to be less accurate in these areas" (PSLC). One bad point identified as surface above the rest results in an erroneous jagged stalagmite peak rising above the actual surface.

2. Bomb Craters

Lidar data sets may also contain scattered points which are incorrectly identified as too-low, or negative blunders. This may be caused when a specular reflection or too-close ground saturates the detector and produces an internal echo. Where vegetation reflections are removed by a "find-the-lowest-point-in-the-vicinity algorithm, true ground points adjacent to the negative blunders may be misidentified as vegetation reflections and removed. The result can be a conical crater that is entirely an artifact" (PSLC).

C. VISUAL ANALYSIS

Years of experience in the Marine Corps reading contour maps have given the author an appreciation for a good map and the skills to recognize a bad map. The surface maps generated at the different reduced point densities were each looked at as a whole by the analyst for a subjective sense of "goodness". From the figures above, the educated reader should be able to discern that the 100% DEM is a good map. The 4 million points that went into this map give it a fineness and resolution that indicates the nature of the ground in that area. As the number of points was reduced by percentages, the visually discerned "goodness" of the map was similarly reduced.

The map remained good for the first several of the reductions, then fell off quickly. In the 100% DEM, details of the bare earth landscape are very fine and the interesting/important features that exist in the region are easy to pick out. When the region was originally selected for further study, the decision was made because of these features. Specifically, in the 100% DEM, the reader can pick put a very distinct water

feature, slopes running down to the water on both sides, a linear road feature and man-made objects and buildings. These features are easily recognizable in the 100%, the 90%, the 66%, 50%, 30%, 10% and 5% DEMs. At the 3% reduction in points, the building features are hard to pick out without prior knowledge of their existence, but the road, slopes and the water are clear. At the 1% reduction, the road feature is unrecognizable, the buildings are no more and are perceived as artifacts, but the water feature is recognizable. Below 1%, the existing ground features are lost in the triangularization from the TINning of the data points assigned as ground in the Plug-In. By 0.1%, any existing ground features are mostly unrecognizable by the DEM created with those points. In this experiment, the DEMs created with data below 0.1% of the original data set are absolutely worthless to an operator.

D. STATISTICS

As described in Chapter IV, the Surface Digital Elevation Maps were further analyzed with the statistical functions available in ENVI. This software program can calculate the different point values between each surface DEM and the original 100% model. The correlation was graphically depicted from this data.

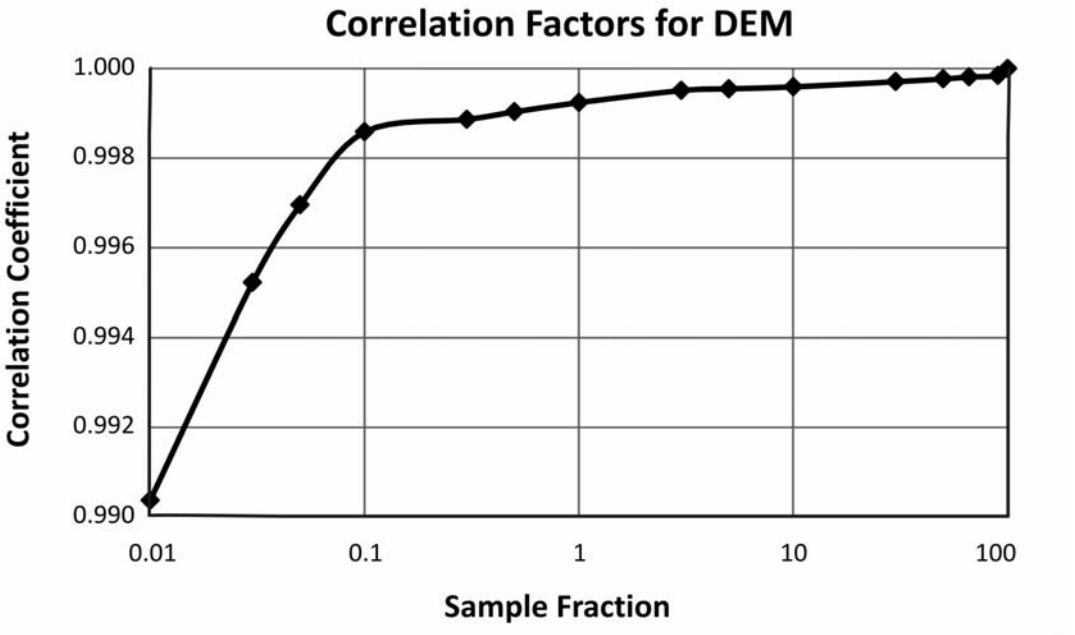

Figure 48. Correlation Factor for each DEM

From the above correlation figure, it can be seen that there is a high correlation between the original data set and each of the reduced point clouds for reductions down to 1% of the original total. For percentage reductions below 0.1%, the data correlation drops off and the covariance, or the measure of how strongly the two DEMs are related to one another (Devore 220) becomes unreliable.

Root Mean Square error analysis was also calculated and the data results exported as a graphic display for visual inspection. After the "calibrated eyeball" visual analysis of the surface DEMS, the RMS data was evaluated in ENVI and is displayed below. The RMS error was calculated using an IDL code written by Angela Puetz to work with ENVI.

$$RMS = \sqrt{\frac{\sum_{i=1}^{n} (X_{1,i}^{2} - X_{2,i})^{2}}{n}}$$

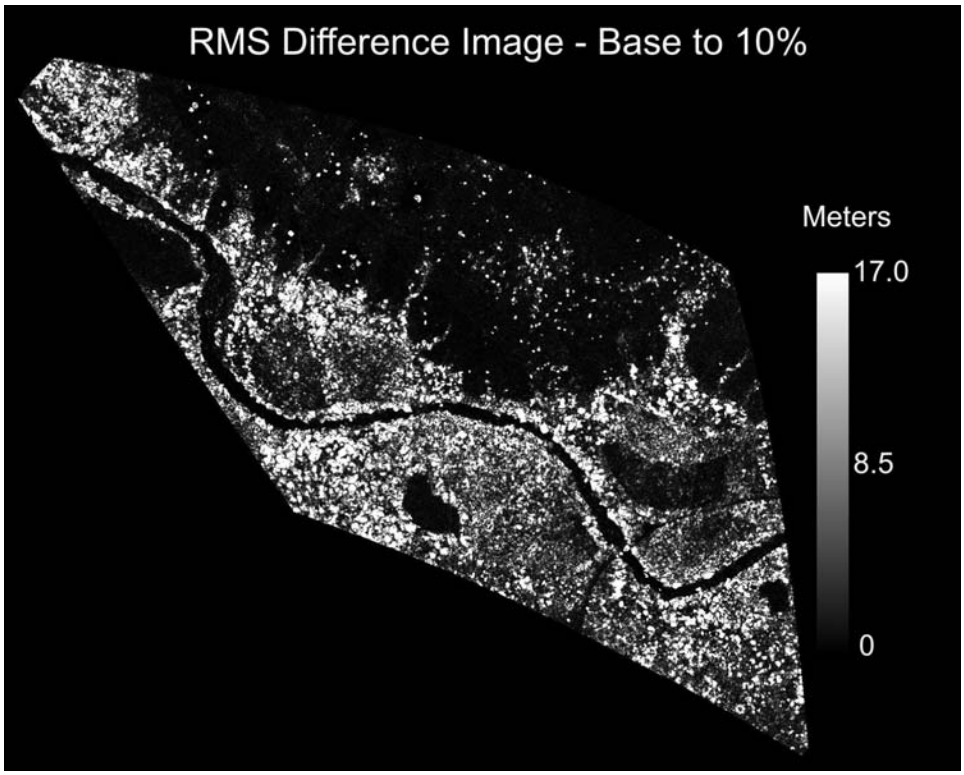

Figure 49. RMS difference between the base DEM image and the 10% data reduction DEM. Bright areas indicate where the two maps differ most.

Another item studied is the number of points selected as surface compared to the total number of collected cloud points. This percentage provided some insight on the quality and accuracy of the surface DEM. At the densest cloud of data points, the Bare Earth Extraction Plug-In selected half of the returns as surface points and at the extreme opposite end, the Plug-In selected less than 1 point as surface for every 123 points examined. In the figure below, the information plotted compares the number of points identified as surface to the total or reduced number of points in the cloud (surface/cloud).

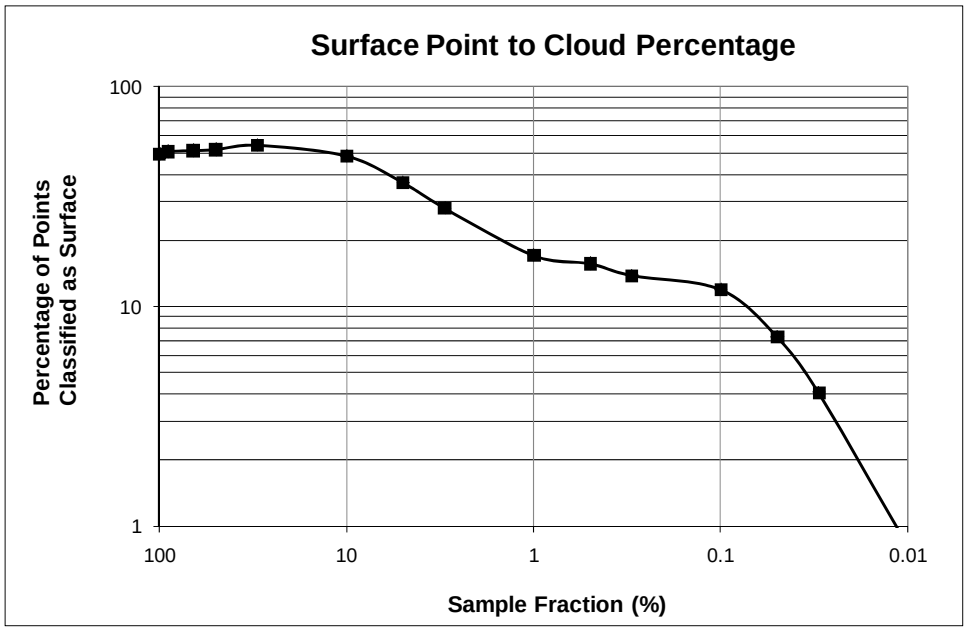

Pts	Fraction
100	49.41
90	50.81
66	51.35
50	51.85
30	54.26
10	48.48
5	36.71
3	28.10
1	17.09
0.5	15.69
0.3	13.86
0.1	11.95
0.05	7.28
0.03	4.06
0.01	0.81

Figure 50. Percentage of surface points identified through the Bare Earth Extractor compared to the total cloud points in the reduced data set

The Bare Earth Extractor Plug-In identified approximately half of the points as ground for the data reductions where greater than 10% of the total point cloud was available, as shown above and indicated with a percentage of 50%. In these cases, the surface DEM was finer and more accurate when compared to the original dataset. As the ratio of total cloud points to those identified as surface points grew, the accuracy and resolution of the DEM fell off.

The algorithm used by this plug-in has a much more difficult time accurately identifying the classification of the points in a less dense point cloud. This is most evident for the .01% reduced data set which has a percentage below 1% of the points

identified as surface points to the total number of points in the point cloud. Such as it was, the plug-in identified only 7 point returns as surface and this DEM was completely useless to navigate in a 1.4 km^2 area. In the 0.1% reduction of the data, the Plug-In was identifying only about 12% of the point cloud as surface. The algorithm is breaking down at these low densities and perhaps will do so when the detector does not receive enough ground returns on other collects to populate a true ground surface DEM adequately.

VII. SUMMARY

The overall results of this research represented by the analysis in Chapter V yield interesting and encouraging results. By looking at multiple DEMs created of the same distinct area from an "exquisite data set" of collected Lidar cloud returns and subsequent percentage reductions of the total, we observe a strong correlation between the amount of data and the accuracy of the DEM generated from that data.

Percent of Data	*Point Cloud Total Points*	*Surface Points*	*Pt Cloud [pts/km^2]*	*Surface [pts/km^2]*
100	8622343	4260249	6064065	2996219
90	7760109	3942705	5457659	2772891
66	5690746	2921962	4002283	2055006
50	4311172	2235412	3032033	1572158
30	2586703	1403544	1819220	987108
10	862234	417996	606407	293975
5	431117	158246	303203	111294
3	258670	72682	181922	51117
1	86223	14738	60641	10365
0.5	43112	6763	30320	4756
0.3	25867	3584	18192	2521
0.1	8622	1030	6064	724
0.05	4311	314	3032	221
0.03	2587	105	1819	74
0.01	862	7	606	5

Table 6. Experimental Point Density

The table above displays the number of points in the original data set and in each percentage reduction of the whole. The region covered by this data was mapped on seven adjacent and consecutive passes from an airborne Lidar. This area was measured to be 1625 meters by 875 meters for a total area of 1421875 square meters (1.42 km^2). By dividing the total points by the total area, the results tabulated above show what amount of points per meter, or resolution, is necessary for an accurate and useful DEM. This

experiment looked at three ways to asses the DEM: with visual maps, with correlation data between the 100% DEM image and each image created with a given percent of the original dataset, and with a comparison between data points selected as surface points compared to the total point cloud. From the previous heuristic and statistical analysis in chapter V we saw the visually dramatic fall of accuracy or "goodness" of the created DEM below 3% of the original data cloud. There is a significant drop off in correlation between the images below 0.1%. The percentage of points classified as surface drops below 10% and again below 0.1%. Taken together, this indicates a need for a collection of no less than 600 points per 100m x 100m area of interest or 60,000 points per km^2 or approximately one point for every four square meters surveyed. For the type of resolution achieved in the 10% reduced data set, 6000 points were collected and analyzed for any 100m x 100m area. Not surprisingly, the more points collected, the better the accuracy and fineness of the DEM. Necessarily, the accuracy desired will depend on the type of mission that is being planned. Certain requirements need centimeter accuracy to identify exact geolocated positions whereas others are good enough to plan with a 1:50,000 scale map that identifies gross features of the terrain and smaller details and less important to the plan. However, the result of this experiment gives military and intelligence planners another planning factor to consider when trying to collect against an area of interest or a potential hostile target.

VIII. CONCLUSION

Suitably accurate surface Digital Elevation Maps can be generated from a point cloud containing 60,000 points per square kilometer of area. Reasonably good to marginally acceptable surface maps can be created with 30,000-18,000 points per km^2. These surface DEMs are only good for gross terrain appreciation and do not accurately show fine details on the ground. Below this number of returns, the software that processes surfaces from the collection of points in the area of interest cannot accurately distinguish and classify surface points from nearby returns from foliage or other objects. Increasing point density from the collection necessarily improves the accuracy of the maps generated from this data.

Although the purpose of this thesis was to assess the production of Digital Elevation Maps using varying density of data points from a Lidar collection, the application of this thesis research may aid future planning officers in their Intelligence Preparation of the Battlespace.

While conducting this research, the author had several ideas on how to apply this to a tactical or intelligence gathering operation. The step-stare approach and off-nadir collection of points with a low divergence, high pulse repetition frequency transmitter in the sensor, an airborne Lidar may be able to covertly collect data on the range to and composition of hostile camps in many different environments, from under jungle canopy or within urban valleys.

The following is a list of potential research areas that would assist in the development of the Lidar field:

- Airborne Lidar collection tactics, techniques and procedures
    - Step Stare collection
    - Off nadir collection
- Identification of man-made objects in a Lidar pint cloud
- Use of fully digitized waveform returns to identify types of foliage

- Use of fully digitized waveform returns to identify ground composition
- Further determine how the type of foliage or ground area affects the required number of points for an accurate DEM
- Compare and evaluate other bare earth extraction algorithms in the creation of DEMs

Lidar offers a capability to produce accurate Digital Elevation Models of areas obscured by a canopy through its foliage penetration. Based on the results of this research, a Lidar collection against an area of interest that contains 60,000 points per square kilometer area of interest will be able to generate an accurate DEM. Although desired accuracy for identifying objects or trails under canopy benefits from additional point density, this result is a baseline for a result previously unattainable with other forms of remote sensing imagery available.

LIST OF REFERENCES

Aggett, Graeme. "Airborne Laser Mapping with LiDAR." Presentation from 2005 GIS Conference Proceedings. <http://gisconference.cas.psu.edu/2005/proceedings/1_tues_0830.pdf>.

"ALHAT: Autonomous Landing and Hazard Avoidance Technology." NASA Jet Propulsion Laboratory. 2 September 2008. < http://www-robotics.jpl.nasa.gov/tasks/showTask.cfm?TaskID=84&tdaID=999986>.

Applied Imagery. "Quick Terrain Modeler Application Notes." 7 September 2008. <http://www.appliedimagery.com/ >.

Araki, H. et al. "Present Status and Preliminary Results of the Lunar Topography by KAGUYA-LALT Mission." Lunar and Planetary Science XXXIX Conference. 10-14 March 2008. pp 1510-1511.

Blair, J. Bryan; Michelle Hofton and Scott B. Luthcke. Wide-Swath Imaging Lidar Development for Airborne and Spaceborne Applications. International Archives of Photogrammetry and Remote Sensing, Volume XXXIV-3/W4 Annapolis, MD, 22-24 Oct. 2001.

Bufton, J. L. Space-based laser altimeter technology and applications. (1996).

Bufton, J. L. Shuttle laser altimeter. (1997).

"CALIOP." National Space Science Data Center website. 10 September 2008. <http://nssdc.gsfc.nasa.gov/nmc/experimentDisplay.do?id=2006-016A-01>.

"CALIPSO Products." CALIPSO QUICKLOOK LIDAR BROWSE IMAGES. <http://www-calipso.larc.nasa.gov/products/lidar/browse_images/>.

"CALIPSO." National Space Science Data Center website. 10 September 2008. <http://nssdc.gsfc.nasa.gov/nmc/spacecraftDisplay.do?id=2006-016A>

Canadian Space Agency. "MET Station – Lidar." 5 September 2008 <www.space.gc.ca>.

Carswell, Allan I. et al. "LIDAR for Mars Atmospheric Studies on 2007 Scout Mission 'phoenix'." 22nd Internation Laser Radar Conference (ILRC 2004), Proceedings of the Conference held 12-16 July, 2004 in Matera, Italy. Edited by Gelsomina Pappalardo and Aldo Amodeo. ESA SP-561. Paris: European Space Agency, 2004, p. 973.

Cassini-Huygens. Jet Propulsion Laboratory website. 10 September 2008. <http://saturn.jpl.nasa.gov/overview/index.cfm>.

"Chang'e." National Space Science Data Center website. 11 September 2008. <http://nssdc.gsfc.nasa.gov/nmc/spacecraftDisplay.do?id=2007-051A>.

"Clementine." National Space Science Data Center website. 10 September 2008. <http://nssdc.gsfc.nasa.gov/nmc/spacecraftDisplay.do?id=1994-004A>.

"Country of Honduras." 14 September 2008. <http://www.honduras.com>.

Degnan, John J. "Thirty Years of Satellite Laser Ranging." Keynote Speech, Proceedings of the Ninth International Workshop on Laser Ranging Instrumentation, Canberra, Australia, November 7-11, 1994.

Devore, Jay L. Probability and Statistics for Engineering and the Sciences. Toronto, Ontario, Canada: Thomson Learning, 2004.

Dini, Gh.; Sabzevari, M. "Producing High Scale Topographical Maps, Using Space Images." Geoscience and Remote Sensing Symposium, 2005. IGARSS '05. Proceedings. 2005 IEEE International Volume 3, 25-29 July 2005 Page(s):1651 – 1653.

Dubayah, Ralph, et al. "The Vegetation Canopy Lidar Mission." University of Maryland Mission Paper. 8 September 2008. <http://www.geog.umd.edu/vcl/vcltext.html>.

Earth Observatory. "Vegetation Canopy Lidar." 8 September 2008. <http://earthobservatory.nasa.gov/Library/VCL/printall.php>.

"ENVI Capabilities." ITT Visual Information Solutions. 14 September 2008. <http://www.ittvis.com/ProductServices/ENVI/Capabilities.aspx>.

"GeoTIFF." 14 September 2008. <http://www.remotesensing.org/geotiff/geotiff.html>.

Gesch, D. B. "Accuracy assessment of a global elevation model using shuttle laser altimeter data." (1998).

"GLAS." National Space Science Data Center website. 10 September 2008. <http://nssdc.gsfc.nasa.gov/nmc/experimentDisplay.do?id=2003-002A-01>.

Harding David J. "Geoscience applications of airborne and spaceborne lidar altimetry"

Harding, D. J., Carabajal, C. C., Luthcke, S. B., & Gesch, D. B. "Application of the shuttle laser altimeter in an accuracy assessment of global 1-kilometer digital elevation data." <http://www.isprs.org/commission3/lajolla/pdf/p81.pdf>.

Harrington, J. D. and Mike Buckley. "NASA REVEALS NEW DISCOVERIES FROM MERCURY." NASA Press Release: 08-166. July 3, 2008.

Hohl, Thomas. "Representing the relief of Orienteering maps with the aid of airborne laser scanning." 18 Nov 2004. Gymnasium Kirschgarten Basel, Switzerland.

"ICESat." National Space Science Data Center website. 10 September 2008. <http://nssdc.gsfc.nasa.gov/nmc/spacecraftDisplay.do?id=2003-002A>.

IKG Research. "Automatic methods for the fusion, reduction and consistent combination of complex, heterogeneous geoinformation." Retrieved 30 April 2008 <http://www.ikg.uni-hannover.de/forschung/vw_stiftung/index.en.html>.

"ILAP Bare Earth Extraction Plug-In Operator's Manual." Johns Hopkins University Applied Physics Laboratory. Laurel, Maryland. 2006.

Isenburg, Martin. "Visualizing LIDAR in Google Earth." 24 June 2008. <http://www.cs.unc.edu/~isenburg/research>.

Jones, Thomas D. "Shooting for the Moon." Aerospace America. May 2008: 20-22.

"Kaguya." Japan Aerospace Exploration Agency website. 24 June 2008. <http://www.isas.jaxa.jp/e/enterp/missions/kaguya/index.shtml>.

Kalin, David A. Foliage Penetration Overview. FOPEN Workshop. National Geospatial-Intelligence Agency, Reston, VA. 26 June 2008.

Keller, John; Gordon Chin and Thomas Morgan. "Lunar Reconnaissance orbiter: Instrument Suite and Objectives." IAC-07-A3.6.A.03 25 September 2007.

Krabill, W.B.; Collins, J.G.; Link, L.E.; Swift, R.N.; Butler, M.L. "Airborne Laser Topographic Mapping Results." Photogrammetric Engineering and Remote Sensing. 50.6 (1984): 685-694.

LAPF. "SLA-02 Data Products Distribution Site." 7 July 2008. <http://denali.gsfc.nasa.gov/lapf_web>.

"Laser Altimeter." National Space Science Data Center website. 10 September 2008. <http://nssdc.gsfc.nasa.gov/nmc/experimentDisplay.do?id=1971-063A-05> <http://nssdc.gsfc.nasa.gov/nmc/experimentDisplay.do?id=1972-031A-05> <http://nssdc.gsfc.nasa.gov/nmc/experimentDisplay.do?id=1972-096A-09>.

"LOLA." Lunar Reconnaissance Orbiter website. 11 September 2008. <http://lunar.gsfc.nasa.gov/lola.html>.

"Mars Global Surveyor." National Space Science Data Center website. 9 September 2008. <http://nssdc.gsfc.nasa.gov/nmc/spacecraftDisplay.do?id=1996-062A>.

"Mars Observer." National Space Science Data Center website. 10 September 2008. <http://nssdc.gsfc.nasa.gov/nmc/spacecraftDisplay.do?id=1992-063A>.

"Mars Polar Lander." National Space Science Data Center website. 10 September 2008. <http://nssdc.gsfc.nasa.gov/nmc/spacecraftDisplay.do?id=1999-001A> <http://nssdc.gsfc.nasa.gov/nmc/experimentDisplay.do?id=1999-001A-03>.

McGarry, Jan and Zagwodzki, Tom. "A Brief History of Satellite Laser Ranging: 1964 – present* (a GSFC Perspective)." Presentation by NASA/GSFC/694. 7 April 2005.

"Mercury Laser Altimeter (MLA)." Johns Hopkins University Applied Physics Laboratory Messenger website. 9 September 2008. <http://messenger.jhuapl.edu/instruments/MLA.html>.

"Messenger." National Space Science Data Center website. 9 September 2008. <http://nssdc.gsfc.nasa.gov/nmc/spacecraftDisplay.do?id=2004-030A>.

"Mission Overview." Lunar Reconnaissance Orbiter website. 11 September 2008. <http://lunar.gsfc.nasa.gov/mission.html>.

"MOLA." Goddard Space Flight Center website. 24 June 2008. <http://mola.gsfc.nasa.gov/>.

Mukai, T. et al. "An overview of the LIDAR observations of asteroid 25143 Itokawa." Advances in Space Research 40. 2007. pp 187-192.

"NASA 'Altair' Lunar Lander." 18 Dec 2007. NASA. 28 August 2008. <http://www.nasa.gov/mission_pages/constellation/altair/index.html>.

NGA. "National Geospatial-Intelligence Agency Home." 7 September 2008. <http://www1.nga.mil/Pages/Default.aspx>.

Olsen, R. C. Remote Sensing from Air and Space. Bellingham, WA: SPIE Press, 2007.

Optech Gemini Product Information. "Gemini ALTM 167." 31 August 2008. <http://www.optech.ca/pdf/Gemini167.pdf>.

Optech Inc. "About Lidar." 25 August 2008 <http://www.optech.ca/aboutlaser.htm>.

"Payloads." China's Lunar Exploration Program website. 11 September 2008. <http://210.82.31.82/> <http://www.clep.org.cn/index.asp?modelname=index_zt_kxtc>.

Phoenix News. "The Evolution of Dust over the Phoenix Lander." 30 May 2008. <http://jpl.nasa.gov/news/phoenix/images-all.php?fileID=11015>.

PSLC. "Puget Sound Lidar Consortium – Data". 16 September 2008. <http://pugetsoundlidar.ess.washington.edu/lidardata/index.html>.

"Quick Terrain Modeler Training." National Geospatial Intelligence College Course Handout. Applied Imaging. Silver Spring, MD. 2008.

Riegl, USA. "Last Pulse Measuring Technique." 25 August 2008 <http://www.rieglusa.com/principle_operation/e_gi009.htm>.

Roth, M. W., Hunnell, J. C., Murphy, K. E., & Scheck, A. E. (2007). "High-Resolution Foliage Penetration with Gimbaled Lidar." Proceedings of SPIE. Vol. 6550 65500K-1-65500K-9.

Science@NASA. "What Neil & Buzz Left on the Moon." 7 September 2008. <http://science.nasa.gov/headlines/y2004/21jul_llr.htm>.

Shaffer, Steven. "Using ArcGIS for Radar Analysis and Map Production for USA NAIP Program." ESRI Federal User Conference Proceedings. 14 Mar 2008. <http://gis.esri.com/library/userconf/feduc08/papers/453.pdf>.

Spatial Resources website. 14 September 2008. <http://www.spatialresources.com/id78.html>.

Sjogren, William L. "Final Report Apollo Laser Altimeter Analysis S-216." Jet Propulsion Laboratory. Pasadena, California. January, 1975.

"STS/LITE." National Space Science Data Center website. 10 September 2008. <http://nssdc.gsfc.nasa.gov/nmc/spacecraftDisplay.do?id=LITE>.

The Purdue OWL Family of Sites. 26 Aug. 2005. The Writing Lab and OWL at Purdue and Purdue University. 27 August 2008 <http://owl.english.purdue.edu>.

Ullrich, Andreas. Et al. "Improvements in DTM generation by using full-waveform airborne laser scanning data." 25 August 2008. <http://www.riegl.com/airborne_scannerss/airborne_photo_gallery/downloads/Ullrich_et_al_2007_Moskau_engl.pdf>.

"VCL." Internet Encyclopedia of Science. 8 September 2008. <http://www.daviddarling.info/encyclopedia/V/VCL.html>.

"WFF GLAS." Hydropheric and Biospheric Sciences Laboratory website. 11 September 2008. <http://glas.wff.nasa.gov/>.

Xinhua News Agency. "New moon photos taken by Chang'e-1 released." 10 December 2007. 11 September 2008. <http://english.hanban.edu.cn/english/China/234956.htm>.

Young, Jamie. "LiDAR for Mapping and GIS". Earth Imaging Journal website. 16 September 2008. <http://www.eijournal.com/LiDar_Mapping.asp>.

THIS PAGE INTENTIONALLY LEFT BLANK

APPENDIX – RANDOM_PTS_FROMXYZ.PRO IDL CODE

The following text is the code written by Angela Puetz of the Naval Postgraduate School Remote Sensing Center to randomly select points from the XYZ file of Lidar cloud data. This code was run 14 times over the data subset to generate each of the reduced file sets analyzed.

```
dir = 'P:\LIDAR\Penlight\'   & cd, dir

file_dir = 'P:\LIDAR\Penlight\Anderson_Research\Strip30-36subset\'
file_dir = 'C:\Documents and Settings\bcanders\My Documents\Strip30-36subset\'
output_dir = file_dir

pct = [3.0, 5.0] ;Percentage to reduce file size to

file = 'Subset30-36.xyz'
pos = strpos( file, '.')
tf = strmid( file, 0, strlen(file)-4)
outfile = file_dir + tf

hdr = strarr(3)

data = double([0, 0, 0, 0])
temp = double([0, 0, 0])
temp2 = 7
openr, 1, file_dir+file
readf, 1, hdr
print, 'input file: ', file_dir+file
print, 'output file:', outfile
npts = 0l
;stop
hdr1 = ' '
WHILE ~ EOF(1) DO BEGIN
   readf, 1, hdr1
   npts = npts+1
ENDWHILE
help, npts
close, 1

openr, 1, file_dir+file
readf, 1, hdr
data = dblarr(4, npts)
for index = 0L, npts-1  DO BEGIN
   readf, 1, temp, temp2
   data(0:2, index) = temp
   data(3, index) = temp2
ENDfor
close, 1



;data = data(*,1:n_elements(data))

FOR i=0, n_elements(pct)-1 DO BEGIN
  nreduced = long(npts*pct(i)/100.)
```

```
   if (nreduced  lt 2) then  nreduced = 2
  print, 'original number of pts:', npts
  print, 'number of reduced pts:', nreduced

  ;Reduce dataset to percentage of original
 seed = 1
  reduced_pts = RANDOMU(seed,nreduced)
  index = sort( reduced_pts)
  reduced_pts = reduced_pts(index) * npts
  reduced_pts = long( reduced_pts)

  data_2 = data(*,reduced_pts)

  ;Output reduced data set is ASCII format
  dir = output_dir

pcti = fix(pct(i)*100)
  outfile_temp = outfile+'_'+string(pcti, "(I5.5)")+'_pct.xyz'
  print, 'output file:', outfile_temp


  openw, 2, outfile_temp
  printf, 2, 'Points taken from: ', file
  aa = string(pct(i), "(f8.2)")
  bb = string(npts, "(I8)")
  cc = string(nreduced, "(I8)")
  lable = 'Reduced to: '+ aa +'%   Original # of pts: '+bb+ ' Reduced # of pts:
'+cc
  print, lable
  printf, 2, lable
  printf, 2, 'x, y, z, intensity'
  for j=0L, nreduced-1 do begin
    printf, 2, data_2(0:2,j), fix(data_2(3,j)), format = "( f19.12, 2x, f20.12,
2x, f16.12, i4   )"
  endfor
  close, 2
ENDFOR

END
```

INITIAL DISTRIBUTION LIST

1. Defense Technical Information Center
   Ft. Belvoir, Virginia

2. Dudley Knox Library
   Naval Postgraduate School
   Monterey, California

3. R. C. Olsen
   Naval Postgraduate School
   Monterey, California

4. Marine Corps Representative
   Naval Postgraduate School
   Monterey, California

5. Director, Training and Education
   MCCDC, Code C466
   Quantico, Virginia

6. Director, Marine Corps Research Center
   MCCDC, Code C40R
   Quantico, Virginia

7. Marine Corps Tactical Systems Support Activity
   (Attn: Operations Officer)
   Camp Pendleton, California

8. Head, Information Operations and Space Integration Branch
   PLI/PP&O/HQMC
   Washington, DC